



Identifying New Probes of Essential Targets in *Mycobacterium tuberculosis*

Citation

Wellington, Samantha Ann. 2017. Identifying New Probes of Essential Targets in *Mycobacterium tuberculosis*. Doctoral dissertation, Harvard University, Graduate School of Arts & Sciences.

Permanent link

<http://nrs.harvard.edu/urn-3:HUL.InstRepos:41142058>

Terms of Use

This article was downloaded from Harvard University's DASH repository, and is made available under the terms and conditions applicable to Other Posted Material, as set forth at <http://nrs.harvard.edu/urn-3:HUL.InstRepos:dash.current.terms-of-use#LAA>

Share Your Story

The Harvard community has made this article openly available.
Please share how this access benefits you. [Submit a story](#).

[Accessibility](#)

Identifying New Probes of Essential Targets in
Mycobacterium tuberculosis

A dissertation presented

By

Samantha Ann Wellington

to

The Committee on Higher Degrees in Chemical Biology

in partial fulfillment of the requirements

of the degree of

Doctor of Philosophy

in the subject of

Chemical Biology

Harvard University,
Cambridge Massachusetts

May 2017

© 2017 *Samantha Wellington*

All rights reserved.

Identifying New Probes of Essential Targets in *Mycobacterium tuberculosis***Abstract**

Despite the availability of effective treatments, *Mycobacterium tuberculosis* (Mtb) remains a public health crisis. An estimated 9 million people are infected with Mtb every year, resulting in 1.5 million deaths. Efforts to control the tuberculosis epidemic are stymied by a lengthy treatment period, a large reservoir of latently infected individuals, and the emergence of multi- and extensively drug-resistant strains of Mtb.

Drugs with novel mechanisms of action are urgently needed in order to address these challenges, but standard screening methods are failing to identify these types of compounds. While numerous functions have been characterized as essential for the survival of Mtb, very few are inhibited by current drugs. Furthermore, few existing drugs are able to kill the non-replicating, phenotypically drug-resistant state of Mtb thought to contribute to lengthy treatment times and latent infections. This research explores the mechanisms of new small molecule inhibitors against Mtb, thereby expanding our knowledge of the bacteria's inner-workings and identifying new therapeutic targets.

Chapter 2 describes the identification of a novel azetidine, BRD4592, that kills Mtb through allosteric inhibition of tryptophan synthase (TrpAB), a previously untargeted enzyme. Given that Mtb can scavenge tryptophan from its environment, questions of TrpAB's *in vivo* essentiality are of top importance. Building on our discovery of BRD4592 and utilizing additional inhibitors of amino acid synthesis, we explore the mycobacterial response to amino acid starvation (Chapter 3). We show TrpAB is required for the *in vivo*

survival of Mtb and although the inhibitors induce a protective response to cell stress, the response does not prevent eventual cell death.

Finally, Chapter 4 details the characterization of four compounds active against non-replicating Mtb. One of the compounds binds nickel and cobalt and disrupts metal ion homeostasis. The other three compounds act as prodrugs, requiring modification by Mtb enzymes for activity. Through this work, we discovered that the Mtb enzyme MymA can function as an activating enzyme. MymA is not only responsible for activating one of our newly identified compounds, but also can activate ethionamide, an existing antitubercular drug. Together, the compounds identified in this dissertation provide tools to better understand Mtb biology and, ultimately, to combat the Mtb epidemic.

Table of Contents

TITLE PAGE	I
COPYRIGHT PAGE	II
ABSTRACT	III
TABLE OF CONTENTS	V
ACKNOWLEDGEMENTS	VII
CHAPTER 1: NEW DRUG TARGETS FOR <i>MYCOBACTERIUM TUBERCULOSIS</i>	1
ATTRIBUTIONS	2
ABSTRACT	2
SECTION 1.1. BACKGROUND	3
SECTION 1.2. STRATEGIES FOR DISCOVERING MTB THERAPEUTICS	5
SECTION 1.3. NEW DRUG TARGETS FOR MTB	7
<i>Macromolecular Synthesis</i>	7
<i>Energy Metabolism</i>	16
<i>Inhibitors with Complex Mechanisms</i>	19
<i>Emerging Targets</i>	20
SECTION 1.4. CHALLENGES AND PROSPECTS FOR MOVING FORWARD	27
CHAPTER 2: IDENTIFICATION OF A SPECIFIC ALLOSTERIC SMALL-MOLECULE INHIBITOR OF <i>MYCOBACTERIUM TUBERCULOSIS</i> TRYPTOPHAN SYNTHASE ..	31
ATTRIBUTIONS	32
ABSTRACT	34
SECTION 2.1. BACKGROUND	35
SECTION 2.2. RESULTS	40
<i>Identification of an azetidine that targets tryptophan synthase stereospecifically</i> ..	40
<i>BRD4592 is an allosteric inhibitor of Mtb TrpAB</i>	44
<i>BRD4592 stabilizes closed, active states of the β subunit</i>	49
<i>Crystal structures reveal BRD4592 binds the TrpAB protein-protein interface</i>	53
<i>BRD4592 has a multifaceted mechanism of inhibition</i>	60
SECTION 2.3. DISCUSSION	64
SECTION 2.4. MATERIALS AND METHODS	69
CHAPTER 3: EXPLORING CENTRAL METABOLISM AS A THERAPEUTIC TARGET: MYCOBACTERIAL RESPONSES TO AMINO ACID STARVATION	87
ATTRIBUTIONS	88
ABSTRACT	89
SECTION 3.1. BACKGROUND	90
SECTION 3.2. RESULTS	93

<i>Mtb TrpAB is essential in vivo</i>	93
<i>Probing the bactericidal response to L-Trp starvation</i>	98
<i>Mycobacterial response to starvation of branched-chain amino acids</i>	99
SECTION 3.3. DISCUSSION	101
SECTION 3.4. MATERIALS AND METHODS.....	104
CHAPTER 4: NEW COMPOUNDS AGAINST NON-REPLICATING MYCOBACTERIUM TUBERCULOSIS	109
ATTRIBUTIONS.....	110
ABSTRACT	111
SECTION 4.1. BACKGROUND	112
SECTION 4.2. RESULTS	113
<i>Characterization of a metal-binding aminothiazole</i>	113
<i>The aminothiazole perturbs metal-responsive genes</i>	114
<i>Identification of non-toxic analogues of TK010-016R</i>	117
<i>Mycobacterial response to non-toxic analogues</i>	117
<i>EthA is required for activity of compounds 1 and 2</i>	120
<i>MymA is required for thiooxadiazole 3 activity</i>	127
<i>Optimization of the thiooxadiazole scaffold for replicating and non-replicating activity</i>	129
<i>MymA activates thiooxadiazole 3</i>	132
<i>Evidence for MymA activation of ethionamide</i>	134
<i>Selection for loss of function of mymA in clinical strains</i>	138
SECTION 4.3. DISCUSSION	143
SECTION 4.4. MATERIALS AND METHODS	148
CHAPTER 5: SUMMARY AND PERSPECTIVES	154
SECTION 5.1. SUMMARY OF FINDINGS	155
SECTION 5.2. CONCLUSIONS AND FUTURE DIRECTIONS	158
REFERENCES	161

Acknowledgements

I would like to thank Deb Hung for her continual guidance and support. I would also like to thank my dissertation advising committee for their encouragement and feedback over the years: Stuart Schreiber, Dan Kahne, and Eric Rubin. Thank you also to Mike Gilmore and Stew Fisher for mentorship and enthusiasm throughout my training.

The Hung lab has been an engaging and enjoyable environment for my training, for which I am grateful, and many members of the lab deserve additional acknowledgement for collaboration and mentorship. Drug discovery is truly a team endeavor and I am grateful to have had the opportunity to work with and receive training from several talented and enthusiastic scientists. This research would not have been possible without the incredible collaboration the Joachimiak lab. Nor would it have been possible without the resources and collaboration of numerous Broad Scientists.

I am incredibly thankful for the community I've found in Boston. My classmates and close friends have brought joy, excitement, and support as we navigate our training together. I have also found a second community at Y2Y Harvard Square where I've been lucky enough to work alongside several deeply caring and committed individuals. Y2Y has given me a much-needed complement to my scientific endeavors, has shown me what true passion and teamwork can accomplish, and has introduced me to so many individuals I admire and sincerely care for.

Finally, my family deserves the highest acknowledgement of all. I would like to thank them for their endless curiosity about my science as well as their continuous support in everything I do.

Chapter 1: New drug targets for *Mycobacterium tuberculosis*

Attributions

The following chapter is being prepared as a review article by S. Wellington and D. Hung.

Chapter 1: New drug targets for *Mycobacterium tuberculosis*

Samantha Wellington^{1,2,3}, Deborah T. Hung^{1,2,3}

¹ Broad Institute, Cambridge, MA 02142 USA

² Department of Genetics, Harvard Medical School, Boston, MA 02115 USA

³ Department of Molecular Biology and Center for Computational and Integrative Biology, Massachusetts General Hospital, Boston, MA 02114 USA

Abstract

After decades of relative inactivity, the *Mycobacterium tuberculosis* (Mtb) drug discovery field has recently been revitalized. This large increase in efforts to discover new antitubercular therapeutics has brought several insights into the biology of Mtb and promising new therapies such as bedaquiline, which inhibits ATP synthase and delamanid, a nitroimidazole that inhibits both mycolic acid synthesis and energy production. Despite these advances, in order to meet the WHO END TB goal of reducing tuberculosis incidence by 90% by 2035, the field desperately needs compounds with novel mechanisms of action capable of inhibiting multi- and extensively-drug resistant Mtb as well as non-replicating Mtb. This review addresses recent efforts to discover inhibitors with new targets as well as strategies for tackling such a difficult challenge.

Section 1.1. Background

Mycobacterium tuberculosis (Mtb) is the world's leading cause of death due to an infectious disease¹. Decades after the introduction of an effective treatment regimen containing isoniazid, rifampin, ethambutol, and pyrazinamide, Mtb continues to pose a major global health threat. Though highly effective against drug-sensitive strains, the front-line antibiotics are slow, requiring 6-9 months of treatment to cure an infection. The lengthy treatment time often results in patient non-compliance, fueling the development of multi- and extensively drug-resistant tuberculosis (M/XDR-TB)². In cases of drug resistance, patients undergo a 2-year regimen involving thousands of pills and injections with cure rates of 50% for MDR-TB and only 20% for XDR-TB¹. The rising prevalence of multidrug resistant strains clearly necessitates the development of new therapeutics with unique mechanisms of action for which there will not be cross-resistance to current therapies.

Mtb typically causes lung infections where it inhabits numerous cell types, including alveolar macrophages. Infecting bacteria reside inside phagosomes, preventing phago-lysosomal fusion³. In humans, pulmonary infection with Mtb stimulates the formation of granulomas which are dense clusters of immune cells that create a harsh environment of hypoxia, nutrient deprivation, reactive nitrogen and oxygen species, and low pH³⁻⁶. *In vitro*, these environmental stresses have each been shown to induce a non-replicating state in Mtb that is, to varying degrees, phenotypically drug-resistant^{7,8}. It is hypothesized that *in vivo*, subpopulations of dormant bacilli that are phenotypically resistant to standard antibiotics are responsible for the lengthy time required for Mtb treatment and serve as a reservoir from which drug-resistant bacteria emerge^{8,9}.

Researchers believe that by targeting this subpopulation, they may be able to shorten treatment time. There has, therefore, been great interest in developing compounds that have efficacy against non-replicating Mtb. In an attempt to find such compounds, numerous screens have been conducted in conditions meant to simulate the *in vivo* environment, including screens against a nutrient-deprivation model⁷, a hypoxia model¹⁰, and a multi-stress model¹¹ as well as against Mtb inside macrophages^{12,13}.

Despite this recent activity, a decades-long gap in efforts to discover novel antitubercular compounds has resulted in a sparse drug development pipeline². Current antibiotics target a narrow range of biological processes and, with the exception of pyrazinamide, the current front line antitubercular drugs have little efficacy against non-replicating Mtb^{7,14-17}. Recent investment in antitubercular drug discovery has created several promising leads and new therapeutic targets, but there remains a lack of drugs with novel mechanisms of action in preclinical development to feed into the pipeline as current trials succeed or fail^{2,14}. Researchers have therefore been exploring new approaches to treat Mtb, focusing on targets that confer efficacy against M/XDR-TB and against non-replicating bacilli. Overall, there is general consensus that new antitubercular therapeutics should (1) be effective against M/XDR-TB, requiring drugs with new mechanisms of action, (2) be effective against non-replicating Mtb, with the goal of shortening treatment time, and (3) be compatible with current antitubercular therapeutics and with HIV therapeutics, as individual suffering from tuberculosis are often co-infected with HIV^{2,9,18}.

Section 1.2. Strategies for discovering Mtb therapeutics

Scientists employ several methods to identify new lead compounds for the treatment of Mtb (Fig. 1.1). Phenotypic whole-cell screening, in which one is searching for compounds that inhibit bacterial growth, has produced most current antibiotics¹⁹. These methods require the least prior knowledge about potential targets and identify only compounds that both permeate the cell and have an effect on Mtb survival. Target identification of screening hits remains one of the greatest challenges of whole-cell screening² and many new chemical scaffolds identified through this type of screening have redundant mechanisms¹⁹. Further, whole-cell screening has historically been carried out in conditions dissimilar from the *in vivo* environment, limiting the translation of activity in the screen to activity in *in vivo* models. Screens in conditions meant to mimic the *in vivo* state^{7,11} and screens against Mtb inside macrophages^{12,13,20} are beginning to address this issue.

To date, the other main branch of drug discovery has relied on target-based methods. In this case, a protein target is determined to be essential for the bacterium and then researchers either design inhibitors based on substrates or transition states (structure/mechanism-based discovery)²¹⁻²⁶ or screen for compounds that bind the protein²⁷ or inhibit the protein's function *in vitro*²⁸⁻³⁰. This approach enables the development of compounds with desired mechanisms, but requires detailed knowledge of the target and also requires validation of “on-target” activity within the cell. Compounds developed through target-based approaches often do not have activity against whole cells due to their inability to permeate the bacterial cell wall or due to incorrect assumptions about the essentiality of the target. Both GlaxoSmithKline and AstraZeneca recently

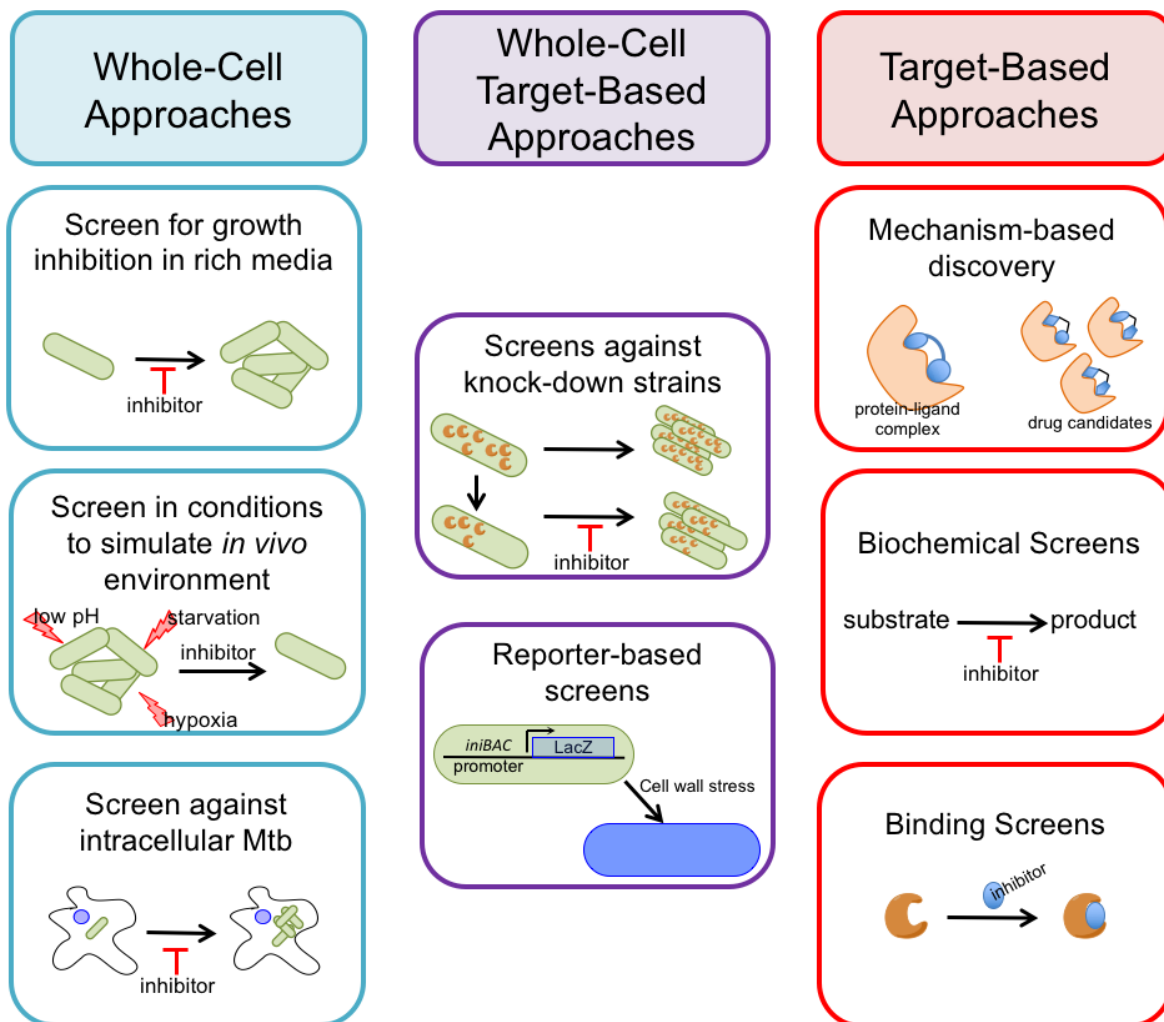


Figure 1.1. Drug discovery strategies in Mtb. Researchers employ numerous strategies for drug discovery. To date, target-based approaches have failed to produce cell-permeable clinical candidates while whole-cell screening suffers from challenges identifying novel targets. Recently, researchers have bridged the two methods creating target-specific whole-cell screening methods.

published highly significant reviews detailing the results of a combined 135 high-throughput screens against various bacterial targets^{14,31}. In both cases, despite enormous effort, target-based discovery failed to progress a single drug to the clinic.

Whole-cell target-based screening bridges these classic approaches. In this case, small molecules are screened against strains with essential proteins knocked-down¹⁶ or strains engineered to report the activity of a specific enzyme or pathway^{10,32,33}. These approaches can focus screens toward the discovery of compounds with new mechanisms of action, while ensuring hits are cell permeable. As this type of screening is just beginning to be adopted for the discovery of novel Mtb therapeutics, its success remains largely untested. The collective result of these screening and drug development campaigns are several new lead compounds, many of which are in preclinical development or clinical trials (Table 1.1). While there are too many potential targets to discuss within one review, the rest of this chapter highlights targets against which there has been the most progress (cell wall synthesis, protein synthesis, and energy metabolism) as well as emerging targets in exciting new areas such as central metabolism.

Section 1.3. New drug targets for Mtb

Macromolecular Synthesis

Cell Wall

Mtb has an unusual cell wall composed of a peptidoglycan layer covalently attached to arabinogalactan, which is attached to very long 60-90 carbon fatty acids

Table 1.1. Mtb inhibitors in development.

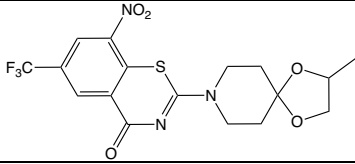
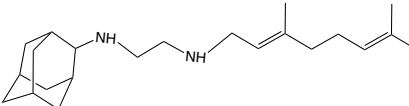
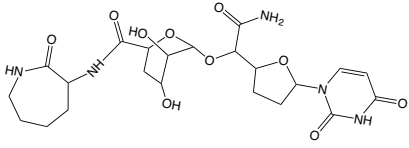
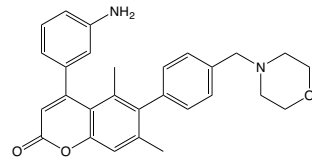
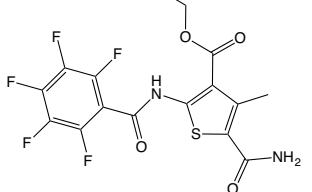
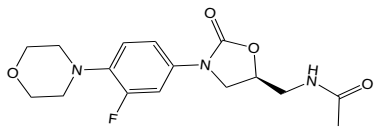
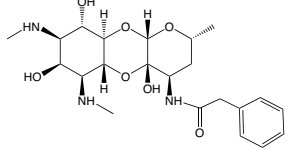
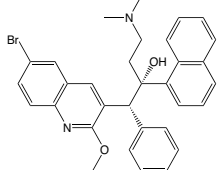
Target	Function	Inhibitors	Representative structure	Stage of development
<u>Cell Wall Synthesis</u>				
DprE1	epimerizes decaprenylphosphoryl ribose	BTZs ³⁴		Preclinical
MmpL3	trehalose monomycolate transport	SQ109 ³⁵		Phase II clinical trials
MurX (translocase I)	Transforms Park's nucleotide to lipid I	Capuramycin ³⁶		Preclinical
FadD32	activates meromycolic acid branch from FAS-II	Diarylcoumarin ³⁷		Research
Pks13	Joins meromycolic acid to alpha-alkyl fatty acid	Thiophenes ³²		Research
<u>Protein Synthesis</u>				
Ribosome		Oxazolidones ³⁸		Phase II and III Clinical Trials
		Spectinamides ³⁹		Preclinical
<u>Energy Metabolism</u>				
ATP Synthase	ATP Synthase	Bedaquiline ⁴⁰		Approved in United States

Table 1.1 continued

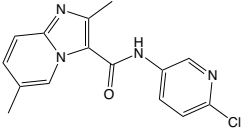
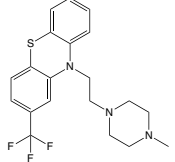
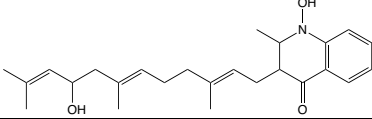
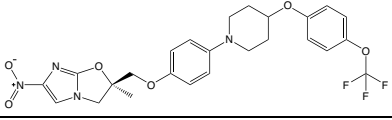
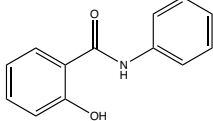
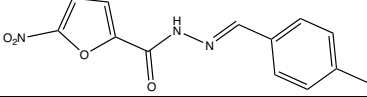
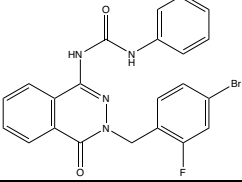
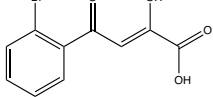
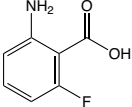
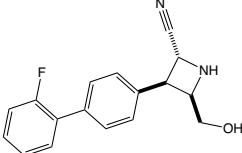
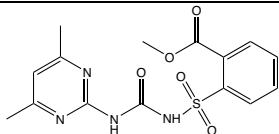
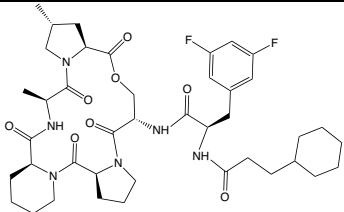
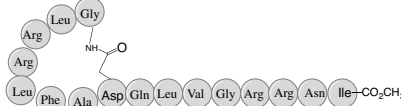
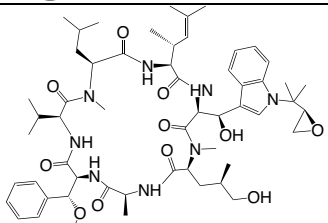
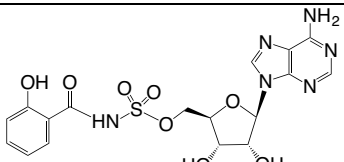
QcrB	member of electron transport chain	Imidazopyridine (Q203) ²⁰		Phase I Clinical Trials
NDH-2	member of electron transport chain	Phenothiazines ⁴¹		Research
MenA	menaquinone synthesis	Aurachin RE ¹⁷		Research
Mycolic acid synthesis/ Cytochrome c oxidase		Nitroimidazoles ⁴²		Delamanid approved in European Union
<u>Glyoxylate shunt</u>				
ICL	Carbohydrate Metabolism	Salicylanilides ⁴³		Research
		Hydrazones ⁴⁴		Research
		Phthalazines ⁴⁵		Research
GlcB	Carbohydrate Metabolism	Phenyl-diketo acids ²³		Research
<u>Amino Acid Biosynthesis</u>				
TrpE (or TrpD)	Tryptophan biosynthesis	Fluorinated anthranilates ²⁶		Research
TrpA	Tryptophan biosynthesis	Azetidine nitrile (Chapter 2)		Research

Table 1.1 continued

IlvB1	Branched-chain amino acid biosynthesis	Acylsulfonamides ⁴⁶		Research
<u>Clp Protease</u>				
ClpP	Protease	ADEPs ⁴⁷		Research
ClpC1	Protease	Lassomycin ⁴⁸		Research
		Cyclomarin A ⁴⁹		Research
<u>Mycobactin synthesis</u>				
MbtA	Mycobactin (siderophore) synthesis	Salicyl-AMS ²⁴		Research

called mycolic acids³⁵. Lipids, such as the well-described virulence factor phthiocerol dimycocerosate (PDIM) intercalate into the long hydrophobic chains of the mycolic acids creating something akin to a second lipid bilayer^{2,35}. This extremely hydrophobic cell wall creates a strong barrier to xenobiotics and is quite different from Gram-positive cell walls which contain a single lipid membrane and thick peptidoglycan layer and from Gram-negative cell walls with their highly impermeable double membrane⁵⁰. Two of the front-line antitubercular drugs, isoniazid and ethambutol, as well as several second-, third-, and fourth-line antibiotics act by inhibiting the synthesis of cell wall components². As one of the most well-validated antimicrobial targets, the cell wall remains an epicenter of drug development. The past several years of research has brought new cell wall-active compounds with unique targets in the biosynthesis pathway.

In 2009, a class of benzothiazinone (BTZ) compounds (Table 1.1) was found to act by covalently binding the active site of decaprenylphosphoryl- β -D-ribose 2' epimerase (**DprE1**)³⁴. DprE1, in concert with DprE2, epimerizes decaprenylphosphoryl ribose to decaprenylphosphoryl arabinose in an essential step of cell wall arabinogalactan and lipoarabinomannan biosynthesis (Fig. 1.2)⁵¹. Following the initial discovery of BTZs, several groups independently reported additional DprE1 inhibitors identified through unbiased, whole-cell phenotypic screens against Mtb^{12,19,52-54}. The very diverse chemical structures of these inhibitors prompted investigation into the basis for the redundant identification of this target and apparent promiscuity of DprE1. Unexpectedly, it was found that DprE1 localizes to the periplasmic space, making it more accessible to drugs and likely explaining its vulnerability⁵¹. BTZs have since been modified into a series of piperazine-containing benzothiazinone (PBTZs), which show greater potency, safety, and

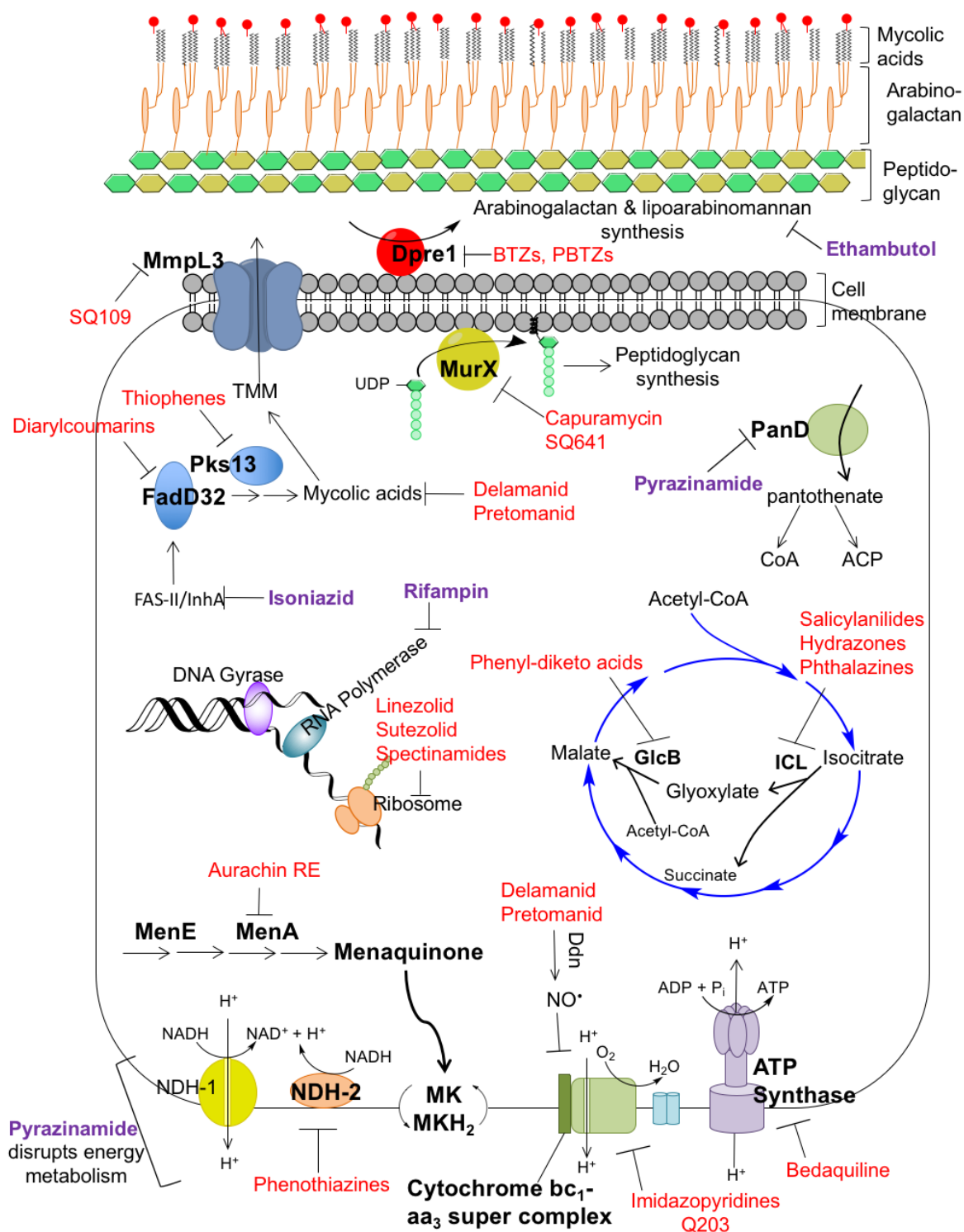


Figure 1.2. Overview of Mtb drug targets as well as examples of compounds that inhibit them. Frontline drugs (isoniazid, ethambutol, pyrazinamide, and rifampin) are shown in purple. Of note, pyrazinamide has a very complex mechanism involving disruption of energy metabolism⁵⁵ and potentially inhibition of pantothenate synthesis and trans-translation⁵⁶. Several pathways are under investigation as new therapeutic targets for the treatment of Mtb, including numerous emerging targets against which no compounds have reached pre-clinical or clinical development.

efficacy in animal models of mycobacterial infection^{57,58}. The DprE1 inhibitors PBTZ169 and BTZ043 have progressed to pre-clinical development.

Reminiscent of the discovery of DprE1 inhibitors, in 2012, three groups independently published unique small molecules that inhibit the previously untargeted **MmpL3**^{35,59,60}. These studies implicated MmpL3 in the transport trehalose monomycolate (TMM), a mycolic acid-containing cell envelope lipid, from the cytoplasm to the periplasm (Fig. 1.2) and demonstrated that inhibition of MmpL3 disrupts cell wall biosynthesis. Quickly thereafter, several groups reported additional chemical scaffolds that inhibit MmpL3^{19,61-64}. Again, the location of MmpL3 in the cell membrane is thought to be a key factor in the large number of unrelated compounds that inhibit its function. Multiple classes of MmpL3 inhibitors demonstrate antitubercular activity in mice, further supporting MmpL3 as a valuable drug target⁶¹⁻⁶³. SQ109, a 1,2-diamine structurally related to ethambutol, was already in clinical trials at the time it was found to inhibit MmpL3 and has now progressed through phase II trials⁵⁹. Recently, it has been suggested that SQ109 also targets other processes in the bacterium, including menaquinone biosynthesis and electron transport, which may account for its potency and relatively low frequency of resistance⁶⁵.

A third cell wall biosynthesis target is **MurX (translocase I)**, an essential enzyme required for peptidoglycan synthesis (Fig. 1.2). Interest in MurX arose from the discovery that capuramycin, a natural product isolated from *Streptomyces griseus*, acts by inhibiting the enzyme³⁶. MurX inhibitors kill Mtb *in vitro* much more quickly than most FDA-approved antitubercular therapeutics⁶⁶. Because capuramycin and its analogs suffer from poor solubility, cell permeability, and oral absorption, researchers have focused on target-

based screening to identify inhibitors of the enzyme⁶⁷ and on medicinal chemistry to improve the physiochemical properties of the compound. Promisingly, IV administration of a phospholipid-based nanoemulsion formulation of a semi-synthetic analog of capuramycin, SQ641, has proven effective in a murine tuberculosis model and Sequella Inc. is currently pursuing SQ641 as a therapeutic for the treatment of mycobacterial and Gram-positive infections⁶⁸.

Several other enzymes involved in cell wall biosynthesis are being investigated as emerging drug targets, including **FadD32** and **Pks13**. FadD32 activates the meromycolic acid branch from FAS-II after which Pks13 joins it to the alpha-alkyl fatty acid branch from FAS-I in essential steps of mycolic acid biosynthesis (Fig. 1.2)³². A group of diarylcoumarins were shown to inhibit FadD32 *in vitro*, inhibiting mycolic acid synthesis in whole cells and resulting in bactericidal activity against Mtb³⁷. Similarly, genetic evidence implicated Pks13 as the target of a class of thiophene compounds found to inhibit mycolic acid biosynthesis and researchers went on to demonstrate the thiophenes inhibit an essential FadD32-dependent function of Pks13 *in vitro*³². A separate study found that mutations in *pks13* confer resistance to an unrelated benzofuran⁶⁴.

Cell wall synthesis inhibitors with different targets can have additive or even synergetic effects^{37,66}, and so, the development of multiple drugs that act by inhibiting the cell wall will continue to have utility. Though effective at combating drug-sensitive and drug-resistant Mtb, these types of inhibitors are, however, highly effective only against replicating, aerobically growing bacteria⁶⁹. Thus, it is critical to look at targets other than cell wall synthesis in order to find new drugs with the ability to kill non-replicating Mtb.

Protein Synthesis

Protein synthesis inhibitors are a mainstay in the treatment of other bacterial infections and there has been great interest in developing similar inhibitors effective against Mtb. More than 70 years ago, streptomycin, an inhibitor of the bacterial ribosome, was the first antibiotic discovered to be effective against Mtb⁷⁰. In *in vitro* systems, protein synthesis inhibitors, such as chloramphenicol and tetracycline, inhibit the Mtb ribosome, but these antibiotics fail to inhibit growth of the whole organism⁷¹. This intrinsic resistance is attributed to the impermeability of the mycobacterial cell wall to these drugs.

Nearly 20 years ago oxazolidinones were discovered to inhibit a very early stage of protein synthesis in Gram-positive bacteria and to have activity against whole Mtb cells^{38,72}. Linezolid, eperezolid, and sutezolid (formerly PNU-100480) were evaluated in murine models of Mtb infection, with sutezolid demonstrating greater activity than linezolid⁷². At the time, linezolid was already in clinical trials for other indications and was soon to be approved for the treatment of skin infections and hospital-acquired pneumonia. A full decade later, sutezolid was again evaluated in murine models. The studies confirmed previous results, demonstrating that sutezolid is 1-2 orders of magnitude more effective against Mtb in mouse models compared to linezolid⁷³. Sutezolid also has clear bactericidal activity in mice, while linezolid's activity is much weaker and less clearly bactericidal⁷³.

Linezolid has been used off label to treat multi-drug resistant Mtb for several years, which has allowed a number of retrospective studies to be conducted; these studies suggest that linezolid has efficacy against MDR-TB⁷³⁻⁷⁶. In recent years, prospective clinical trials have been conducted to gain more robust data on linezolid's efficacy. In

M/XDR-TB patients with limited other options, linezolid has proven successful in achieving culture conversion with no relapse⁷⁷. The major challenge of linezolid treatment is the high risk of severe adverse side effects, including myelosuppression and neuropathy, which are experienced by as many as 82% of patients receiving linezolid⁷⁷. These side effects are usually reversible, subsiding when the dose of linezolid is decreased or when linezolid is temporarily halted. However, at lower doses, is an increased risk of drug resistance emerging⁷⁸. Researchers are experimenting with intermittent dosing at higher concentrations of linezolid to reduce the risk of side effects and resistance⁷⁸. Meanwhile, sutezolid has advanced through phase II clinical trials⁷⁹.

Recently, semi-synthetic spectinomides have been developed as additional protein synthesis inhibitors³⁹. Spectinomycin is a natural product with narrow-spectrum antitubercular activity resulting from its inhibition of ribosome translocation, a different molecular mechanism than that of the oxazolidinones. The efflux pump Rv1258c limits the potency of natural spectinomycin, but using structure-based design, Lee *et al.* developed spectinomycin analogs that are unaffected by this pump. These analogs were shown to have a high safety margin in mice and have moved to pre-clinical development³⁹. Such efforts have the potential to deliver highly effective treatments against MDR-TB with fewer negative side effects than existing alternatives.

Energy Metabolism

Disruption of energy metabolism has been an area of great progress in antitubercular drug development. ATP homeostasis and the maintenance of an energized membrane are particularly vulnerable targets in hypoxic non-replicating bacteria⁶⁹. There

is precedence for this mechanism of action in pyrazinamide, a front-line Mtb therapeutic that disrupts the membrane potential of bacilli and is more effective against non-replicating bacteria than against replicating cultures⁵⁵. Two recently approved drugs and many compounds in clinical trials act by disrupting energy production or homeostasis.

In 2005, a diarylquinoline, bedaquiline (also known as TMC207 or R207910) was found to have bactericidal activity against MDR-TB strains and in a murine model of infection as well as activity against non-replicating Mtb⁴⁰. Point mutations in *atpE*, part of the F₀ subunit of **ATP synthase**, confer resistance to bedaquiline, suggesting the drug targets the proton pump of the enzyme (Fig. 1.2)⁴⁰. In 2012, the first in its class, bedaquiline was also the first new TB therapeutic to be approved by the US Food and Drug Administration in 40 years. Though bedaquiline has been associated with severe safety risks, it remains useful for the treatment of MDR-TB and is part of ongoing trials evaluating new regimens for their ability to shorten MDR-TB treatment⁸⁰.

QcrB, a subunit of the cytochrome bc₁-aa₃ complex, has also been explored as a therapeutic target. Cytochrome b is responsible for transferring electrons to cytochrome c and is an essential member of the electron transport chain required to generate the proton gradient used by ATP synthase (Fig. 1.2)^{20,81}. An imidazopyridine amide (IPA) Q203 was found to target the cytochrome bc₁ complex, triggering a rapid reduction in intracellular ATP in both replicating and hypoxic non-replicating Mtb²⁰. Similar compounds were identified through whole-cell screening, with genetic evidence again suggesting the compounds inhibits QcrB⁸². Q203 is effective against M/XDR-TB as well as in murine models of infection²⁰ and is currently in phase I clinical trials⁸³.

Another enzyme under consideration as a therapeutic target is **NDH-2**, a membrane-bound type II NADH dehydrogenase encoded by either *ndh* or *ndhA* that transfers electrons from NADH to menaquinone (Fig. 1.2)⁸¹. Phenothiazine analogs were found to specifically target NDH-2, inhibiting both Ndh and NdhA⁴¹. These phenothiazines inhibit electron transport in Mtb, suppressing growth in a mouse model of acute infection⁴¹. The compounds are also highly effective against non-replicating Mtb under a variety of stress conditions including low pH, starvation, and nitric oxide exposure⁸⁴. Separately, NdhA was implicated in the mechanism of a 2-mercapto-quinazolinone when it was found that mutations upstream *ndhA* resulting in increased *ndhA* expression confer resistance to the compound⁶⁴.

Finally, menaquinone (MK) biosynthesis is also being explored as a target in energy generation. MK is a lipid soluble electron carrier essential for the transfer of electrons between components of the electron transport chain (Fig. 1.2)⁸¹. **MenA** and **MenE**, two of the enzymes required for the synthesis of menaquinone in Mtb, are essential for growth in mice¹⁷. Aurachin RE, a natural product isolated from *Rhodococcus erythropolis*, was discovered to inhibit MenA, resulting in potent killing of non-replicating Mtb in a low oxygen assay¹⁷. Aurachin RE itself has significant problems as a therapeutic due to interactions with anti-HIV drugs and so current efforts are focused on developing inhibitors based on the Aurachin RE structure that have fewer interactions and liabilities¹⁷. There have also been efforts to develop mechanism-based inhibitors of MenE²¹.

Energy generation inhibitors, like bedaquiline, tend to kill Mtb slowly *in vitro* and in early bactericidal activity (EBA) studies^{85,86}. This does not, however, preclude them from having the potential to shorten treatment time. Pyrazinamide also has limited efficacy in

EBA studies, but its introduction shortened standard therapy by 3 months⁵⁵. Compounds that are specifically active against non-replicating Mtb may not rapidly kill replicating bacteria but could contribute to faster cures by eradicating the subpopulation of non-replicating bacteria thought to exist *in vivo*. This hypothesis remains to be rigorously tested and the development of compounds with activity against only non-replicating Mtb will provide insight into the utility of targeting this state.

Inhibitors with Complex Mechanisms

Several nitroimidazole compounds are in clinical development including delamanid (OPC-67683) and pretomanid (PA-824), which are in clinical trials for the US, and TBA-354 and DC-159 in preclinical development. Delamanid was approved in the European Union for the treatment of MDR-TB in 2014⁸⁷. Delamanid was discovered in program to search for antitubercular agents that inhibit mycolic acid synthesis⁸⁸. Though no specific enzyme in cell wall synthesis has been identified as the target of these compounds, detection of ¹⁴C-labeled fatty acids and mycolic acids shows that delamanid inhibits the synthesis of methoxy- and keto-mycolic acids, but not alpha-mycolic acids (Fig. 1.2)^{88,42}; this is in contrast to isoniazid, which inhibits the synthesis of all mycolic acid classes. Also unlike isoniazid, the nitroimidazoles are active against non-replicating Mtb⁴².

Interestingly, both delamanid and pretomanid rely on functional copies of Fgd1, an F420-dependent glucose-6-phosphate dehydrogenase, and Ddn, a deasaflavin-dependent nitroreductase, for activity^{42,88,89}. Ddn converts pretomanid into three metabolites in a process that generates reactive oxygen species, including nitric oxide (NO)⁸⁹. It is hypothesized that the NO reacts with cytochrome c oxidase, interfering with

respiration and depriving the bacilli of essential energy sources (Fig. 1.2)^{69,89}. The structure activity relationships governing activity of pretomanid against hypoxic, non-replicating Mtb do not correlate with activity against aerobic, logarithmically growing Mtb, suggesting a different mechanism of action against each state⁶⁹. It is unlikely that the effects on mycolic acid synthesis are responsible for the activity against non-replicating Mtb as no other mycolic acid synthesis inhibitors have activity against non-replicating Mtb⁸⁹. It is instead believed the activity against non-replicating bacilli is derived from the compounds' disruption of energy generation. Along with pyrazinamide and SQ109, which are reported to affect multiple targets^{56,65}, the nitroimidazole compounds demonstrate that multi-target activity may be highly desirable for conferring increased potency and activity against multiple physiological states of Mtb.

Emerging Targets

Numerous additional targets are being explored using *in vitro* assays against purified proteins and against whole Mtb cells. Though compounds with these novel mechanisms are further from the clinic and often untested *in vivo*, these new targets are promising leads for the treatment of drug-resistant and non-replicating Mtb and they highlight the strategies researchers are using to identify compounds with completely new mechanisms of action (See Fig. 1.1 for overview of strategies).

Glyoxylate Shunt

Increasingly, researchers are looking to new essential processes for drug targets. Validation and inhibition of targets in central metabolism poses a unique challenge as

metabolic pathways tend to be very robust, allowing for stable function over many environmental conditions and metabolic enzymes may be essential in one condition, but not in another^{15,90,91}. For example, FASII inhibitors are potent against Gram-positive organisms *in vitro*, but ineffective *in vivo* due to the abundance of fatty acids available in human serum⁹⁰. Further complicating drug discovery against central metabolic targets, the active sites of these enzymes are usually evolved to accommodate hydrophilic substrates and are typically shallow – an unfavorable starting point for drug design, which often relies on hydrophobic interactions for potency^{15,92}. Nevertheless, several processes in central metabolism, including the glyoxylate shunt and amino acid biosynthesis have been areas of recent interest for killing Mtb.

In the absence of carbohydrates, most microorganisms use the glyoxylate shunt for growth on fatty acids or acetate with the end result of glucose production from fatty acids^{93,94}. Although standard Mtb media uses glycerol and glucose carbon sources, fatty acids are the primary carbon source of Mtb *in vivo*^{94,95}. In the glyoxylate pathway, ICL converts isocitrate to succinate and glyoxylate and malate synthase (**GlcB**) catalyzes the production of malate from glyoxylate and acetyl-CoA (Fig. 1.2). The first enzyme in the glyoxylate shunt, isocitrate lyase (**ICL**) is essential for the survival of Mtb in mouse lungs and in non-replicating states. Mtb has two functional isocitrate lyases, Icl1 and Icl2⁹⁴. Both *icl1* and *icl2* are upregulated in bacilli isolated from mouse lungs⁹³. Deletion of *icl1* or *icl2* individually has little effect on Mtb fitness, but deletion of both genes results severe attenuation in mice⁹⁴. Thus, compounds likely must inhibit both enzymes to be effective. The ICL inhibitor 3-nitropropionate (3-NP) has little effect on Mtb grown on glycerol or glucose, but completely eliminates Mtb growth on fatty acids and in murine

macrophages⁹⁴. 3-NP is neurotoxic in mice, but several groups have attempted to develop other inhibitors of Mtb isocitrate lyase. These include salicylanilide derivatives^{22,43}, hydrazones⁴⁴, and phthalazines⁴⁵ each of which show only partial inhibition of ICL and high IC₅₀s *in vitro*, with whole-cell activities against replicating and non-replicating Mtb in the micromolar range.

GlcB has also been explored as a drug target. Researchers have attempted to use structure-guided discovery to design active-site inhibitors of the enzyme with a degree of success. For example, phenyl-diketo acid derivatives designed to inhibit GlcB *in vitro* have activity against whole Mtb cells under replicating and low-oxygen conditions, and reduce Mtb CFU in an acute mouse model of infection²³. Though an abundance of evidence supports the hypothesis that *Mtb* uses fatty acids as a primary nutrient source during infection, high throughput screening often uses media containing glycerol as the primary carbon source^{94,95}. Because the glyoxylate shunt is not required for growth on glucose or glycerol, screens in standard mycobacterial growth media will not identify ICL or GlcB inhibitors⁹⁵. Efforts to develop inhibitors against ICL and GlcB highlight the necessity of validating targets *in vivo* as well as the importance of conducting screens in conditions that are similar to the *in vivo* environment.

Amino Acid Biosynthesis

Another emerging target in central metabolism is amino acid biosynthesis. Mounting evidence suggests that Mtb's endogenous biosynthetic machinery for several amino acids is required for survival during an infection^{26,96}, but it also appears that Mtb responds differently to various amino acid starvations^{97,98}. While deletion or inhibition of

some amino-acid-synthesizing genes results in Mtb cell death *in vitro* (e.g. tryptophan, histidine, and methionine), other amino acid starvations (e.g. proline and leucine) are better tolerated, producing a static response^{97,98}. This is more complicated *in vivo*, where Mtb can scavenge nutrients from host cells²⁶, resulting in gene essentialities that are heavily dependent upon the environment. Among the twenty amino acids, tryptophan, and branched-chain amino acid synthesis, in particular, have been the focuses of recent drug discovery efforts^{26,99}.

First, tryptophan biosynthesis has long been recognized as essential for Mtb *in vitro* and *in vivo*⁹⁷. Recent reports have shown that the dependence *in vivo* is at least partially due to the effect of CD-4 T-Cell-produced interferon- γ (IFN γ)²⁶. Host macrophages contain some level of tryptophan, which can be scavenged by resident Mtb. However, upon IFN γ stimulation, a host enzyme degrades tryptophan pools increasing Mtb's reliance on its endogenous tryptophan biosynthesis²⁶. Building on the knowledge that tryptophan biosynthesis is essential for Mtb during *in vivo* infections, Zhang *et al.* tested halogenated anthranilates, which are structural mimetics of tryptophan intermediates, and found them to be effective against Mtb *in vitro* and in a murine model of infection²⁶. Other groups have used computational modeling to predict potential inhibitors of the active site of tryptophan synthase, the final enzyme in tryptophan biosynthesis¹⁰⁰. Interestingly, deletion of *trpD*, further upstream in tryptophan biosynthesis results in slower cell death than deletion of *trpA*. While the basis for these differences is unknown, it underscores the necessity of studying each potential target within a given metabolic process.

Branched-chain amino acid (leucine, isoleucine, and valine) synthesis has also been an area of recent activity. *ilvB1* codes for acetohydroxyacid synthase, which is the first dedicated enzyme in the branched-chain amino acid biosynthetic pathway, and is essential in the absence of supplemented amino acids. When the gene is deleted, Mtb is severely attenuated, losing viability *in vitro* and failing to grow in mice⁹⁶. Herbicides and antimicrobial agents have been developed based on the chemical sulphometuron methyl, which has been demonstrated to inhibit branched-chain amino acid synthesis^{46,99}. Importantly, these inhibitors are potent against Mtb *in vitro* and in restricting the growth of Mtb in the lungs of infected mice⁹⁹. Despite this progress, much work remains to define nutrient availability during Mtb infection of humans and the essentiality of each amino acid synthesis pathway.

ClpP Protease

ClpP, in conjunction with the ClpX/ClpC ATPase subunits, forms a proteasome that degrades misfolded or damaged proteins and is essential for Mtb viability *in vitro*¹⁰¹. In Mtb, the proteolytic core is formed from two rings of ClpP1 or ClpP2, which interact with a ring of ClpC or ClpX¹⁰². A series of acyldepsipeptides (ADEPs) was found to inhibit the growth of Gram-positive firmicutes by activating the ClpP protease, resulting in the unregulated degradation of essential proteins⁴⁷. In Mtb, however, ADEPs significantly reduce proteolytic activity by disrupting the interaction between the proteolytic core and the regulatory ATPase¹⁰². Unlike in other bacteria, the ClpP protease is indispensable for Mtb growth and the primary mechanism of ADEPs against mycobacteria is believed to be inhibition of proteolytic activity rather than unregulated degradation¹⁰¹.

Multiple classes of cyclic peptides, including cyclomarin A⁹⁰ and lassomycin⁹¹, have been found to act against the **ClpC1 ATPase** of the protease^{48,49}. Such peptides bind ClpC1 in a manner that is not competitive with ATP and have bactericidal activity against both replicating and non-replicating Mtb. Interestingly, despite acting on the same target protein, the cyclic peptides have quite different mechanisms. Cyclomarin A was found to increase proteolytic activity of the protease against a model substrate in whole mycobacterial cells⁴⁹. Lassomycin, on the other hand, increases ATPase activity while inhibiting proteolytic activity, thus preventing the essential degradation of specific proteins within the cell⁴⁸. More recently, researchers have completed a whole-cell targeted screen using a GFP-based reporter of ClpP activity³³. The pilot screen identified bortezomib, an inhibitor of the human 26S proteasome, as an inhibitor of Mtb ClpP1P2 activity and validated this mechanism-based approach of whole-cell screening for proteasome inhibitors³³.

Pantothenate Synthetase

Several groups have been working to develop inhibitors of pantothenate synthetase (**PanC**), an essential enzyme involved in the synthesis of pantothenate, which is a precursor for both coenzyme A (CoA) and acyl carrier protein (ACP). While humans lack *panC* homologs, *panC* has been shown to be essential for Mtb survival in mice^{16,28}. Additionally, pantothenate synthesis was recently implicated as part of the mechanism of pyrazinamide against Mtb, via the observation of *panD* mutations amongst pyrazinamide-resistant strains⁵⁶. Techniques to identify PanC inhibitors have primarily focused on finding compounds that inhibit or bind the protein *in vitro* using fragment-based screening,

rational design based on reaction intermediates, and unbiased screening of small compound libraries^{27-29,103}. Such efforts have resulted in inhibitors of PanC with varying degrees of activity, some with IC₅₀s in the nanomolar range. A few of these compounds have activity against whole Mtb cells, though their MICs remain in the high micromolar range. Recently, a whole-cell target-based screen against PanC was carried out by Abrahams *et al.*¹⁶. This screen identified compounds with activity against whole Mtb cells and increased activity against cells depleted for PanC. None of these compounds, however, have activity against the purified PanC enzyme.

Part of the challenge in targeting PanC could be that Mtb is not particularly sensitive to pantothenate depletion¹⁰⁴, with *panC* deletions resulting in a static, rather than bactericidal, response⁹⁸. Interestingly, disruption of genes further downstream in the CoA pathway is bactericidal, perhaps making them better targets in the pathway¹⁰⁴. As in tryptophan biosynthesis, the basis for these differences is not understood, but they highlight that not all targets within a single pathway are equal in terms of effect on the bacterial cell and support the need for rigorous target validation *in vivo*.

Iron Uptake

Human serum and tissue is an iron-poor environment, and so, pathogens must synthesize iron-chelating siderophores for survival and virulence^{105,106}. Mtb produces two siderophores: mycobactin, which is cell wall-associated and carboxymycobactin, which is secreted¹⁰⁷. The enzymes involved in mycobactin synthesis are essential *in vitro* in media with low concentrations of iron and in animal models of infection¹⁰⁷. Several groups have attempted the rational design of inhibitors of enzymes involved in mycobactin synthesis²⁴.

The first compound developed, 5'-O-[N-salicyl-sulfamoyl adenosine] (salicyl-AMS), potently inhibits **MbtA** *in vitro* and inhibits the growth of Mtb in iron-deplete media²⁴. Salicyl-AMS was recently shown to have modest activity in a murine model of Mtb infection, providing *in vivo* proof of concept for this new antitubercular target¹⁰⁶. However, at higher doses, severe toxicity to the mice was observed¹⁰⁶. This toxicity was potentially due to off-target effects or drug metabolites as mammals do not have homologues of mycobactin biosynthesis enzymes. Several groups are attempting to improve the specificity and the pharmacokinetic properties of this original compound¹⁰⁸⁻¹¹¹.

Researchers have also been exploring salicylate synthase (**MbtI**) as target within the mycobactin biosynthesis pathway. Inhibitors have been created using rational-design based on substrate or proposed transition state structures, while others were discovered through *in vitro* high throughput screening^{25,30,112,113}. To date, inhibitors active against the enzyme *in vitro* have not translated to inhibitors with potent whole-cell activity.

Section 1.4. Challenges and Prospects for Moving Forward

Despite significant improvement compared with 10-15 years ago, the number of novel series in clinical development for the treatment of tuberculosis remains low¹⁸. Compounds with novel mechanisms of action are unrepresented and target-based screening has failed to yield a single antimicrobial drug^{9,14,18}. Though whole-cell screening has resulted in viable hits, the same mechanistic targets have been uncovered in multiple screens, highlighted by the numerous DprE1 and MmpL3 inhibitors identified simultaneously by multiple research groups^{37,52-54,57,59-62}. These may be the most accessible and vulnerable targets in Mtb, but these redundant hits are also a product of

the screening methods employed. Rather than whole-cell screens conducted in rich media or target-based screens, the field has begun to use what we know about Mtb *in vivo* to combine the two^{7,11,18,33,114}. There is a growing shift toward *in vitro* growth conditions that better mimic the *in vivo* environment and toward pathway directed whole-cell screening, either by screening based on a pathway-relevant metric other than cell death (e.g. upregulation of *iniBAC* operon to identify cell wall inhibitors¹⁶) or by screening against strains depleted of essential protein targets^{16,32,33}.

Limiting the utility of these whole-cell target-based approaches is our lack of understanding about which genes and functions are truly essential *in vivo*. We are just beginning to explore targets such as the glyoxylate shunt and iron acquisition, which are required for survival *in vivo* but not *in vitro* in rich media. As our understanding of Mtb pathogenesis grows, it should be possible to use newly validated drug targets to develop more relevant screens that fuel the next generation of Mtb therapeutic leads. To find compounds potent against the non-replicating state, we will likely need to turn to these previously unexplored targets. To date, the cell wall has been a very attractive target due to its vulnerability and accessibility, but no cell wall synthesis inhibitors show activity against non-replicating bacteria⁶⁹. While novel cell wall synthesis inhibitors will continue to be critical in treating drug-resistant Mtb, to meet the goal of targeting non-replicating bacteria and shortening treatment time, we will need move beyond enzymes in cell wall biosynthesis.

Screening in conditions similar to the *in vivo* environment, rather than target-based whole-cell screening, eliminates the need to identify appropriate targets beforehand and can lead to important discoveries in biology through investigation of targets that emerge.

Additionally, many of the most successful antibiotics have multiple targets and this is exactly what makes them so effective while also limiting resistance^{14,65}. Target-based screening may restrict the opportunity for such discovery. However, whole-cell screening comes with its own challenges. Despite many advances, the field continues working to develop *in vitro* models that accurately recapitulate the *in vivo* environment and targets still must be shown to be required for survival *in vivo* once identified as *in vitro* essential through a whole-cell screen. Additionally, target identification after whole-cell screening is very difficult, creating a bottleneck that slows drug development and results in attrition, with compounds dropping out of pipelines due to an inability to determine their mechanisms¹⁴.

Of course, the future of Mtb drug discovery lies in some intermediate. We will continue to learn more about Mtb, building better *in vitro* models and better target-based whole-cell screening, both of which will be important for the discovery of novel inhibitors. To reach the 2035 WHO END TB goal of reducing tuberculosis deaths by 95%, the field must move into new target space, rather than continuing to rely on the 4 traditional pillars of antibacterial therapy: cell wall synthesis, protein synthesis, DNA replication and transcription. This will require creative strategies and new approaches to screening and drug discovery.

This dissertation details efforts to identify novel inhibitors of both replicating and non-replicating Mtb. By screening new chemical matter, we discovered a highly potent allosteric inhibitor of tryptophan synthase, a new molecular target in Mtb (Chapter 2). Further, we show that tryptophan synthase is essential *in vivo* and study the basis for the bactericidal response to tryptophan starvation (Chapter 3). Additionally, we identify new

compounds that kill non-replicating Mtb and by studying their mechanisms identify metal ion homeostasis as a vulnerable target in Mtb and also identify MymA as a new activating enzyme in Mtb (Chapter 4). This research provides probes for the future study of Mtb and highlights the power of screening and of chemical genetics to uncover promising targets and new biological insights.

Chapter 2: Identification of a specific allosteric small-molecule inhibitor of *Mycobacterium tuberculosis* tryptophan synthase

Attributions

The work in this chapter was submitted as a manuscript by S. Wellington *et al.* to *Nature Chemical Biology* and reformatted for this dissertation. Sections on the *in vivo* essentiality of tryptophan synthase were removed from the manuscript and included in this dissertation as part of chapter 3. Additionally, supplemental materials from the manuscript were integrated into this chapter. This chapter contains highly collaborative research with contributions listed at the end.

Chapter 2: Identification of a specific allosteric small-molecule inhibitor of *Mycobacterium tuberculosis* tryptophan synthase

Samantha Wellington^{1,2,3}, Partha P. Nag^{1,9}, Karolina Michalska^{4,5,9}, Stephen E. Johnston¹, Robert P. Jedrzejczak^{4,5}, Virendar K. Kaushik¹, Anne E. Clatworthy³, Noman Siddiqi⁶, Patrick McCarren¹, Besnik Bajrami¹, Natalia I. Maltseva⁴, Stewart L. Fisher¹, Andrzej Joachimiak^{4,7}, Stuart L. Schreiber^{1,8}, Deborah T. Hung^{1,2,3}

¹ The Broad Institute, Cambridge, MA 02142 USA

² Department of Genetics, Harvard Medical School, Boston, MA 02115 USA

³ Department of Molecular Biology and Center for Computational and Integrative Biology, Massachusetts General Hospital, Boston, MA 02114 USA

⁴ Center for Structural Genomics of Infectious Diseases, University of Chicago, Chicago, IL 60637 USA

⁵ Structural Biology Center, Argonne National Laboratory, Argonne, IL 60439, USA

⁶ Harvard T.H. Chan School of Public Health, Boston, MA 02115 USA

⁷ Department of Biochemistry and Molecular Biology, University of Chicago, Chicago, IL 60637 USA

⁸ Department of Chemistry and Chemical Biology, Harvard University, Cambridge MA 02138 USA

⁹ These authors contributed equally to this work.

Abstract

The discovery of antibiotics with novel targets is greatly needed, but has been slow and challenging. While there are numerous functions required for cell survival and growth, only a small fraction of these processes – primarily those involved in macromolecular synthesis – are inhibited by current antibiotics. Targeting metabolic enzymes has been the focus of recent interest, but effective inhibitors have been difficult to identify. Here, we describe a novel azetidine, BRD4592, which kills *Mycobacterium tuberculosis* (Mtb) through allosteric inhibition of tryptophan synthase (TrpAB), a previously untargeted metabolic enzyme that is highly allosterically regulated. BRD4592 binds the protein–protein interface of TrpAB and acts via a complex mechanism affecting multiple steps in the overall TrpAB reaction, giving rise to inhibition that is not easily overcome by changes in metabolic environment and is, in fact, enhanced by increases in substrate or product concentration. This work thus supports the effectiveness of allosteric inhibition for targeting proteins that are naturally highly dynamic and suggests a framework for the discovery of a next generation of allosteric inhibitors.

Section 2.1. Background

Resulting in 9.6 million infections and 1.5 million deaths in 2014, *Mycobacterium tuberculosis* (Mtb) has now surpassed HIV as the leading cause of death worldwide due to an infectious disease¹. The rise of multidrug resistance necessitates a deeper understanding of this complex bacterium in order to facilitate the development of more efficient treatments, including therapeutics with novel mechanisms of action^{2,9,18}. Recent efforts to discover new antitubercular agents have brought novel insights into Mtb biology along with promising new therapies such as bedaquiline, which inhibits ATP synthase⁴⁰, and delamanid, a nitroimidazole that inhibits mycolic acid synthesis and disrupts energy production^{88,69}. Despite some promising advances, however, many of the recently identified antitubercular compounds found in whole-cell screening disproportionately hit cell wall targets including MmpL3, DprE1, FadD32, and Pks13^{12,35,37}, perhaps because of the vulnerability imparted by their relatively high accessibility to xenobiotics. Thus, the excitement from uncovering different chemical scaffolds in these efforts has been dampened by the redundancy of the identified targets (*i.e.*, MmpL3 and DprE1)^{19,52-54,57,59-62,115} and the failure to capitalize on the plethora of other targets that should seemingly be available. This slow progress in identifying and developing new antitubercular candidates is likely a product of both the types of chemical libraries screened and the methods used for their screening.

In order to uncover new chemical matter with activity against Mtb, we took advantage of a diversity-oriented synthetic (DOS) library that contains rich stereochemical and skeletal diversity of compounds to perform whole-cell screening against wild-type (WT) Mtb. We identified a novel chiral azetidine derivative, BRD4592, which has

bactericidal activity exclusively in one of eight stereoisomeric forms. We go on to show that BRD4592 allosterically inhibits Mtb tryptophan synthase (TrpAB) – an enzyme catalyzing the last two steps of L-tryptophan (L-Trp) biosynthesis¹¹⁶ (Fig. 2.1a).

TrpAB is encoded by *trpA* and *trpB*, which correspond to the α and β subunits of the functional $\alpha\beta\alpha$ heterotetramer¹¹⁶. The α subunits convert indole-3-glycerol phosphate (IGP) to glyceraldehyde 3-phosphate (G3P) and indole, while the β subunits, using pyridoxal 5'-phosphate (PLP) as a cofactor, catalyze the β -replacement reaction in which indole displaces the hydroxyl group of L-Serine (L-Ser) to produce L-Trp¹¹⁶ (Fig. 2.1a, 2.2). Decades-long studies of *Salmonella typhimurium* TrpAB have shown that indole is transferred from the α subunit to the β subunit along a 25 Å hydrophobic channel¹¹⁶⁻¹¹⁸ to react with an L-Ser-PLP adduct¹¹⁹. Because L-Trp is the most energetically costly amino acid¹²⁰, requiring the equivalent of over 70 ATP molecules¹²¹, its biosynthesis is typically exquisitely regulated both at the transcriptional level of the operon as well as the allosteric level of the enzyme complex¹²⁰. Notably, the enzymatic activities and substrate channeling between the two active sites of TrpAB are coordinated by complex allosteric regulation between the subunits to optimize indole utilization^{116,122,123}, perhaps making the enzyme primed for allosteric inhibition by small molecules.

Here we present the first comprehensive report describing Mtb TrpAB and its inhibition by BRD4592. Through detailed kinetic, thermodynamic, and structural characterization, we demonstrate that BRD4592 is an allosteric, mixed-type inhibitor binding to a novel site with a highly unique mechanism of inhibition. Specifically, BRD4592 potently inhibits both reactions of the TrpAB enzyme allosterically through its

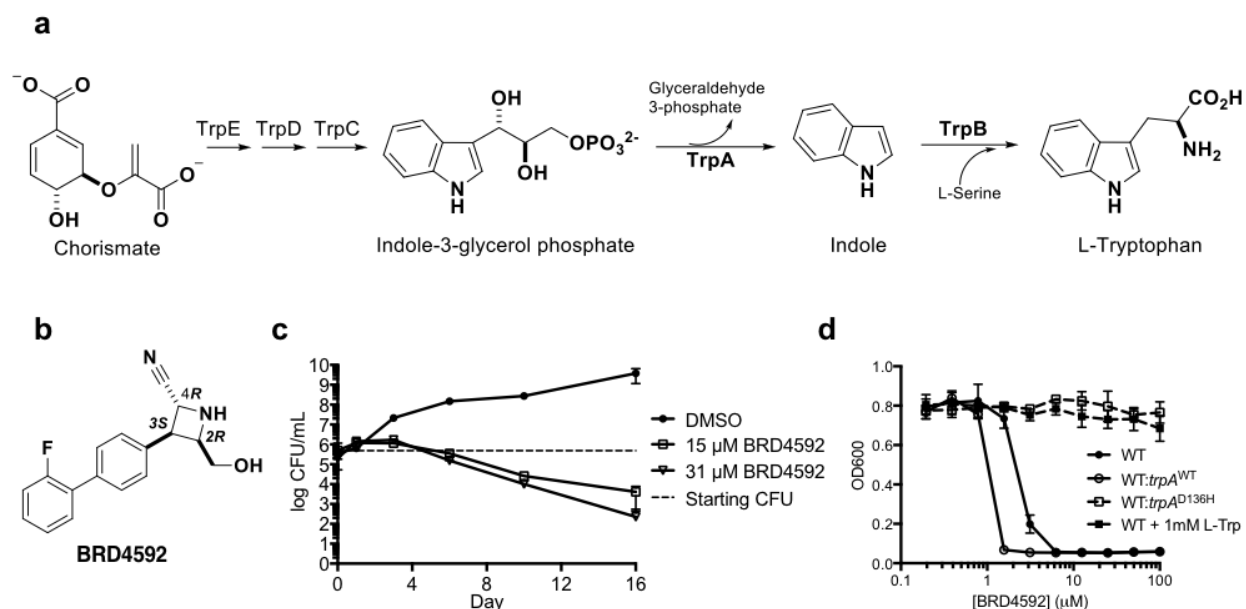
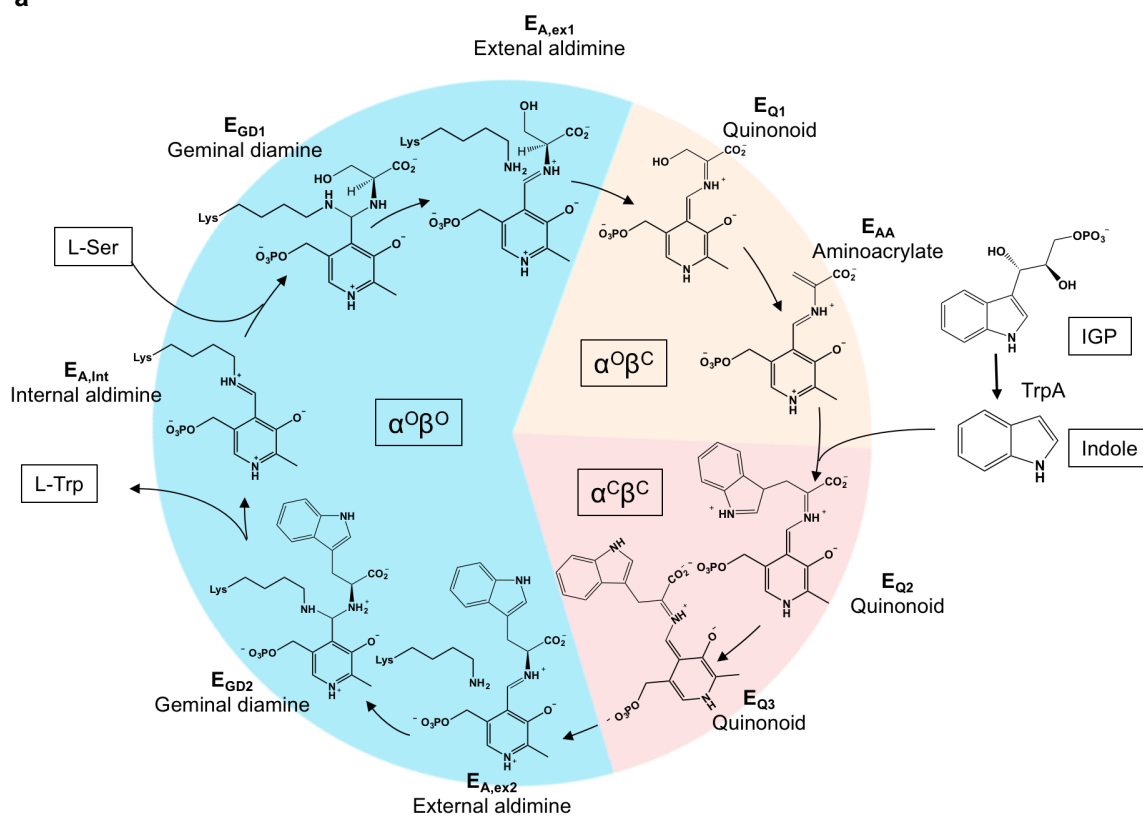


Figure 2.1. BRD4592 activity against Mtb. (a) L-Trp biosynthesis pathway (b) Chemical structure of BRD4592 (c) Kill kinetics showing a decrease in colony forming units (CFU) of Mtb grown in rich media containing BRD4592. (data are mean \pm s.d. for three biological replicates and are representative of three independent experiments). (d) Dose response showing growth (measured by OD₆₀₀) of WT Mtb as well as WT Mtb with an episomal copy of WT or mutated *trpA* (WT:*trpA*^{WT} and WT:*trpA*^{D136H}, respectively) treated with BRD4592. WT + 1 mM L-Trp is H37Rv grown in media supplemented with L-Trp. Growth of WT:*trpA*^{D136H} and WT + 1 mM L-Trp is unaffected by BRD4592. (data are mean \pm s.d. for four replicates and are representative of three independent experiments).

a



long-range interactions with the α and β subunits. These interactions result in a combination of effects including, paradoxically, stabilization of active conformations of the enzyme complex, which have increased affinity for substrates and products, as well as stabilization of the interaction between the α and β subunits. The compound's multi-component mechanism is highly unique and results in inhibition that is not overcome by changes in the metabolic environment. Collectively, our findings demonstrate the effectiveness of a strategy to target conditionally essential metabolic enzymes using allosteric small molecules and suggest general principles for allosteric probe discovery.

Section 2.2. Results

Identification of an azetidine that targets tryptophan synthase stereospecifically.

We screened the Broad Institute DOS library, which at the time comprised 82,762 compounds synthesized using the build/couple/pair strategy^{126,127}, against log-phase Mtb using a previously reported GFP-based assay¹⁹. From this screen, the azetidine BRD4592 ((2R,3S,4R)-3-(2'-fluoro-[1,1'-biphenyl]-4-yl)-4-(hydroxymethyl)azetidine-2-carbonitrile) (Fig. 2.1b) was determined to have *in vitro* activity with an MIC₉₀ of 3 μ M against Mtb. The compound contains three stereogenic centers and only the BRD4592 stereoisomer is active, suggesting a high degree of target specificity. Similarly to the delayed bactericidal response observed in bedaquiline treatment of Mtb⁸⁶, after several days of treatment, BRD4592 reduces the colony forming units (CFUs) of Mtb cultures by 2-3 logs (Fig. 2.1c). The compound also has comparable activity against a diverse panel of clinical isolates of Mtb, including drug-resistant strains (Table 2.1). Importantly, BRD4592 is specific with a CC₅₀ against hepG2 cells >100 μ M and no activity in 36

Table 2.1: Activity of BRD4592 against various Mtb strains

Strain	Description	BRD4592 MIC (μM)
H37Rv (WT)	Wild-type <i>M. tuberculosis</i>	3
BAA-812	Clinical isolate, isoniazid resistant	3
01-R0348	Clinical isolate, isoniazid and streptomycin resistant	1.6
98-01436	Clinical isolate, streptomycin resistant	1.6
CI-10	Clinical isolate, Beijing SolDB4 family, ofloxacin resistant	1.6
CI-14	Clinical isolate, T1 SpolDB4 family, ofloxacin and isoniazid resistant	3
HN-878	Clinical isolate, Beijing SpolDB4 family, pan-sensitive	3
CI-11	Clinical isolate, H3 SpolDB4 family, pan-sensitive	1.6
AS2	Clinical isolate, LAM10-CAM SpolDB4 family, pan-sensitive	3
AS4	Clinical isolate, T1 SpolDB4 family, pan-sensitive	3
CI-5	Clinical isolate, T2 SpolDB4 family, pan-sensitive	3
CDC1551	Clinical isolate, X3 SpolDB4 family, pan-sensitive	3
CI-4	Clinical isolate, EAI2-Manilla SpolDB4 family, pan-sensitive	1.6
RM1	H37Rv TrpA D136G	>100
RM2	H37Rv TrpA D136H	250
RM3	H37Rv TrpA D136G	>250
RM4	H37Rv TrpA G66V	>250
RM5	H37Rv TrpA D136G	125
RM6	H37Rv TrpA D136H	>125
RM7	H37Rv TrpA D136G	125
RM8	H37Rv TrpA D136G	125
RM9	H37Rv TrpA D136G	125
RM10	H37Rv TrpB N185S	31
RM11	H37Rv TrpB N185S	31
RM12	H37Rv TrpA P65Q	62.5
RM13	H37Rv TrpA D136N	125
RM14	H37Rv TrpA D136G	125
RM15	H37Rv TrpA G66A	>250
RM16	H37Rv TrpA D136G	125
WT: <i>trpA</i> ^{WT}	H37Rv harboring pUV3583c_ <i>trpA</i> ^{WT}	1.5
WT: <i>trpA</i> ^{D136H}	H37Rv harboring pUV3583c_ <i>trpA</i> ^{D136H}	>100
H37RvΔ <i>trpA</i>	H37Rv containing a clean deletion of <i>trpA</i>	N/A*
H37RvΔ <i>trpA</i> :: <i>trpA</i>	H37RvΔ <i>trpA</i> harboring pUV3583c_ <i>trpA</i> ^{WT}	2

* H37RvΔ*trpA* must be grown in media supplemented with L-Trp and so, BRD4592 was not tested against this strain.

** RM1-16 are spontaneous BRD4592-resistant mutants isolated from WT H37Rv.

screens reported in PubChem (substance SID 131446886) against 19 unique and diverse targets including enzymes involved in DNA repair, bacterial glycoprotein synthesis, Mtb biotin synthesis, and bacterial protein synthesis as well as against whole-cell *Trypanosoma cruzi*, *Cryptococcus neoformans*, and *Plasmodium falciparum*.

To determine the mechanism of action of BRD4592, we selected for resistant Mtb mutants. Spontaneous mutants were obtained at a frequency of about 8×10^{-8} and each had an MIC₉₀ at least 10-fold greater than the parent strain (Table 2.1). All resistant mutants studied contained point mutations in *trpA* (Rv1613) corresponding to alterations in three amino acids, α D136, α G66, and α P65, or in *trpB* (Rv1612) corresponding to alterations in residue β N185 (Table 2.1; Fig. 2.3a). Episomal expression of mutated *trpA*, but not wild-type *trpA*, was sufficient to confer resistance to BRD4592 in WT Mtb, showing that the resistant allele is dominant (Fig. 2.1d).

To assess if BRD4592 may be more broadly active, we tested it against a panel of Gram-negative and Gram-positive bacterial species. We found that BRD4592 is active against several mycobacterial species, but does not affect the growth of any other bacteria tested (Fig. 2.3b). Interestingly, by sequence alignment, we found α G66 is conserved in all sensitive mycobacterial species (Fig. 2.3c). These data, coupled with the observation that non-glycine substitutions at this position confer resistance to BRD4592 in Mtb (Table 2.1), indicate that substitutions at the α 66 position are the cause of the intrinsic resistance of non-mycobacteria to BRD4592.

In order to complement the genetic data identifying TrpAB as the potential target of BRD4592, we obtained metabolic evidence supporting this same conclusion. Addition of L-Trp to the growth media rescues Mtb from the lethal effects of BRD4592 (Fig. 2.1d).

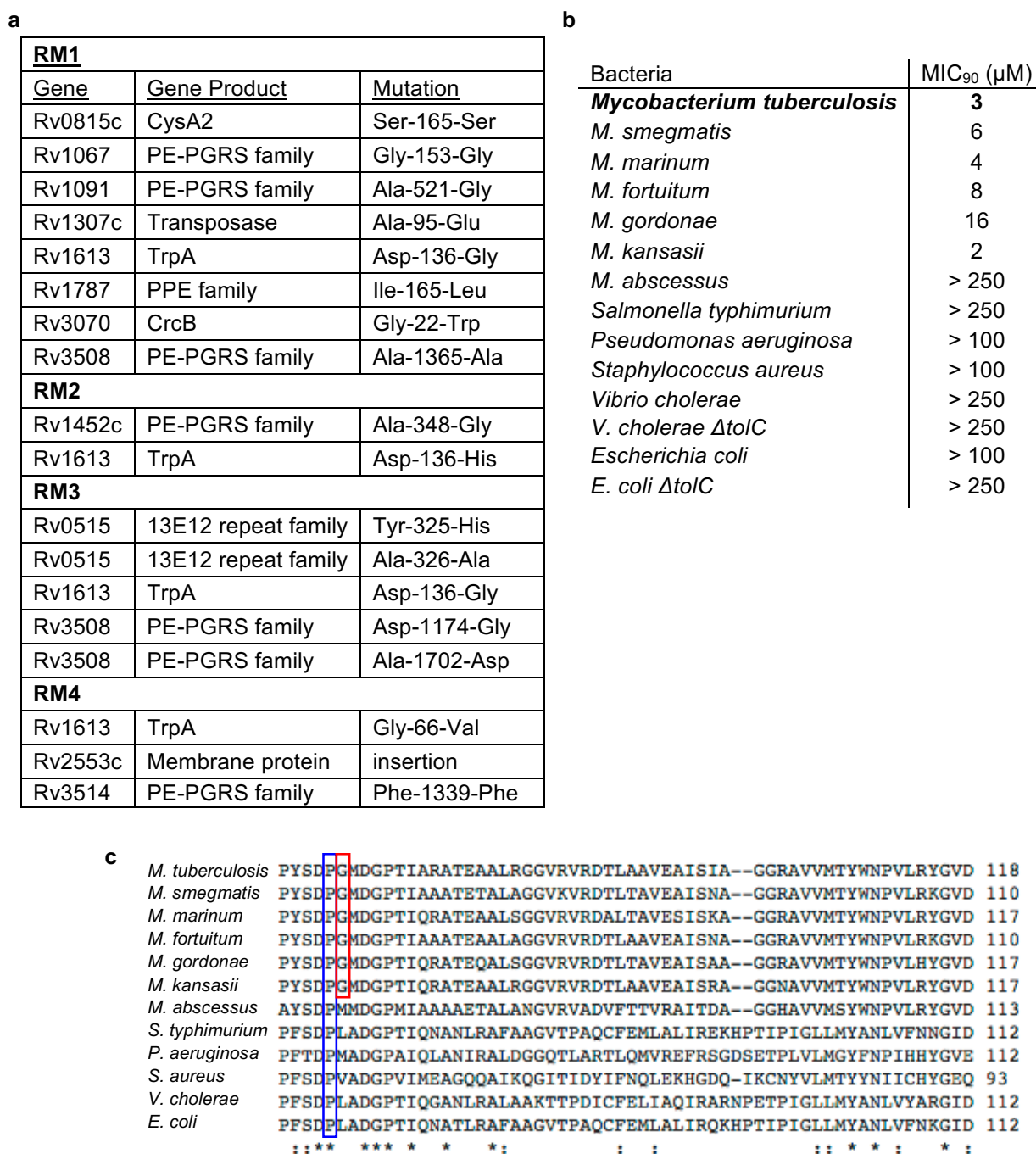


Figure 2.3. Activity of BRD4592 against selected bacterial species. (a) Mutations identified in BRD4592-resistant Mtb mutants. (b) MIC₉₀ of BRD4592 against selected bacteria, including strains engineered to be more permeable than wild-type (*V. cholerae* Δ*tolC* and *E. coli* Δ*tolC*). (c) Alignment of the amino acid sequence of TrpA from multiple bacteria. αP65 (blue box) is conserved across all species tested, while αG66 (red box) is not. All bacteria that have an amino acid other than Gly at α66 are resistant to BRD4592.

Taken together, these data implicate TrpAB as the physiological target of BRD4592 in Mtb.

BRD4592 is an allosteric inhibitor of Mtb TrpAB. With these data in hand, we investigated the effect of the compound on recombinant Mtb TrpAB. To study the α reaction in the presence of L-Ser bound at the β site (IGP \rightarrow indole + G3P), we measured G3P production using a modified fluorescence-based assay¹²⁸. At L-Ser concentrations ≥ 0.1 mM, the α reaction is rate determining and therefore, the overall reaction can also be studied by this method. To follow the overall reaction with IGP and L-Ser as substrates (IGP + L-Ser \rightarrow G3P + L-Trp), we developed a complementary LC-MS method to separate and quantify indole and L-Trp simultaneously. With L-Ser and indole as substrates, we also used this assay to measure β subunit activity specifically (indole + L-Ser \rightarrow L-Trp).

We first characterized the kinetic mechanism of Mtb TrpAB to demonstrate that it is similar to previously characterized TrpAB complexes. We determined $K_M^{apparent, L-Ser} = 0.50 \pm 0.12$ mM and $K_M^{apparent, IGP} = 32.6 \pm 8.1$ μ M, with $k_{cat} = 19.6 \pm 3.9$ min⁻¹ (Fig. 2.4a, 2.5a, b). These values are in a similar range to those reported for *E. coli* TrpAB¹²⁹. Reciprocal plots of velocity versus L-Ser and IGP concentrations are linear (Fig. 2.5c, d), indicating that Mtb TrpAB, like the *E. coli* enzyme, uses a double displacement mechanism in which the reaction proceeds via two distinct half-reactions¹²⁹ with either IGP or L-Ser binding first¹²⁸.

We then interrogated which step(s) of the TrpAB reaction BRD4592 inhibits. Under balanced conditions ($[substrate] = K_M$), BRD4592 potently inhibits both the α and β

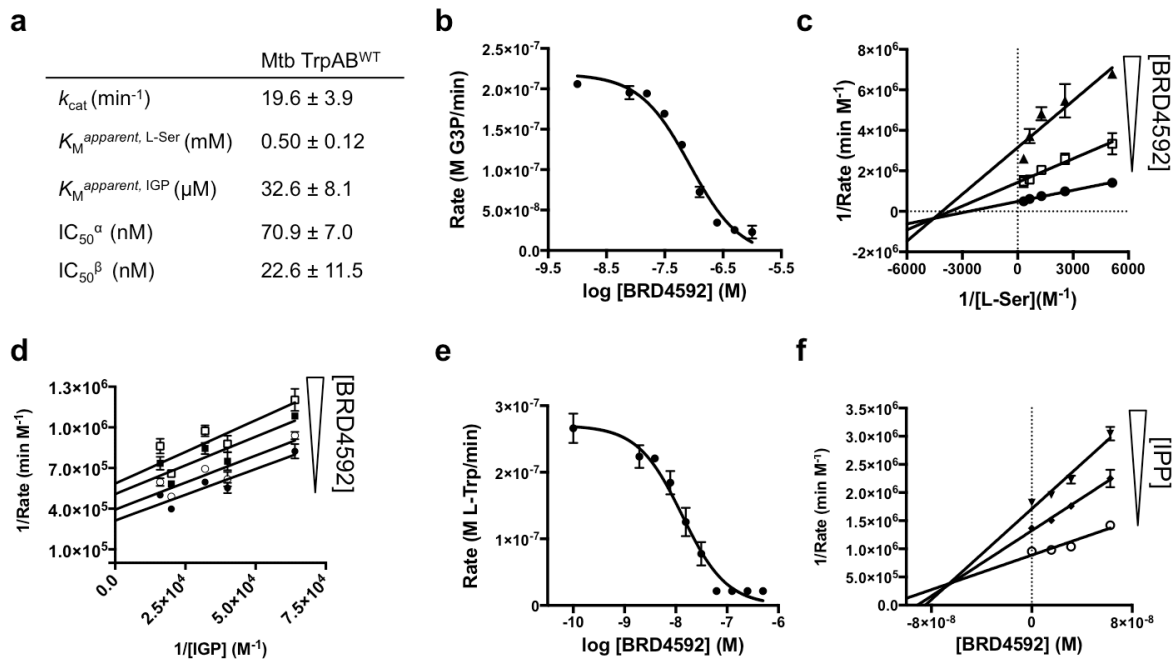


Figure 2.4. BRD4592 inhibition of TrpAB *in vitro*. (a) Kinetic parameters for Mtb TrpAB and IC_{50} of BRD4592 against the α and β reactions (IC_{50}^{α} and IC_{50}^{β} , respectively). (data are mean \pm s.e.m. for at least four independent experiments with three technical replicates each). (b) BRD4592 inhibits TrpAB G3P production from IGP and L-Ser in a dose-dependent manner. (c) Double reciprocal plot of 1/Rate vs. 1/[L-Ser] at various [BRD4592] showing that BRD4592 is a mixed-type inhibitor with respect to L-Ser ($K_i^{apparent, BRD4592} = 40.5 \pm 1.7$ nM, $\alpha = 0.81 \pm 0.06$). (d) Double reciprocal plot of 1/Rate vs. 1/IGP concentration at various [BRD4592] showing that BRD4592 is uncompetitive with respect to IGP ($\alpha K_i^{apparent, BRD4592} = 62.9 \pm 13.0$ nM). (e) BRD4592 inhibits Mtb TrpAB L-Trp production from indole and L-Ser in a dose-dependent manner. (f) 1/Rate vs. [BRD4592] measured over varying concentrations of IGP-mimetic IPP. BRD4592 and IPP inhibit Mtb TrpAB in an additive manner. (data for b-f are mean \pm s.d. for three technical replicates and are representative of at least three independent experiments).

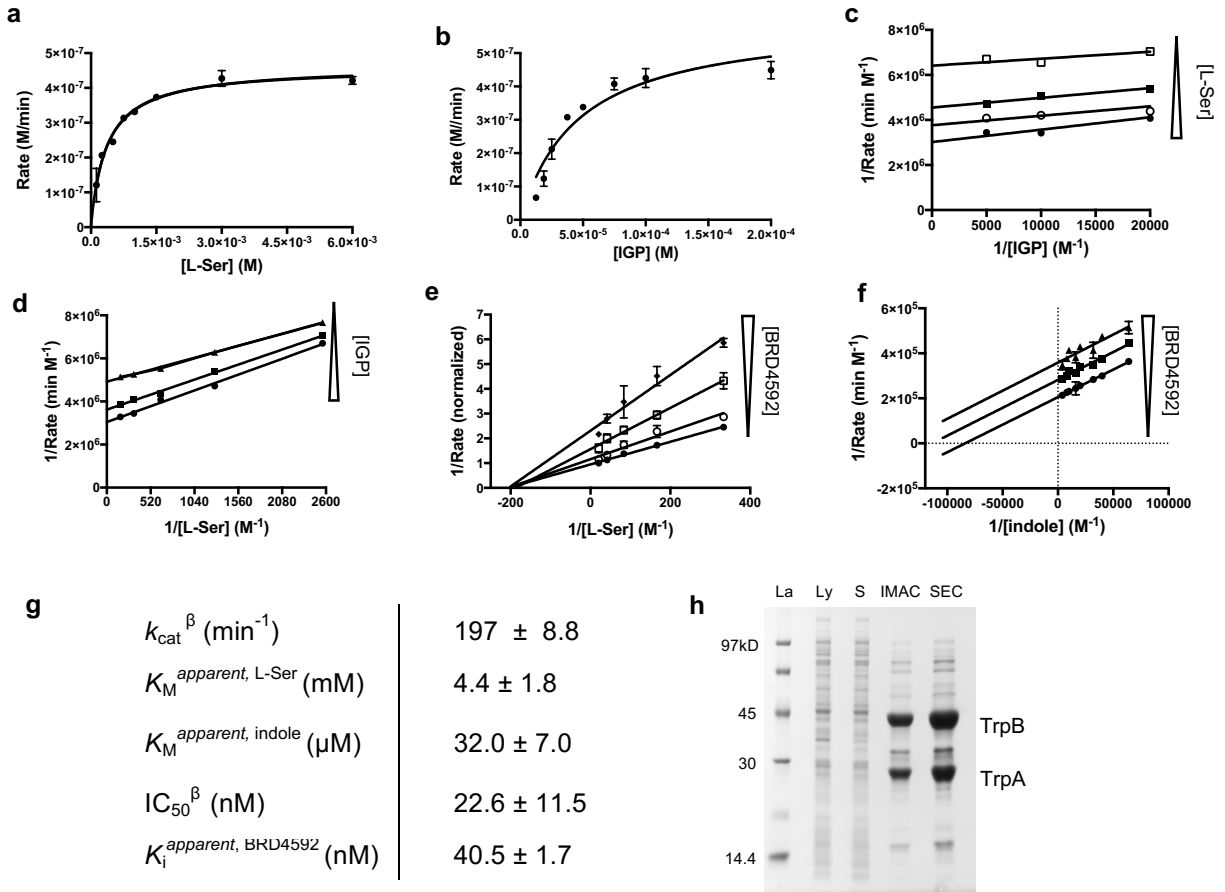


Figure 2.5. Kinetic characterization of Mtb TrpAB. (a) Rate of the TrpAB reaction vs. [L-Ser] under conditions of saturating [IGP]. (b) Rate of the TrpAB reaction vs. [IGP] under saturating [L-Ser]. The sigmoidal shape suggests cooperativity between L-Ser and IGP binding. Fitting of an allosteric sigmoidal kinetic model yields a hill coefficient of 1.7 ± 0.3 , indicating positive cooperativity. (c) Double reciprocal plot of $1/\text{Rate}$ vs. $1/[\text{IGP}]$ at varying [L-Ser]. (d) Double reciprocal plot of $1/\text{Rate}$ vs. $1/[\text{L-Ser}]$ at varying [IGP]. The linear nature of the double reciprocal plots is similar to data reported for *E. coli* TrpAB¹²⁸ and suggests Mtb TrpAB uses a double displacement reaction characterized by two distinct half reactions¹²⁹. (e) Double reciprocal plot of $1/\text{Rate}$ vs. $1/[\text{L-Ser}]$ at saturating [indole] and varying [BRD4592]. In the TrpAB TrpB half reaction indole and L-Ser react to yield L-Trp and H_2O . Production of L-Trp from indole and L-Ser is measured by LC-MS. BRD4592 is noncompetitive vs. L-Ser ($R^2 = 0.92$), binding TrpAB equally well with or without L-Ser. (f) Double reciprocal plot of $1/\text{Rate}$ vs. $1/[\text{indole}]$ at saturating [L-Ser] and varying [BRD4592]. BRD4592 is uncompetitive vs. indole ($R^2 = 0.9616$). (g) Table of kinetic parameters of TrpAB in the TrpB half reaction. Values are mean \pm s.e.m and all data are representative of at least three independent experiments consisting of technical quadruplicates. (h) Gel of TrpAB purification. Lane 1: Ladder (La); 2: lysate (Ly); 3: Supernatant (S); 4: TrpAB following immobilized metal affinity chromatography (IMAC); 5: TrpAB following size exclusion chromatography (SEC).

reactions equally, with an IC_{50}^{α} (against the α reaction) of 70.9 ± 7.0 nM and an IC_{50}^{β} (against the β reaction) of 22.6 ± 11.5 nM (Fig. 2.4b, 2.4e, 2.5e-g). TrpAB enzymes containing the amino acid substitutions α G66V and β N185S each showed a much higher BRD4592 IC_{50}^{α} (>1000 nM and 239.3 ± 3.1 nM, respectively), which correlates with the higher whole-cell MIC_{90} of BRD4592 against Mtb harboring these mutant enzymes. These data provide further evidence that inhibition of TrpAB is indeed responsible for the activity of BRD4592 against whole Mtb cells.

The fact that both steps of the reaction are affected suggests that BRD4592's mechanism is more complex than simple inhibition of one of the individual active sites. To understand this phenomenon better, we examined the relationship between BRD4592 and substrate binding. Under saturating [IGP], we found BRD4592 is a mixed-type inhibitor versus L-Ser, with $K_i^{apparent, L-Ser} = 40.5 \pm 1.7$ nM and $\alpha = 0.81 \pm 0.06$ (Fig. 2.4c). The low α value ($\alpha < 1$) indicates that BRD4592 binds TrpAB more tightly when L-Ser is also bound¹²⁹, and isothermal calorimetry (ITC) confirmed this finding (Fig. 2.6a, b). We found that BRD4592 is uncompetitive versus IGP under saturating [L-Ser], with $\alpha K_i^{apparent, IGP} = 62.9 \pm 13.0$ nM (Fig. 2.4d). Together, these data support a model in which BRD4592 is an allosteric inhibitor of both reactions where substrate binding to either subunit enhances inhibitor affinity.

To confirm that BRD4592 is indeed an allosteric inhibitor of the α reaction and demonstrate that it behaves distinctly from direct inhibitors of the α active site, we compared BRD4592 to previously developed IGP substrate mimetics including indole-propanol phosphate (IPP), F6 and F9^{122,130}. Unlike BRD4592, these substrate mimetics

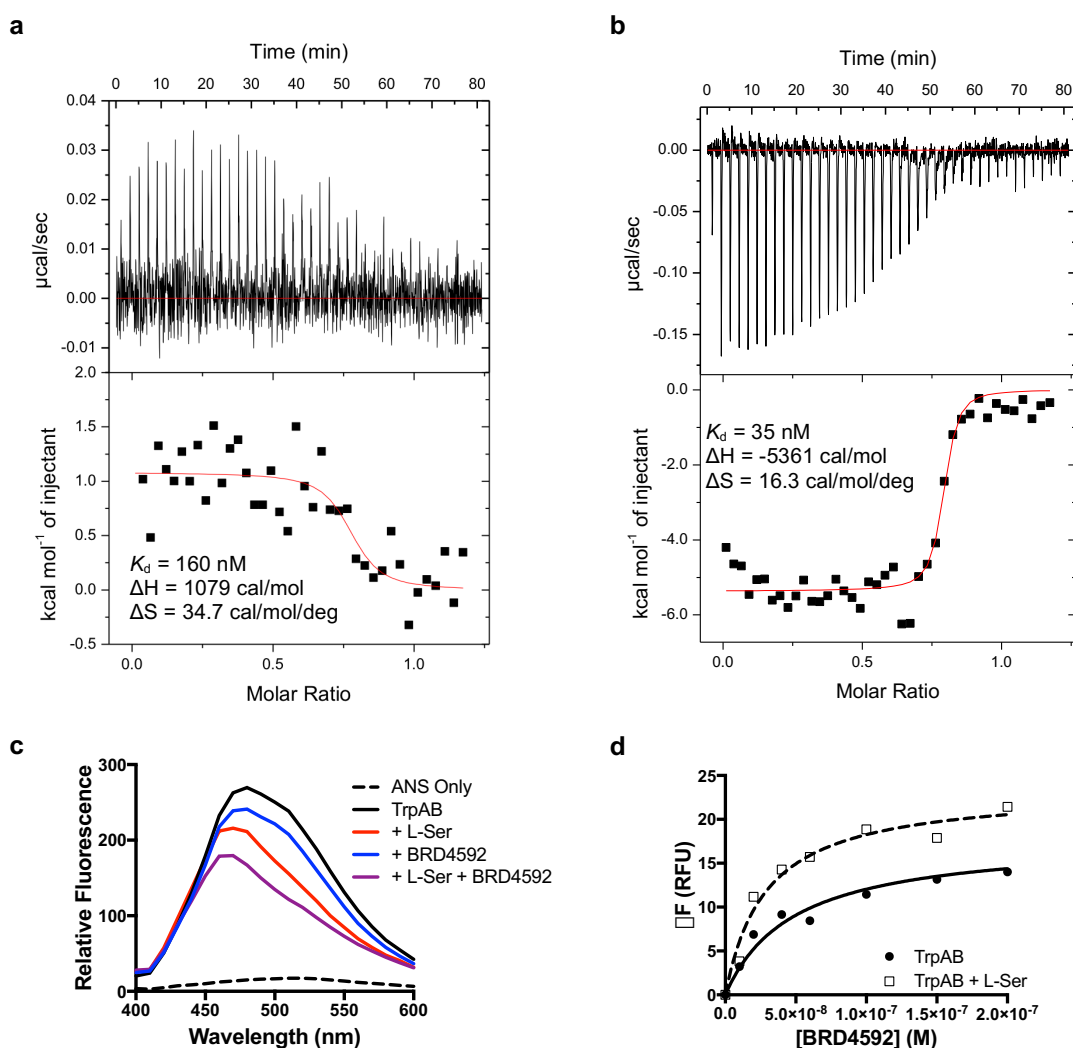


Figure 2.6. Binding of BRD4592 to TrpAB. (a) Isothermal calorimetry of BRD4592 titrated into TrpAB. (b) Isothermal calorimetry of BRD4592 titrated into TrpAB with L-Ser. ITC graphs are representative of two independent experiments. (c) Fluorescence spectrum of 8-anilino-1-naphthalenesulfonic acid (ANS) (dashed line) bound to TrpAB (black line) with L-Ser (red line), BRD4592 (blue line) or L-Ser and BRD4592 (purple line). Small molecules (such as BRD4592) displace ANS from the protein, decreasing ANS fluorescence¹²². This decrease depends on inhibitor concentration and affinity. (d) Change in fluorescence signal from ANS bound to TrpAB over varying concentrations of BRD4592 (open squares; $K_d^{\text{apparent, BRD4592}} = 132 \pm 8 \text{ nM}$) or change in fluorescence signal from ANS bound to TrpAB with L-Ser over varying concentrations of BRD4592 (closed circles; $K_d^{\text{apparent, BRD4592}} = 42 \pm 11 \text{ nM}$). A hyperbola fit to the change in fluorescence was used to calculate the K_d^{apparent} of BRD4592. Values are mean \pm s.e.m. for three independent experiments.

are competitive with IGP¹³⁰. Moreover, these α active site inhibitors are orders of magnitude less potent than BRD4592 (IPP, F6, and F9 IC_{50}^{α} = 255 \pm 41 μ M, 2.6 \pm 0.02 mM, and 1.3 \pm 0.08 mM, respectively). Further, in contrast to these α site ligands that have limited efficacy against the Mtb β reaction, BRD4592 equally inhibits both reactions (BRD4592 IC_{50}^{β} = 23 \pm 12 nM compared to IPP IC_{50}^{β} = 4.4 \pm 0.7 mM). Finally, combination inhibition studies of TrpAB with BRD4592 and IPP, indicated that the enzyme is inhibited in an additive manner (Fig. 2.4f). In sum, these data support a model where BRD4592 binds to a different pocket than IPP and operates through a mechanism distinct from that of α active site inhibitors.

BRD4592 stabilizes closed, active states of the β subunit. The α and β subunits of TrpAB interact extensively throughout the catalytic cycle. Each of the subunits initially adopts an open, lowly active conformation (α^O or β^O) and transitions to a closed, highly active conformation (α^C or β^C) as the multi-step reaction proceeds¹¹⁶. Upon L-Ser binding to the open conformation of TrpAB complexed with PLP ($\alpha^O\beta^O$), the substrate is rapidly converted to an aminoacrylate intermediate (E_{AA}) and the communication (COMM) domain of the β subunit, responsible for allosteric interactions between the two subunits¹¹⁶, shifts into a closed, highly active state (β^C) (Fig. 2.2). Likewise, binding of the IGP substrate to the α subunit promotes closing of the α subunit (α^C) via movement of the α 6 loop. In *S. typhimurium*, allosteric activation is mutual, with closing of the β subunit triggering closing of the α subunit and vice versa^{116,125}. Both reactions and indole translocation occur with the enzyme in the closed state ($\alpha^C\beta^C$). Once catalysis is

complete, the enzyme recycles back to the $\alpha^0\beta^0$ state to begin a new catalytic cycle (Fig. 2.2).

Having demonstrated that BRD4592 is an allosteric inhibitor of the α reaction, we turned to understand BRD4592's mode of inhibition against the β reaction. We used the absorbance spectrum of the β subunit PLP cofactor to study the chemical state of cofactor-substrate adducts and, by inference, conformational states of TrpAB¹²². As observed for the *Salmonella* TrpAB enzyme, Mtb TrpAB PLP absorbance spectra are consistent with the β subunit shifting from an open, lowly active state ($E_{A,Int}$) to a closed, highly active state (E_{AA}) upon the addition of L-Ser (Fig. 2.7a, 2.2). Because this shift is associated with changes in absorbance that are dependent upon $[L-Ser]$ ¹²², we could measure the apparent K_d^{L-Ser} in the presence and absence of BRD4592 to be 9.1 ± 1.1 μ M and 83.4 ± 3.2 μ M, respectively (Fig. 2.7b). Importantly, this result suggests that though BRD4592 inhibits the β reaction, in fact, it is promoting the highly active closed conformation of the β subunit.

Using PLP absorbance, we assessed the impact of BRD4592 on other chemical states of TrpAB and found that BRD4592 also stabilizes two additional closed forms of the β subunit: β bound to the indole analog indoline (2,3-dihydro-1H-indole) ($E_{Qindoline}$) and β bound to its product L-Trp (E_{Q3}) (Fig. 2.2, 2.8a, b). We also found that BRD4592 increases affinity of TrpAB for L-Trp 4.5-fold (Fig. 2.8c). These data show that BRD4592 consistently shifts the conformational equilibrium toward chemical states associated with a closed, highly active β subunit. Differential scanning calorimetry (DSC) confirms these findings in that BRD4592 does not stabilize the open, L-Ser-free conformation of TrpAB in a thermal melt (Fig. 2.7c). In contrast, in the presence of L-Ser, BRD4592 binding

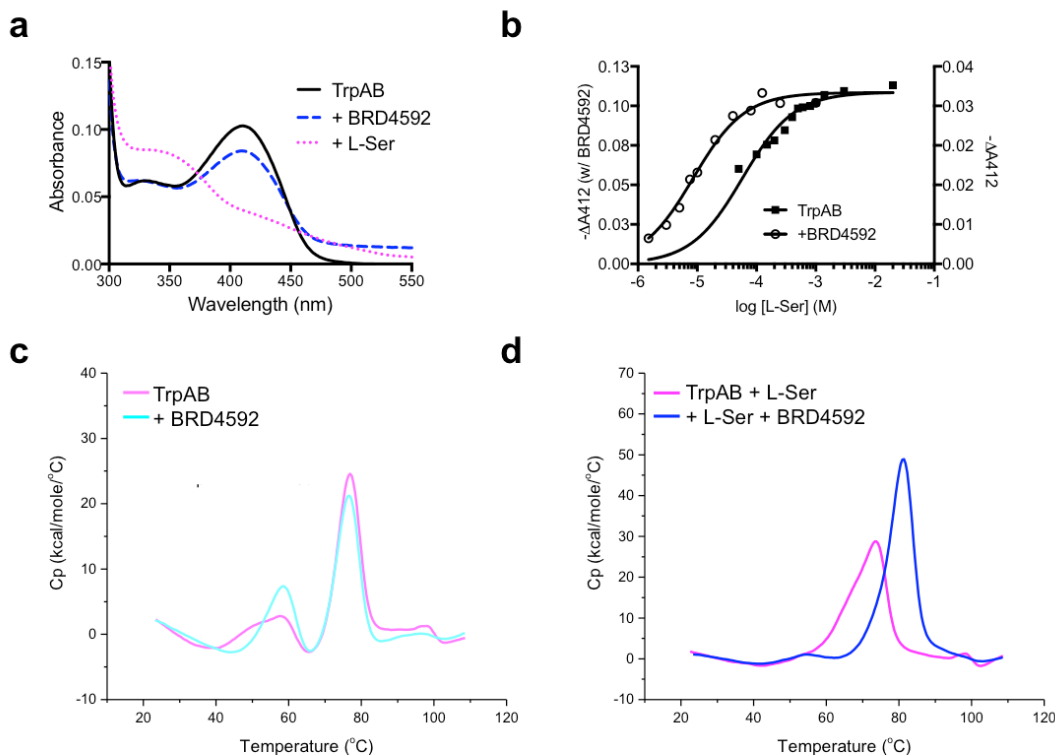


Figure 2.7. BRD4592 stabilizes closed, active states of the β subunit. (a) Absorbance spectrum of the Mtb TrpAB (black solid line) with BRD4592 (blue dashed line) or BRD4592 and L-Ser (pink dotted line). The peak at 412 nm is attributed to a substrate-free PLP adduct that typically assumes an $\alpha^0\beta^0$ conformation ($E_{A,int}$) and the peak at 350 nm is attributed to an $\alpha^0\beta^C$ state (E_{AA}). These spectra are consistent with TrpAB PLP spectra reported for *S. typhimurium*²⁷. (data are representative of three independent experiments). (b) Change in TrpAB absorbance at 412 nm vs. [L-Ser] shows BRD4592 increases TrpAB affinity for L-Ser ($K_d^{apparent, L-Ser} = 83.4 \pm 3.2$ μ M in the absence of BRD4592 and 9.1 ± 1.1 μ M with BRD4592 co-bound). Black squares: TrpAB; Open circles: TrpAB + BRD4592. (data are representative of three independent experiments with K_d reported as mean \pm s.e.m.). (c) DSC of TrpAB with (blue) or without (pink) BRD4592. (d) The same as (c) with the addition of L-Ser to each sample. BRD4592 stabilizes TrpAB + L-Ser against thermal melting, increasing T_m 8°C ($T_m = 73.5 \pm 1.0^\circ\text{C}$ without BRD4592 and $81.6 \pm 0.2^\circ\text{C}$ with BRD4592). (data are representative of four (no BRD4592) or two (TrpAB + BRD4592) independent experiments).

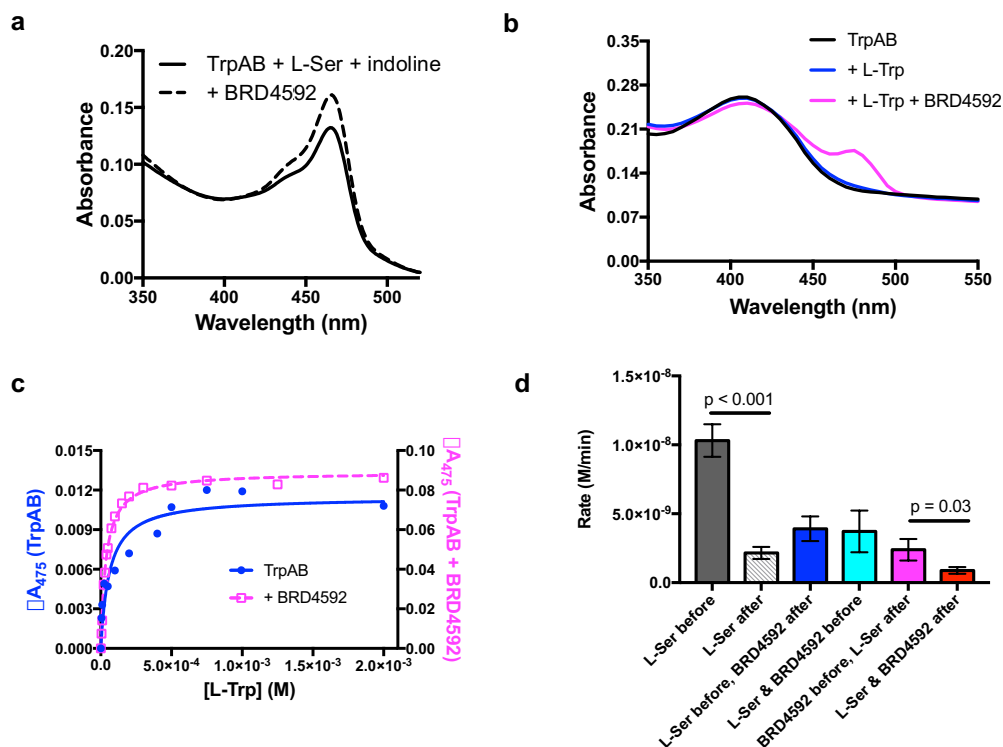


Figure 2.8. Effect of BRD4592 on TrpAB chemical state equilibrium. (a) Absorbance spectrum of Mtb TrpAB with the indole analog indoline and L-Ser (solid line). The peak at 466 nm is consistent with the formation of an indoline-L-Ser-PLP adduct ($E_{Qindoline}$), which is associated with a closed β subunit¹²². Addition of BRD4592 (dashed line) increases the absorbance of this species, indicating that binding of BRD4592 increases the proportion of enzyme in this state. (b) Absorbance spectrum of TrpAB (black line). Upon L-Trp binding (blue line), the enzyme forms two different L-Trp-PLP adducts, one associated with an open β subunit, with maximum absorbance at 415 nm ($E_{A_{18x2}}$), and another associated with a closed β subunit, with maximum absorbance at 475 nm (E_{Q3})¹³¹. At saturating [L-Trp], BRD4592 (pink line) increases absorbance at 475 nm, suggesting BRD4592 increases the proportion of the enzyme in the closed β conformation (E_{Q3}). (c) Change in absorbance of 475 nm light by TrpAB vs. [L-Trp] with BRD4592 (magenta dashed line, $K_d^{L-Trp} = 25 \pm 12 \mu M$) and without BRD4592 (blue line, $K_d^{L-Trp} = 114 \pm 20 \mu M$). K_d is calculated by fitting a hyperbola to the change in absorbance. (d) Jump dilution analysis in which enzyme was pre-incubated with BRD4592 and/or L-Ser, then diluted 100-fold in buffer containing IGP to begin the reaction. There is no apparent difference in rate when TrpAB is pre-incubated with a high concentration of compound (cyan) vs. treated with compound when the reaction is started (blue), indicating a relatively rapid off-rate¹³². However, when the enzyme is pre-incubated with neither L-Ser nor BRD4592 (grey vs. light grey and pink vs. red), rate dramatically drops suggesting the enzyme dissociates upon dilution (also supported by SEC-MALS showing oligomerization depends on protein concentration) and that L-Ser or BRD4592 binding can stabilize α/β subunit interactions. Graphs are representative of two independent experiments. Values are mean \pm s.e.m. for two independent experiments.

increases the T_m of TrpAB in the active β^C conformation by 8°C (Fig. 2.7d). Interestingly, BRD4592 also apparently stabilizes the interaction between the two subunits, stabilizing the enzyme complex against dissociation upon dilution (Fig. 2.8d). Therefore, we conclude BRD4592 specifically stabilizes closed states of the β subunit.

Crystal structures reveal BRD4592 binds the TrpAB protein-protein interface. To understand better how BRD4592 interacts with the enzyme, we solved five crystal structures of Mtb TrpAB including an inhibitor-free/substrate-free form in the lowly active $\alpha^O\beta^O$ state, the aminoacrylate-bound form (E_{AA}) in the $\alpha^O\beta^C$ state (Fig. 2.9a, c), the BRD4592-bound form in the $\alpha^O\beta^O$ state ($\alpha^O\beta^O$ -BRD4592), and the BRD4592-bound E_{AA} form in the $\alpha^O\beta^C$ state ($\alpha^O\beta^C$ -BRD4592), as well as the α G66V mutant in the inhibitor-free/substrate-free form (α G66V β^O).

Mtb TrpAB is structurally heterogeneous, indicating a high degree of flexibility in the enzyme. While all crystals contained two $\alpha\beta\beta\alpha$ heterotetramers per asymmetric unit, significant heterogeneity was observed among the conformations of the β subunits. In Mtb $\alpha^O\beta^O$ structures, the conformations of half of the β subunits were affected by crystal packing, which moves the COMM domain slightly towards the protein core to adopt the β^O open conformation most frequently observed in *Salmonella* TrpAB structures, while the other β subunits, not constrained by neighboring molecules, adopted a more expanded open conformation (β^{eO}) (Fig. 2.10). A characteristic feature of the β^O state is a hydrogen bond between β H294 and β N185, which is also observed in the closed β^C state but absent in β^{eO} . This conformational heterogeneity is reflected in relatively high

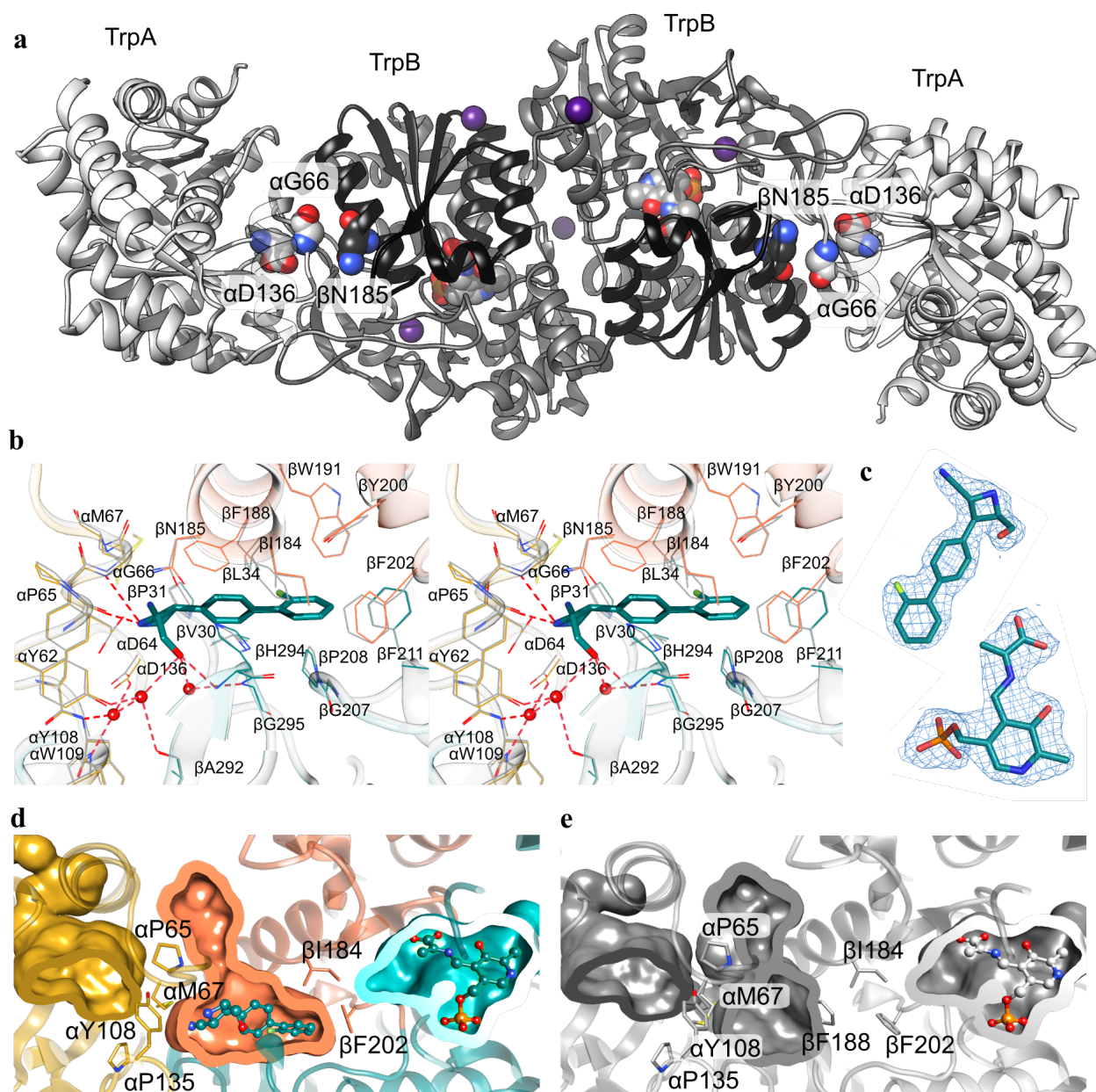


Figure 2.9. Crystal structures of Mtb TrpAB. (a) The overall structure of Mtb TrpAB with L-Ser ($\alpha^o\beta^c$, E_{AA}). The α subunit is shown in light grey and β in dark grey with the COMM domain shown in black. The aminoacylate adducts, positions of BRD4592 resistance mutations and cesium ions (purple) are shown as spheres. (b) Stereoview of BRD4592 binding to $\alpha^o\beta^c$. The α subunit is shown in yellow and β is shown in cyan, with the COMM domain shown in coral. Hydrogen bonds are shown as dashed lines and water molecules are represented as spheres. For reference, the BRD4592 binding site of $\alpha^o\beta^c$ without BRD4592 is superimposed (grey). (c) 2DFo-mFc electron density maps contoured at 1.2σ for BRD4592 and the aminoacylate as seen in the $\alpha^o\beta^c$ - BRD4592 structure. (d) Pockets in the $\alpha^o\beta^c$ -BRD4592 structure. The α pocket is shown in yellow, β pocket (with aminoacylate-PLP adduct) is shown in cyan and inhibitor-binding pocket at the α/β interface is shown in coral. Residues at pocket-pocket interfaces are shown. (e) Pockets in $\alpha^o\beta^c$ with no BRD4592 bound shown as in d.

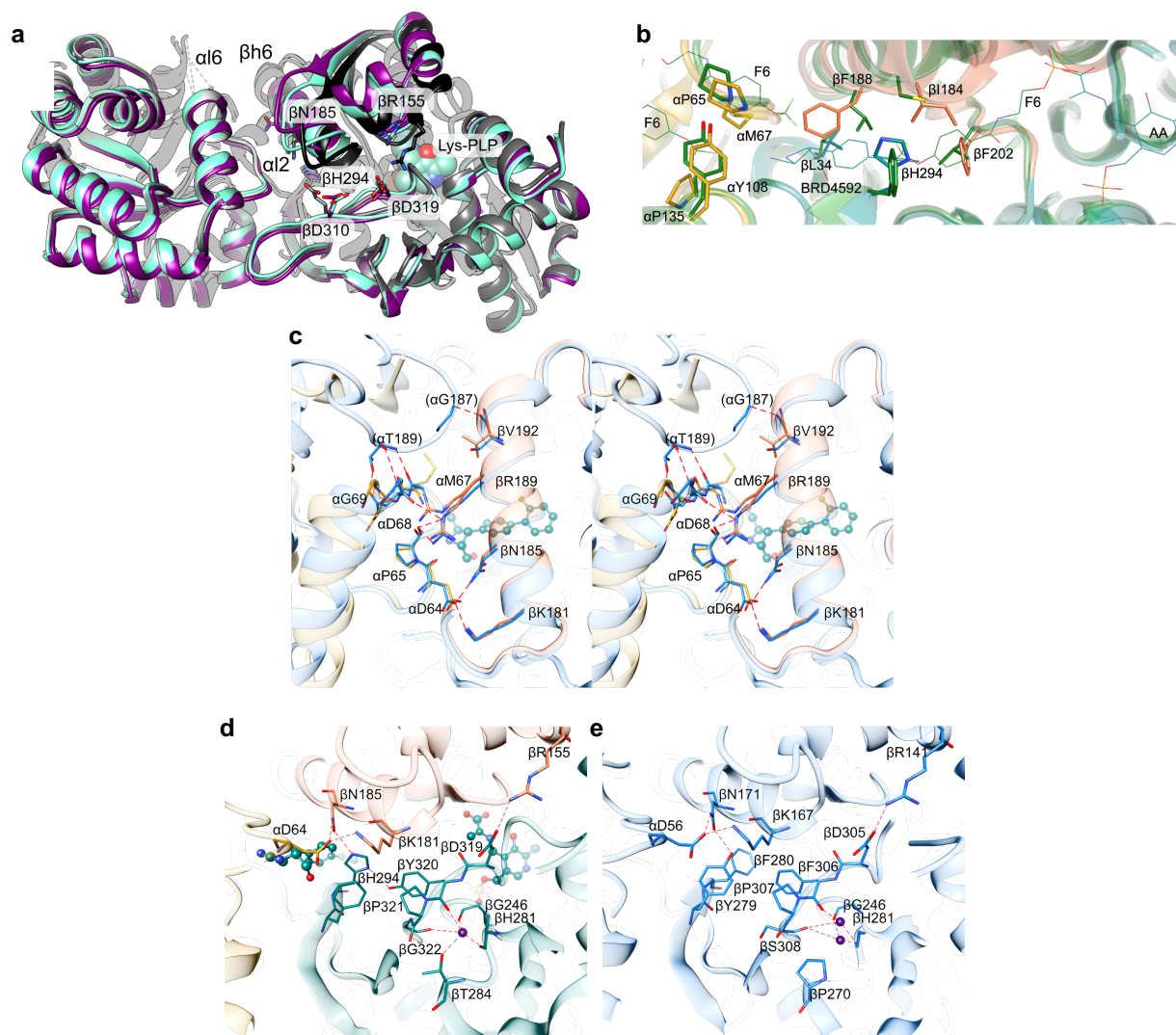


Figure 2.10. Comparisons of Mtb TrpAB. (a) Superposition of the $\alpha\beta$ unit from $\alpha^O\beta^C$ (grey/black), with $\alpha^O\beta^O$ in β^{EO} conformation (chain B, magenta) and $\alpha^O\beta^O$ in β^O (chain D, aquamarine). Residues important for discrimination between conformational states of β are shown as sticks. Lys-PLP from $\alpha^O\beta^O$ is shown as spheres. The β^{EO} state is reminiscent of the conformation seen in only three *Salmonella* TrpAB structures (2J9Z¹³³, 1QOQ¹³⁴, 1KFB¹³⁵) and homologs from *Pyrococcus furiosus* (5E0K¹³⁶, 1WDW¹³⁷) *Francisella tularensis* (5KZM, unpublished), *Streptococcus pneumoniae* (5KIN, unpublished). (b) Superposition of Mtb TrpAB in the $\alpha^O\beta^C$ conformation bound to BRD4592 (α subunit shown in yellow, β subunit in cyan and coral for COMM domain) with the *S. typhimurium* TrpAB homolog saturated with F6 inhibitor (green, PDB 4WX2¹²⁵) showing key differences in the lining of the tunnel. For clarity only fragments of F6 molecules occupying *S. typhimurium* TrpA are shown. Numbering according to Mtb TrpAB. (c) Stereoview of superposition of Mtb $\alpha^O\beta^C$ -BRD4592 (chains C and D, yellow, coral/cyan) with the *S. typhimurium* TrpAB in the $\alpha^C\beta^C$ state (PDB 4HN4, blue). Residue numbering according to Mtb. In parentheses, missing Mtb TrpAB residues corresponding to the shown *S. typhimurium* TrpAB equivalents are provided. BRD4592 is shown as a ball-and-stick cyan model. Hydrogen bonds for *S. typhimurium* TrpAB are shown. (d) Key residues/interactions responsible for allosteric signaling from α to β subunits in Mtb are shown. In (e) analogous elements in *S. typhimurium* TrpAB are shown. Cesium ions are represented by purple spheres. BRD4592 and aminoacrylate are depicted in ball-and-stick representation.

root-mean-square deviation (RMSD) values (ranging from 0.58 - 0.61 Å) for superpositions of all C α atoms in β^{eO} and β^{O} chains.

Consistent with our finding that BRD4592 is an allosteric inhibitor, crystal structures show that BRD4592 binds outside both active sites in a cavity located at the α/β interface (Fig. 2.9b, c). The observed conformational heterogeneity in $\alpha^{\text{O}}\beta^{\text{O}}$ structures affects the binding mode of the BRD4592 molecule, which seems to adopt two somewhat different conformations, associated with the respective positions of the COMM domain in β^{eO} chains (B and H) which shift toward the β^{O} state. On the other hand, the preexisting β^{O} chains (D and F) preserve their original conformations and have their BRD4592 molecules bound in a single state (Fig. 2.11a, b). Given this conformational heterogeneity, structural analysis of $\alpha^{\text{O}}\beta^{\text{O}}$ -BRD4592 is primarily based on the well-ordered chains C (α) and D (β).

The BRD4592 binding pocket intersects the hydrophobic tunnel through which indole presumably travels from the α to the β catalytic site (Fig. 2.9d, e). This novel and adaptable binding site is distinct from the recently reported *Salmonella* TrpAB intra-channel binding site of the F6 inhibitor observed at very high ligand concentrations¹²⁵ (Fig. 2.10b). BRD4592 binding appears to be primarily driven through hydrophobic interactions between BRD4592 aromatic rings and β subunit aromatic side chains, including β F188 and β F202, as well as β subunit branch-chain residues including β I184 and β L34 (Fig. 2.9b). Direct and water-mediated hydrogen bonds connect the secondary amine and the hydroxyl groups of the azetidine ring with both subunits (α D64, α G66, and β H294) (Fig. 2.9b), further contributing to the stability of the enzyme-inhibitor complex and providing a clear explanation for the stereochemical requirements for binding. All

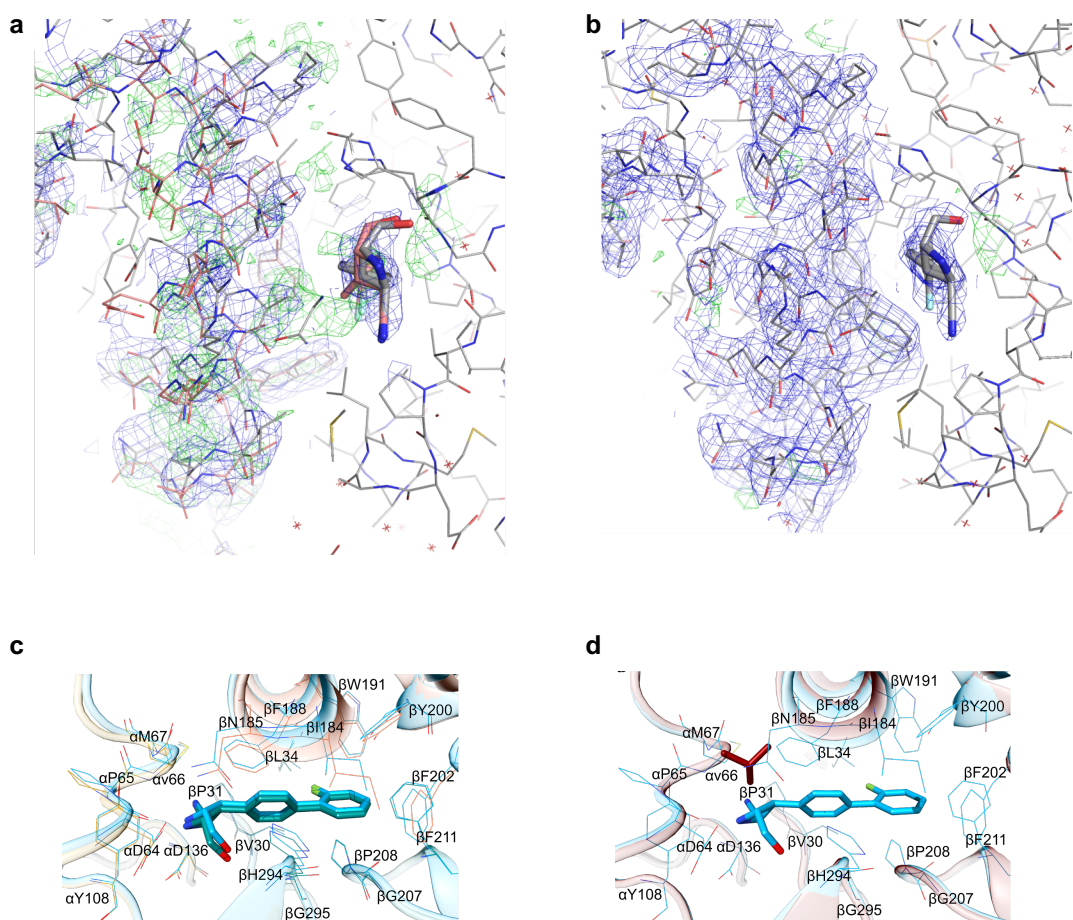


Figure 2.11. Crystal structures of BRD4592 bound to TrpAB. SA-OMIT electron density maps for the $\alpha^o\beta^o$ -BRD4592 structure, (a) chain H, and (b) chain D. 2DFo-mFc (blue) contoured at 1.2σ , DFo-mFc (green) contoured at 3σ . For calculations, atoms corresponding to the lower occupancy conformation (pink) have been removed from chain H (residues 170-200 and BRD4592). The maps are shown only for the double conformation region in chain H and its equivalent in chain D. The side chain of Phe188 has not been modeled for chain H. The discussion in the text is based on well-ordered chain D. (c) Superposition of the BRD4592 binding site from $\alpha^o\beta^o$ -BRD4592 (chain C and D, blue) with $\alpha^o\beta^c$ -BRD4592 (chain C, yellow and D, cyan and coral for COMM domain). In $\alpha^o\beta^c$, several residues are shifted toward BRD4592, resulting in more inhibitor-protein contacts in the $\alpha^o\beta^c$ -BRD4592 structure (67 contacts) compared to the $\alpha^o\beta^o$ -BRD4592 structure (57 contacts) (d) Superposition of the BRD4592 binding site from $\alpha^o\beta^o$ -BRD4592 (blue) with $\alpha G66V^o\beta^o$ (red). In the latter structure only the $\alpha V66$ side chain is shown, in a stick representation. From the structure, we conclude $\alpha V66$ likely prevents BRD4592 binding by sterically blocking the binding site.

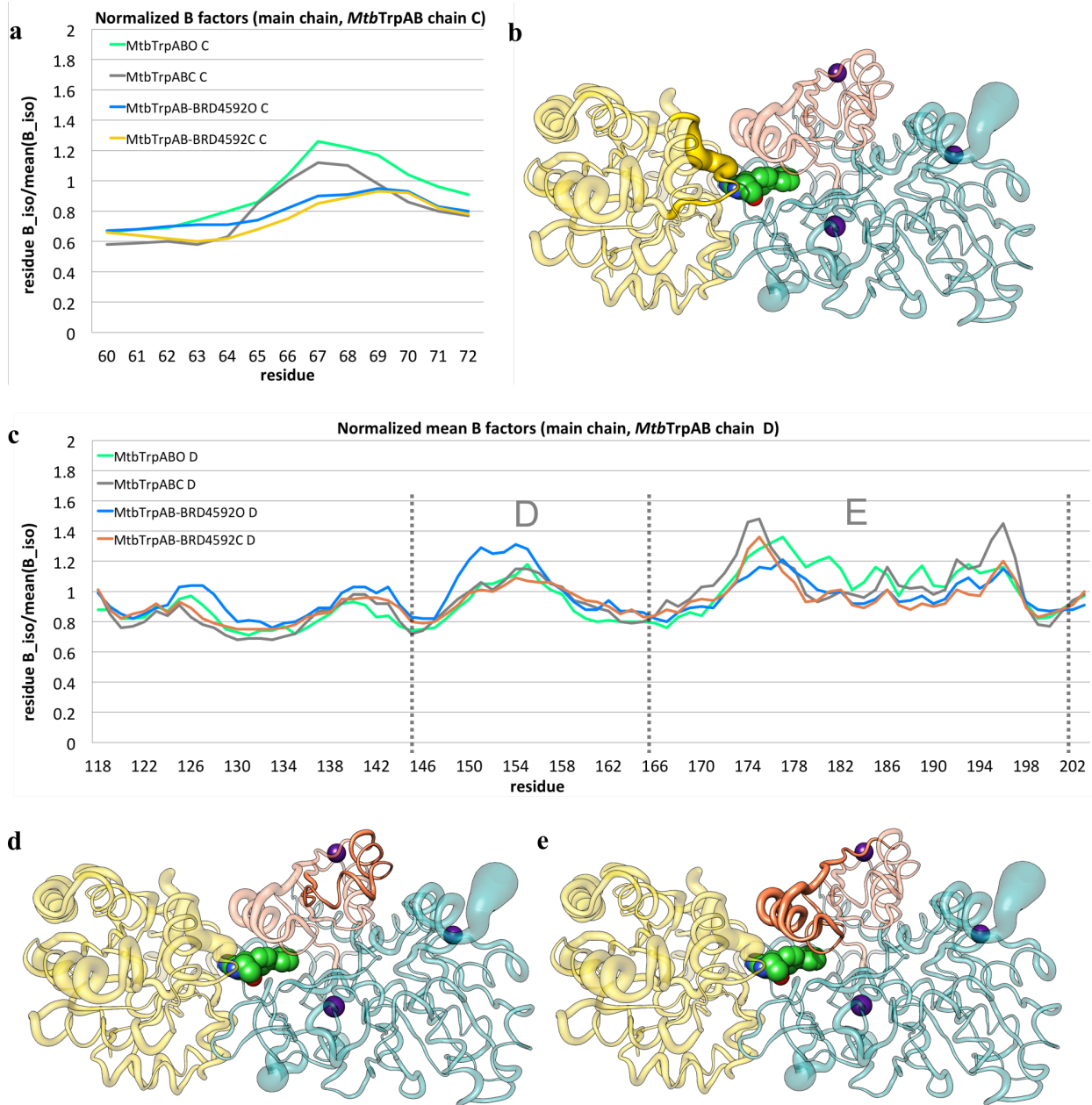


Figure 2.12. Temperature factors analysis for TrpAB structures. (a) Normalized mean main-chain B factors (B^N) plot for the α subunit loop $\alpha 12$ (residues 60-72). In both the $\alpha^O\beta^C$ and $\alpha^O\beta^O$ structures, BRD4592 reduces B factors in $\alpha 12$. (b) $\alpha^O\beta^C$ -BRD4592 structure shown as a tube with thickness proportional to the absolute value of $B^N(\alpha^O\beta^C\text{-BRD4592}) - B^N(\alpha^O\beta^C)$. The α subunit is shown in yellow and the β in cyan, with the COMM domain shown in coral. Cesium ions are shown as purple spheres. The BRD4592 ligand is shown with carbon atoms shown in green. The section corresponding the region plotted in a is shown in an opaque representation. (c) B^N plot for the β subunit from TrpAB structures covering the COMM domain. Sections D and E correspond to opaque regions shown in (d) (residues 145-165) and (e) (residues 166-200, including helix $\beta h6$), respectively. BRD4592 increases B factors for section D in $\alpha^O\beta^O$ and has no effect on the equivalent region in $\alpha^O\beta^C$, while it decreases B factors in section E, which is directly involved in the inhibitor binding and interface interactions, in both $\alpha^O\beta^O$ and $\alpha^O\beta^C$ states.

altered amino acids that were identified in resistant Mtb mutants, such as α G66 and β N185, are clustered along the azetidine-binding site, and the crystal structure of TrpAB with the α G66V mutation suggests that the α V66 isopropyl side chain sterically interferes with BRD4592 binding (Fig. 2.11d).

To understand the impact of L-Ser on the enzyme–BRD4592 interaction, we compared the $\alpha^O\beta^O$ -BRD4592 structure without L-Ser with the $\alpha^O\beta^C$ -BRD4592 structure with L-Ser bound (E_{AA} state). In $\alpha^O\beta^C$ -BRD4592 the inhibitor molecule has more contacts with the protein than in the $\alpha^O\beta^O$ -BRD4592 conformation (67 vs. 57 contacts) (Fig. 2.11c). This is consistent with ITC data showing that BRD4592 binding to Mtb TrpAB is tighter in the presence of L-Ser (Fig. 2.6).

We also find that BRD4592 binding affects the distribution of B factors around the inhibitor-binding site, seemingly reducing protein flexibility. Specifically, the α l2 loop, which contains the catalytic residue α D68, shows lower isotropic B factors in the presence of BRD4592 (Fig. 2.12a, b). A similar effect is observed for helix β h6, an α -subunit-facing section of the COMM domain that forms important activating interactions with the α subunit³⁷ (Fig. 2.12c-e). Multiple studies have established that the geometry of and the bonds formed by loops α l6 and α l2 have a pronounced effect on α subunit activity^{38,39}, with changes in protein elements nearby preventing proper positioning of catalytic residue α D68³⁷. Similar consequences can potentially result from reduced mobility of α l2 in the presence of BRD4592.

BRD4592 has a multifaceted mechanism of inhibition. Together, the biophysical and structural data reveal that BRD4592 is an allosteric inhibitor of both subunits, binding the α/β interface along the tunnel connecting the two. However, the data also point to a more complex mechanism of inhibition since BRD4592 increases enzyme affinity for substrates and products, stabilizes α/β subunit interactions, and shifts equilibrium toward closed, highly active conformations of the enzyme, all effects that are more commonly associated with allosteric activators.

Our results show that there are at least three components of TrpAB inhibition by BRD4592. First, indole production from IGP is prevented, likely due to a reduction in the flexibility in the α 12 loop and β h6 helix, which may interfere with proper positioning of α catalytic residues, and due to stabilization of the E_{AA} conformation of the β subunit, which may prevent further progression through the catalytic cycle. Using high enzyme concentrations, when IGP and L-Ser are used as substrates under saturating concentrations of BRD4592, we find that the α reaction is initially slowed 245-fold ($k_{cat}^{\alpha} = 0.08 \pm 0.01 \text{ min}^{-1}$ versus $19.6 \pm 3.9 \text{ min}^{-1}$ with no BRD4592) (Fig. 2.13c, d)

Second, BRD4592 also potently inhibits the β reaction, such that not all indole produced by the α site reaction is converted to L-Trp (Fig. 2.13e). At saturating concentrations of BRD4592 and high enzyme concentrations, we are initially able to detect production of L-Trp from indole and L-Ser at a rate 750-times slower than the uninhibited enzyme ($k_{cat}^{\beta} = 0.26 \pm 0.01 \text{ min}^{-1}$ and $197 \pm 8.8 \text{ min}^{-1}$, respectively) (Fig. 2.13a). BRD4592 stabilizes TrpAB bound to the indole analogue indoline and is uncompetitive with respect to indole (Fig. 2.8a, 2.5f), suggesting that BRD4592 may trap the enzyme in an indole-bound state, preventing catalytic cycling. Based on the location

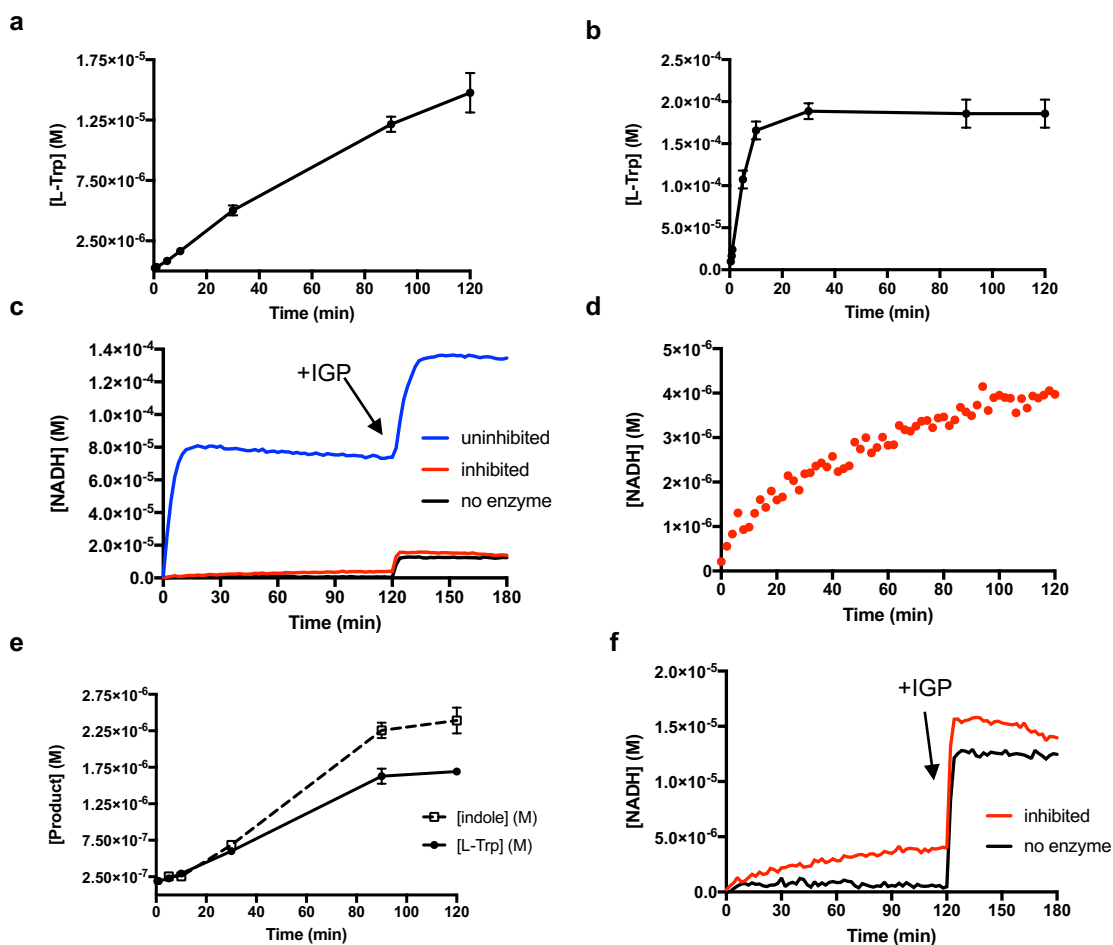


Figure 2.13. Activity of TrpAB under saturating inhibitor. (a) Production of L-Trp by TrpAB from saturating indole and L-Ser under saturating BRD4592. (b) Production of L-Trp under saturating indole and L-Ser, with 10 mM IPP. (c) Activity of TrpAB under saturating IGP and L-Ser with (red) or without (blue) saturating BRD4592, measured using the fluorescence G3P, GAPDH-coupled assay. In the uninhibited reaction, G3P is produced unimpeded until about 80 μ M product. At 120 minutes, additional IGP was added to the reaction. (d) Same as c, zoomed-in to show only the inhibited reaction. Though BRD4592 potentially inhibits the α reaction, the time dependence to inhibition suggests there are additional factors contributing to inhibition, such as stabilization of L-Trp-bound states of the enzyme and product inhibition by indole. (e) Production of L-Trp and indole by TrpAB under saturating IGP, L-Ser, and BRD4592 measured by LC-MS. Both production of L-Trp and indole are slowed significantly compared to uninhibited reactions. Interestingly, both the α and the β reactions stop completely at $[L-Trp] = 1.7$ μ M and $[indole] = 2.4$ μ M. (f) Same as c, zoomed in on the inhibited enzyme. Addition of IGP to the inhibited enzyme does not result in additional G3P production.

of BRD4592 binding, we hypothesize that part of the inhibition mechanism is also to block the movement of indole through the tunnel, which is the substrate's main mode of entry into the β active site^{117,138}. We presume that the observed, albeit slow, conversion of indole to L-Trp may be due to entry of indole via an alternative, less accessible path or to significantly slower entry via the tunnel. In contrast, the α -site ligands (IPP, F6, and F9) do not significantly inhibit the β reaction ($k_{\text{cat}}^{\beta} = 42 \text{ min}^{-1}$ under 10 mM IPP, Fig. 2.13b) despite the fact that they also block the tunnel¹³⁸. It is possible that BRD4592 is simply more effective at blocking the tunnel or that BRD4592 inhibits the β reaction through additional allosteric mechanisms.

Finally, there is a third component to BRD4592's mechanism of inhibition. Under saturating BRD4592, we observe time-dependent inhibition. Initially BRD4592 inhibits both the α and β reactions >200-fold, drastically reducing L-Trp production. However, after a small amount of L-Trp has been produced, the reaction completely stops (Fig. 2.13d, e). Addition of more IGP to this inhibited enzyme complex does not overcome the inhibition (Fig. 2.13f). BRD4592 is a reversible inhibitor, with no evidence of slow binding nor evidence that the azetidine nitrile reacts covalently with TrpAB to explain the time-dependent inhibition (Fig. 2.14). Instead, we hypothesize that this final component is due to product inhibition as BRD4592 increases enzyme affinity for L-Trp and stabilizes closed conformations of the L-Trp-TrpAB complex (Fig. 2.8b, c). Thus, any L-Trp that is produced by the inhibited enzyme may be trapped, preventing further catalytic cycling. By stabilizing multiple substrate- and product-bound states of TrpAB, BRD4592 results in complete inhibition that is not overcome by addition of substrate and is strengthened by any product that is produced. The complexity of BRD4592's mechanism may be the basis for its high

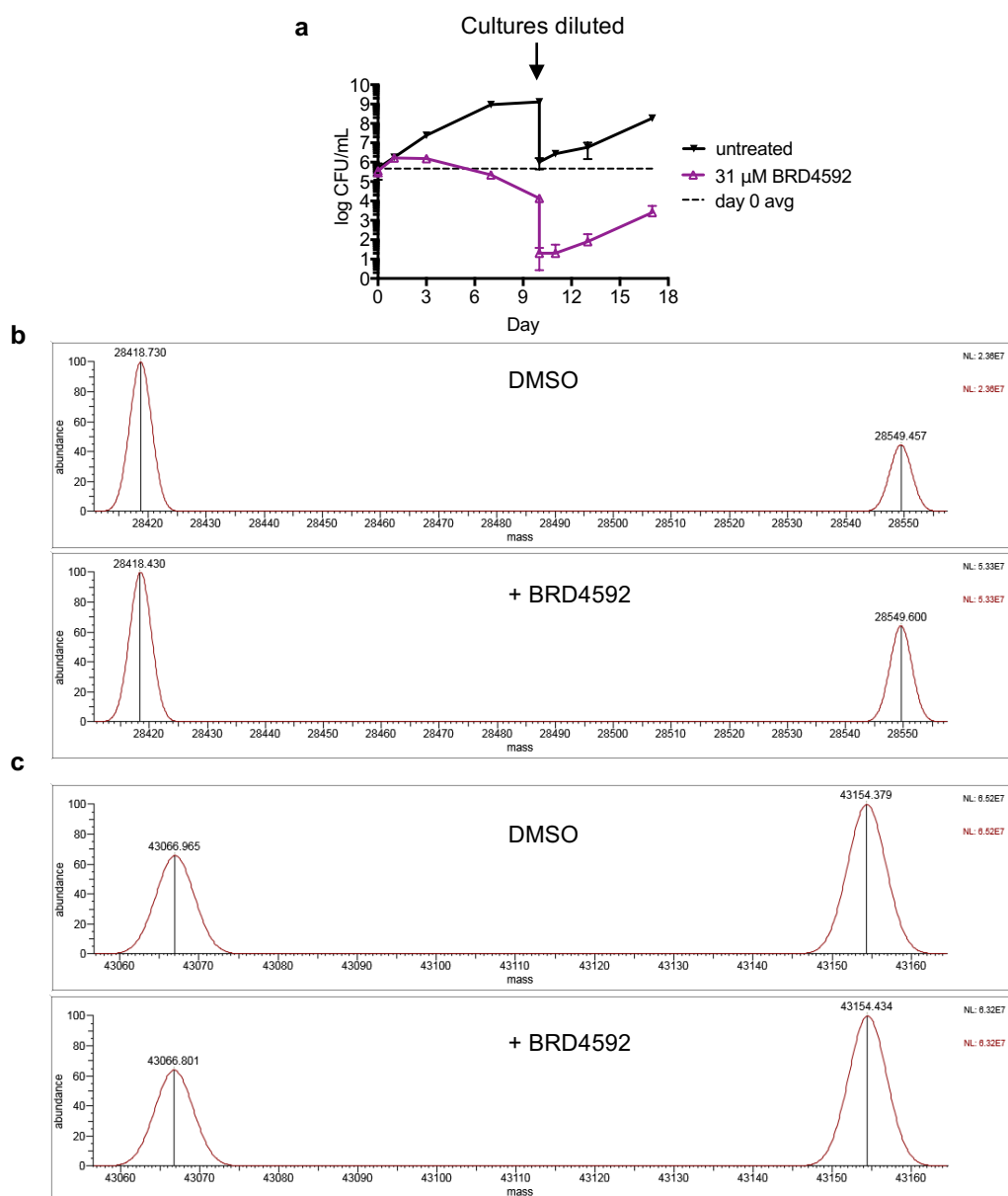


Figure 2.14. BRD4592 does not bind TrpAB irreversibly. (a) Effect of BRD4592 on WT Mtb. When treated with BRD4592, Mtb loses CFU, however, when the culture is diluted 1000-fold after 10 days of treatment, the remaining bacilli resume growth with little lag relative to DMSO controls. This indicates that BRD4592 inhibition of TrpAB is reversible¹³⁹. (b-c) Mtb TrpAB was pre-incubated with DMSO or BRD4592 then analyzed by LC-MS. The molecular weights observed for Mtb TrpAB are consistent with the TrpA protein (b) with a C-terminal 6-His-tag (28.55kDa) and for His-TrpA without its N-terminal methionine (28.42kDa). For TrpB (c), we observe peaks consistent with TrpB without its N-terminal methionine (43.16kDa) and with TrpB without its N-terminal methionine and serine residues (43.07kDa). Pre-incubation with BRD4592 does not change the apparent mass of TrpAB suggesting the inhibitor does not covalently modify the enzyme. Jump dilution experiments in which BRD4592 demonstrates a relatively rapid off-rate (Fig S7d) also indicate that BRD4592 does not bind TrpAB irreversibly.

potency. Though the mechanisms of allosteric inhibitors are rarely characterized in such detail, this study suggests that they may function through extremely complex mechanisms and that this may, in fact, be required for the development of effective inhibitors.

Section 2.3. Discussion

Significant effort is being invested in the discovery of new classes of antibacterial agents with novel mechanisms of action to counter the steady rise of resistance in bacteria including Mtb. We have identified a novel azetidine, BRD4592, with a new molecular target in Mtb. Genetic, metabolic, and biochemical data show that BRD4592 potently inhibits TrpAB, the enzyme catalyzing the final two steps in L-Trp biosynthesis, resulting in time-dependent bactericidal activity. Our data show that BRD4592 binds the protein–protein interface, revealing a new binding site in this well-studied enzyme. Unlike typical inhibitors that bind protein-protein interfaces¹⁴⁰, BRD4592 does not lead to complex disruption and, instead, stabilizes subunit interactions.

Paradoxically, despite a positive effect on enzyme stability and substrate affinity (hallmarks of allosteric activators), BRD4592 inhibits the overall production of L-Trp. BRD4592 binds at a site distant from both catalytic active sites, inhibiting the activity of both subunits without significantly changing the structure of the active sites. It has recently been proposed that allosteric effects, i.e. changes to function resulting from ligand binding outside the active site, need not involve conformational changes at the active site, but can arise from entropy-based changes in protein flexibility¹⁴¹. We suggest that BRD4592 ultimately acts as an inhibitor through a multi-component mechanism. First, by reducing flexibility in the α subunit and by stabilizing the E_{AA} state of the enzyme, BRD4592 inhibits

the α reaction. Next, BRD4592 also stabilizes TrpAB bound to indole and blocks the tunnel between the two active sites, likely hindering access of indole to the β active site, and inhibiting the β reaction. Finally, BRD4592 stabilizes a third state of TrpAB in which the enzyme binds its product L-Trp (E_{Q3}). Therefore, any initial L-Trp that is produced remains bound to TrpAB, preventing further catalytic cycling. To our knowledge, this is the most complicated and multifactorial allosteric inhibitor reported for TrpAB to date, and for allosteric inhibitors in general.

Allosteric inhibition has especially great appeal for targeting metabolic enzymes, which typically have shallow active sites designed to accommodate polar, hydrophilic substrates, characteristics that conflict with drug-like properties required for both target engagement and permeation through cell membranes^{15,92}. Indeed, previously developed α substrate mimetics such as IPP are poor inhibitors against Mtb TrpAB (IC_{50} = 260 μ M, whereas the IC_{50} BRD4592 = 70 nM). Secondly, because of the relatively limited number of substrate entities that are recognized with high affinity, strategies to inhibit enzymes using substrate-like mimetics often result in compounds that have significant off-target effects¹⁴²⁻¹⁴⁴. BRD4592, on the other hand, is not promiscuous, having no activity against hepG2 cells or non-mycobacterial bacteria and a narrow range of activity as reported in PubChem. This positions BRD4592 as a useful probe for understanding the biology of L-Trp biosynthesis, including the intriguing question of why starvation of some amino acids, including L-Trp, results in death for Mtb while starvation of others produces a static response⁹⁷.

There has been great interest in discovering allosteric inhibitors in many disease areas and our findings suggest a path for future discovery. Allosteric inhibitors often

stabilize a specific conformation of their enzyme target to prevent catalytic cycling. For example, a recent allosteric inhibitor of SHP2 functions by stabilizing the enzyme's inactive conformation¹⁴³. In contrast, BRD4592 stabilizes multiple conformational states, resulting in inhibition that is not easily overcome by changes in metabolic environment and is in fact enhanced by increases in substrate or product concentration. Cornish-Bowden has highlighted the extreme rarity of uncompetitive inhibitors and suggested that uncompetitive inhibitors of metabolic enzymes, or mixed-type inhibitors with significant uncompetitive components, are likely to be far more toxic than competitive inhibitors¹⁴⁵. This is due to substantially greater increases in intermediate concentrations as a result of uncompetitive inhibition and the inability of these high substrate concentrations to overcome uncompetitive inhibition. Indeed, we believe BRD4592 clearly demonstrates this principle. Given how diverse the host niche for Mtb can be and that the environment can fluctuate with regard to abundance of various nutrients and metabolites, it is very important for any antitubercular compound targeting central metabolism to be active in a variety of metabolic environments. As such, BRD4592 may represent a prototype of next generation allosteric inhibitors, developed for their complex mechanisms that result in increased potency and provide robust inhibition in the face of changing environmental conditions. Alternatively, these findings raise the possibility that existing allosteric inhibitors function through much more complex mechanisms than previously appreciated.

Finally, our findings suggest that highly dynamic, multi-subunit enzymes with natural allosteric regulation provide prime targets for such allosteric inhibitors. The heterogeneity observed in our collection of Mtb TrpAB crystal structures provides definitive evidence of conformational flexibility in this system, consistent with flexibility

reported in other TrpAB enzymes^{118,119,146}. Such flexibility is considered a critical feature of allosteric proteins, necessary for the communication of signals across protein subunits¹⁴¹. Here, we suggest that the different conformations required by the TrpAB complex throughout its catalytic cycle provide ample opportunity for small molecules to bind and destabilize or, in this case, stabilize certain enzyme states and reduce protein flexibility to prevent catalytic cycling. The complex inhibitory mechanism of BRD4592 indicates that the sensitivity of TrpAB's activity to different conformations makes it particularly vulnerable to inhibitors that can bind and disrupt the transmission of allosteric signals within the enzyme. Highly dynamic enzymes with multiple conformational states and natural allosteric regulation may, therefore, be top candidates for the development of allosteric inhibitors. In addition, this work suggests that understanding the relationship between inhibitor, substrate and product binding is an important aspect of probe discovery, both for the development of more potent inhibitors and for understanding enzyme dynamics and the various ways in which the enzyme's microenvironment could affect probe activity. The adoption of routine assessment of substrate and product interactions will, therefore, be important for the identification and development of allosteric inhibitors. For screening campaigns designed to identify novel allosteric inhibitors, a thorough characterization of confirmed hits with respect to altered affinities of substrates or products can potentially inform the rational prioritization of scaffolds. Thus, our discovery of an extremely unique and complex inhibitor suggests general principles that may lead to new highly potent allosteric inhibitors.

Acknowledgements. We thank J. Gomez, M. Serrano-Wu, and B. Hubbard for helpful discussion. We would also like to thank S. Combs and S. Minami for assistance with *in*

vivo studies. This work was supported by the Broad Institute Tuberculosis donor group, the Pershing Square Foundation, the Bill & Melinda Gates Foundation under grant OPP1032518 (SLS), the National Institute of Allergy and Infectious Diseases, National Institutes of Health, Department of Health and Human Services, under contracts HHSN272200700058C and HHSN272201200026C (AJ) and the U. S. Department of Energy, Office of Biological and Environmental Research, under contract DE-AC02-06CH11357 (AJ). For this work, University of Chicago is a subgrantee of Structural Genomics Consortium under a Bill & Melinda Gates Foundation grant for the Structure-Guided Drug Discovery Coalition (AJ & KM). DTH would like to dedicate this paper to Stuart Schreiber, in honor of his 60th birthday.

Author Contributions. SW performed experiments with Mtb as well as kinetic and biophysical experiments with TrpAB. PPN was responsible for chemistry. KM, NIM, RJ, and AJ were responsible for protein expression and purification, x-ray crystallography, and structure refinement and analysis. SJ and BB developed and performed LC-MS analysis of kinetic assays. VK and SW performed calorimetry. NS, AC, and SW performed *in vivo* experiments. PM contributed to structural analysis and modeling. SLF, AJ, SLS, and DTH advised on experiments and interpretation and together with SW, KM, and PPN wrote the paper.

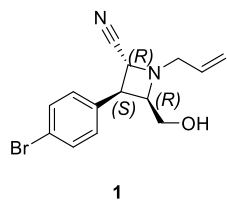
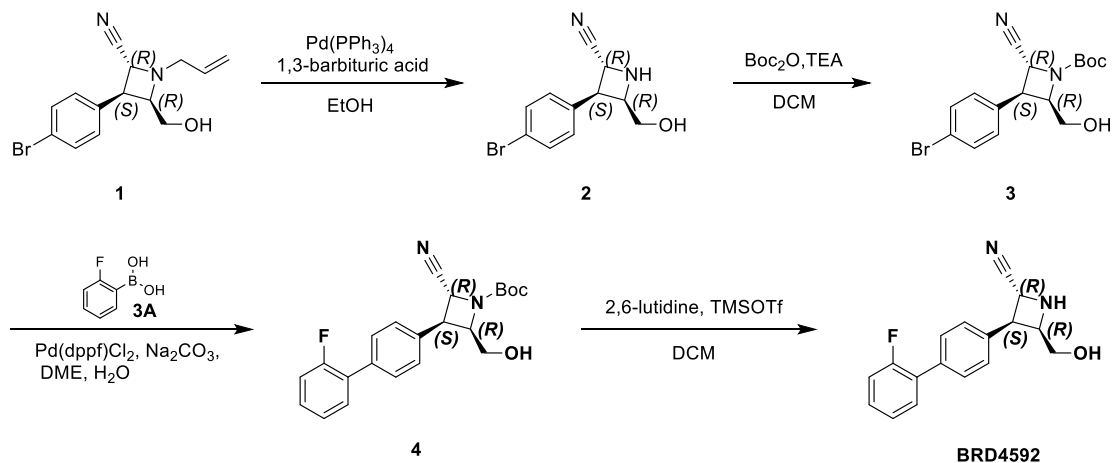
Section 2.4. Materials and Methods

High-throughput screening. The Broad Institute's synthetic Diversity Oriented Synthesis (DOS) library (82,762 compound) was screened against Mtb as previously reported¹⁹. Briefly, replicating Mtb ($OD_{600} = 0.6-0.8$) constitutively expressing GFP was incubated with 25 μ M compound, rifampicin (positive control) or DMSO (negative control) in 384-well plates for 3 days, at which time GFP fluorescence was read using a Spectramax M5. Z-scores were determined per plate and hits were determined using a family-wise error rate (FWER) cutoff of <0.025 . Hits were confirmed using 8 or 9 point dose-response.

Chemistry. All oxygen and/or moisture sensitive reactions were carried out under N_2 atmosphere in glassware that had been flame-dried under vacuum (0.5 mmHg) and purged with N_2 prior to use. All the reagents and solvents were obtained from commercial sources and used without further purification. NMR spectra were recorded on a Bruker 400 (400 MHz 1H , 101 MHz ^{13}C) or Varian (400 MHz 1H , 101 MHz ^{13}C) spectrometer. All chemical shifts are reported in parts per million (δ) with tetramethylsilane as an internal standard. Data are reported as follows: chemical shifts, multiplicity (br = broad, s = singlet, d = doublet, t = triplet, q = quartet, dd = doublets of doublet, m = multiplet; coupling constant(s) (J values) in Hz; integration). Unless otherwise indicated NMR data were collected at 25°C. Flash chromatography was performed using 100-200 mesh Silica Gel with the indicated solvent. LC-MS analysis was performed on a Shimadzu LC-20AB/AD separations module or Agilent 1200 series, operating in ESI (+ or -) ionization mode. Analytes were eluted using a linear gradient of 0.037% TFA/ H_2O (V/V), 0.018%

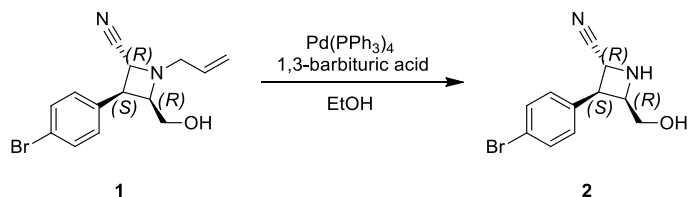
TFA/CH₃CN (V/V) or 10 mM NH₄HCO₃ containing H₂O/CH₃CN mobile phase. Preparative HPLC was performed on a Gilson 281 separations module or Shimadzu LC-8A separations module; MS spectra were recorded using a Waters 3100 with electrospray ionization. Samples were eluted using a linear gradient of 0.1% TFA in H₂O/CH₃CN or 0.04% HCl in H₂O/CH₃CN or 0.2% formic acid in H₂O/CH₃CN, or 10 mM NH₄HCO₃ in H₂O/CH₃CN, or 0.04% NH₄OH in H₂O/CH₃CN. Analytical thin layer chromatography (TLC) was performed on 0.2 mm silica gel plates. Visualization was accomplished with UV light and aqueous potassium permanganate (KMnO₄) stain followed by heating.

Synthesis of BRD4592



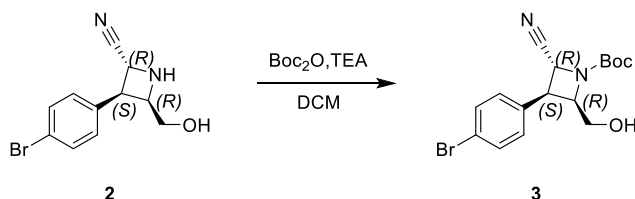
(2R,3S,4R)-1-allyl-3-(4-bromophenyl)-4-(hydroxymethyl)azetidine-2-carbonitrile (1):

For synthesis of **1**, please see Lowe, J.T. *et al.*¹⁴⁷.



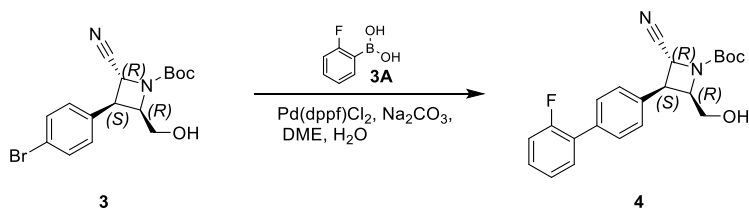
(2R,3S,4R)-3-(4-bromophenyl)-4-(hydroxymethyl)azetidine-2-carbonitrile (2).

To a mixture of (2R,3S,4R)-1-allyl-3-(4-bromophenyl)-4-(hydroxymethyl)azetidine-2-carbonitrile (**1**) (10.00 g, 32.55 mmol, 1.00 equiv) and 1,3-dimethylhexahydro pyrimidine-2,4,6-trione (7.62 g, 48.83 mmol, 1.50 equiv) in EtOH (50 mL) was added $\text{Pd(PPh}_3)_4$ (3.76 g, 3.25 mmol, 0.10 equiv) in one portion at 25°C under N_2 . The mixture was heated to 40°C and stirred for 1.5 hours. TLC indicated reactant was consumed completely. The reaction mixture was concentrated under reduced pressure and the residue was purified by column chromatography (SiO_2 , Petroleum ether/Ethyl acetate = 1:0 to 3:1) to yield **2** (13.00 g, 21.71 mmol, 66% yield) as a red oil. **LCMS** (ESI^+): 268 ($\text{M}+\text{H}$).



Tert-butyl (2R,3S,4R)-3-(4-bromophenyl)-2-cyano-4-(hydroxymethyl)azetidine-1-carboxylate (3). To a mixture of (2R,3S,4R)-3-(4-bromophenyl)-4-(hydroxymethyl)azetidine-2-carbonitrile **2** (13.50 g, 35.38 mmol, 1.00 equiv) and triethylamine (10.74 g, 106.14 mmol, 14.71 mL, 3.00 equiv) in DCM (50

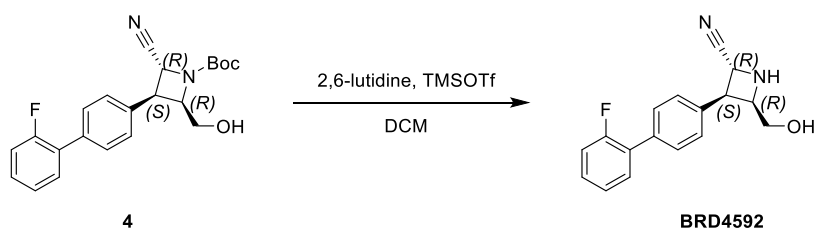
mL) was added di-*tert*-butyl dicarbonate (15.44 g, 70.76 mmol, 16.25 mL, 2.00 equiv) drop-wise at 25°C under N₂. The mixture was heated to 30°C and stirred for 2 hours. TLC indicated reactant was consumed completely. The reaction mixture was quenched with water (200 mL) and the aqueous phase was separated and extracted with DCM (200 mL × 3). The combined organic layers were washed with brine (200 mL), dried over Na₂SO₄, filtered and concentrated under reduced pressure to give a residue. The residue was purified by column chromatography (SiO₂, Petroleum ether/Ethyl acetate=1:0 to 8:1) to yield **3** (9.50 g, 25.61 mmol, 72% yield, 99% purity) as a yellow solid. ¹H NMR (400MHz, CDCl₃) 00MHz, CDCl₃ 61 mmol, 72% yield, 99% purity) as a yellow solid. idue. The residue was purified by column chromatography (SiO₂ 00 mL) and the aq**LCMS** (ESI⁺): 311 (M+H-*tert*-butyl).



***Tert*-butyl(2*R*,3*S*,4*R*)-2-cyano-3-[4-(2-fluorophenyl)phenyl]-4-**

(hydroxymethyl)azetidine-1-carboxylate (4). To a solution of *tert*-butyl (2*R*,3*S*,4*R*)-3-(4-bromophenyl)-2-cyano-4-(hydroxymethyl)azetidine-1-carboxylate **3** (4.00 g, 10.89 mmol, 1.00 equiv) and (2-fluorophenyl)boronic acid (1.68 g, 11.98 mmol, 1.10 equiv) in DME (70.00 mL) and H₂O (30.00 mL) was added Na₂CO₃ (4.62 g, 43.56 mmol, 4.00 eq) and Pd(dppf)Cl₂ (159.37 mg, 217.80 μmol, 0.02 equiv). The mixture was stirred at 90°C for 3 hours after which point LCMS analysis showed completion of the reaction. The reaction mixture was further diluted with H₂O (40 mL) and extracted with ethyl acetate

(100 mL × 3). The combined organic phase was washed with brine (30 mL), dried with anhydrous Na₂SO₄, filtered and concentrated in vacuum. The residue was purified by silica gel chromatography (Petroleum ether/Ethyl acetate=30/1, 5/1) to yield **4** (4.20 g, 9.88 mmol, 90% yield, 90% purity) as a light yellow solid. ¹H NMR (400MHz, CDCl₃) NMR (400MHz) *J* = 6.8 Hz, 2H), 7.43 (dt, *J* = 1.8, 7.7 Hz, 1H), 7.40 - 7.30 (m, 3H), 7.25 - 7.12 (m, 2H), 4.97 (br d, *J* = 3.5 Hz, 1H), 4.84 (br s, 1H), 4.20 - 4.10 (m, 1H), 3.70 - 3.60 (m, 1H), 3.40 (br d, *J* = 11.0 Hz, 1H), 1.56 (s, 9H). **LCMS** (ESI⁺): 327 (M+H-*tert*-butyl).



(2*R*,3*S*,4*R*)-3-(2'-fluoro-[1,1'-biphenyl]-4-yl)-4-(hydroxymethyl)azetidine-2-carbonitrile; (BRD4592).

To a solution of *tert*-butyl (2*R*,3*S*,4*R*)-2-cyano-3-[4-(2-fluorophenyl)phenyl]-4-(hydroxymethyl)azetidine-1-carboxylate **4** (4.20 g, 10.98 mmol, 1.00 equiv) in DCM (120 mL) was added 2,6-lutidine (7.06 g, 65.88 mmol, 7.67 mL, 6.00 equiv) and TMSOTf (12.20 g, 54.90 mmol, 9.92 mL, 5.00 equiv). The resulting solution was stirred under N₂ for 16 hr at 20°C. LCMS showed the reaction was complete. The mixture was concentrated, MeOH (100 mL) was added, and stirring was resumed at 40°C for 30 min. The solution was concentrated and purified by preparative scale HPLC (neutral condition). After lyophilization, 1.5 g of purified solid was obtained. The solid was then dissolved in MeCN (100 mL) and filtered to remove some floccules. The filtrate was concentrated, water (50 mL) was added, and after lyophilization, BRD4592 (1.26 g, 100% purity) was isolated as

a white solid. ^1H NMR (400 MHz, DMSO- d_6) δ 7.54 – 7.48 (m, 3H), 7.40 (br d, J = 7.9 Hz, 3H), 7.32 - 7.25 (m, 2H), 5.00 - 4.91 (m, 1H), 4.54 (t, J = 4.8 Hz, 1H), 4.29 (t, J = 8.1 Hz, 1H), 3.95 (br s, 1H), 3.27 (br s, 1H), 3.22 - 3.13 (m, 1H). ^{13}C NMR (101MHz, DMSO- d_6) δ = 160.80, 158.36, 136.01, 134.16, 131.14, 130.05, 129.97, 129.12, 129.09, 128.43, 125.44, 121.88, 116.70, 116.48, 62.24, 61.88, 47.27, 45.15. HRMS (ESI) calcd for $\text{C}_{17}\text{H}_{15}\text{FN}_2\text{O}$ $[\text{M} + \text{H}]^+$ 282.1168, found 282.1171.

Bacterial strains and growth conditions. *Mtb* (Mtb) H37Rv was used for all experiments unless otherwise noted. Mtb was grown at 37°C in Middlebrook 7H9 supplemented with 10% OADC and 0.2% Tween-80 and 0.05% glycerol or on Middlebrook 7H10 plates supplemented with 10% OADC and 0.5% glycerol. H37Rv ΔtrpA was grown in the same medias supplemented with 1 mM L-Trp. The plasmid pUV3583c was used to constitutively overexpress *trpA* in WT H37Rv and H37Rv $\Delta\text{trpA}::\text{trpA}$.

M. marinum, *M. smegmatis* (mc²155), *M. goodii* (ATCC #14470), *M. intracellulare* (ATCC #13950), *M. kansasii* (ATCC #12478), *M. abscessus* (ATCC #19977), *M. fortuitum* (ATCC #6841), *Salmonella typhimurium* (SL1344), *Pseudomonas aeruginosa* (PA01), *Staphylococcus aureus* Newman, *Vibrio cholerae* (O395 and C6706), *V. cholera* O395 ΔtolC , *Escherichia coli* (K12), and *E. coli* ΔtolC . *M. smegmatis* was grown in Middlebrook 7H9 supplemented with albumin, dextrose, and saline. All other mycobacteria were grown in 7H9 supplemented with 10% OADC, 0.2% glycerol and 0.05% Tween-80. *S. typhimurium* was grown in Mueller-Hinton Broth and in N-minimal media¹⁴⁸. All other strains were grown in LB, M9 minimal medium, and M9 media

supplemented with casamino acids. Activity of BRD4592 was tested in both rich and minimal media.

Determination of dose response curves, MIC₉₀s. Bacteria were grown to mid-log phase, then added to 96 well plates at OD₆₀₀ = 0.025 and grown in the presence varying [BRD4592] for 2 weeks. Growth was assessed by reading OD₆₀₀. The minimal inhibitory concentration, MIC₉₀, was defined as the minimum concentration that inhibited growth by 90% relative to a DMSO control.

For growth curves, Mtb was grown to mid-log phase and diluted to OD₆₀₀ = 0.0025 in inkwells containing the indicated amounts of BRD4592 in triplicate. Aliquots were plated to determine colony forming units (CFU) at the time points indicated.

Generation of resistant mutants. The agar MIC of BRD4592 was determined by plating bacteria on agar containing a dose response of compound in a 96-well format. Resistant mutants were generated by plating 1×10^9 bacteria on agar containing 2X, 4X, and 10X the agar MIC. Four independent parent clones are used in order to avoid the selection of drug-resistant siblings. Colonies were inoculated into liquid media containing 2X the liquid MIC of the compound. These cultures were retested in a liquid MIC assay to confirm resistance and used to generate genomic DNA for whole genome sequencing.

TrpA sequences and alignment. FASTA sequences for TrpA from each bacteria were downloaded from UniProt (uniprot.org) and aligned using the multiple sequence alignment tool Clustal Omega from EMBL-EBI¹⁴⁹.

Mtb *trpAB* gene cloning. The *trpB-trpA* operon was amplified from the genomic DNA of *Mtb* H37Rv using the following primers:

5'-GGAGTAAAGATAATGAGTGCTGCCATCGCCGAAC and

5'-GTGATGGTGATGATGTGCGGACATCCCTAGTCGTACC using KOD HOT START polymerase in the presence of 2.5 M monohydrate betaine. PCR product was purified and treated with T4 polymerase in the presence of dGTP according to previously published methods^{150,151} followed by ligation independent cloning (LIC) to pMCSG81

(<http://dnasu.org/DNASU/GetVectorDetail.do?vectorid=661>)^{152,153}. Vector pMCSG81 expresses proteins with the non-cleavable C-terminal 6 His tag. The expression of Mtb TrpB from the polycistronic operon was satisfactory but Mtb TrpA expression was rather low. Altering the ribosome-binding site (rbs) upstream of the *trpA* gene improved expression level. Polymerase Incomplete Primer Extension (PIPE) cloning was performed as described previously^{154,155} using the two primers:

5'-GTTTAACTTTAAGAAGGAGATATACATATGGTGGCGGTGGAACAGAGC and

5'-CTCCTTCTTAAAGTTAAACACCATTTCAGTCGTTGCCAGCAAGCCAAAC

generating MtbTrpB-MtbTrpA-pMCSG81 plasmid. To further increase the expression of the TrpA subunit the *trpA* gene alone was inserted using LIC into vector pMCSG81-pRSF with resistance to kanamycin and the RSF origin of replication (primers

5'-GGAGTAAAGATAATGGTGGCGGTGGAACAGAGC and

5'- GTGATGGTGATGATGTGCGGACATCCCTAGTCGTACC). The resulting plasmid was named *Mtb*TrpA-pMCSG81-pRSF. For production of stable Mtb TrpAB complex *E. coli* BL21-Gold (DE3) was co-transformed with both vectors.

Mtb TrpAB expression. MtbTrpB-MtbTrpA-pMCSG81 and MtbTrpA-pMCSG81-pRSF were co-transformed to *E. coli* BL21-Gold (DE3) and selected against ampicillin (150 µg/mL) and kanamycin (30 µg/mL) in LB media supplemented with 40 mM K₂HPO₄ and 2 g glucose per liter (LB-PO₄-glucose media). A starter culture was grown overnight at 37°C and 200 rpm. On the following morning 12 liters of LB-PO₄-glucose media with antibiotics was inoculated with overnight culture. After reaching OD₆₀₀ of 1.0, the culture was cooled to 20°C and supplemented with 50 µM pyridoxal 5'-phosphate (PLP) and protein expression was induced with 0.3 mM IPTG. The growth was continued for another 20 hours at 20°C at 190 rpm. An additional LB media culture of 6 liters with only MtbTrpA-pMCSG81-pRSF was grown under the same conditions. Finally, cells harvested from 12 L of MtbTrpB-MtbTrpA-pMCSG81 and 6 L of MtbTrpA-pMCSG81-pRSF were suspended in buffer A (150 mM KCl, 50 mM HEPES:NaOH pH 7.5, 20 mM imidazole pH 8.0, 5% glycerol, 1mM TCEP, 1 mM PLP, 1 mM L-Ser). The cell suspension was frozen and stored at -80°C. αG66V and βN185S mutants were overexpressed in the same conditions using appropriate plasmid combination.

αG66V and βN185S mutants. PIPE cloning procedure was performed on plasmids MtbTrpB-MtbTrpA-pMCSG81 and MtbTrpA-pMCSG81-pRSF. The following primers: 5'-GGACCCGGTCATGGACGGCCCCACCAT and 5'-CGTCCATGACCGGGTCCGAATACGGAAC were used for amplification resulting in MtbTrpB-MtbTrpA(G66V)-pMCSG81 and MtbTrpA(G66V)-pMCSG81-pRSF. An identical procedure was performed to create MtbTrpB(N185S)-MtbTrpA-pMCSG81 using the

following primers: 5'- GACGCCATCAGTGAGGCGTTCCGGGATTGGGTT and 5'- GAACGCCTCACTGATGGCGTCTTTGAGCGTTTTCGA. Both proteins were purified as described for the wild-type enzyme.

Mtb TrpAB purification. Frozen cells were thawed and sonicated (5 min total time, 130W power output) and spun at 30,000 g at 4°C for 1 hour. The initial Ni²⁺-affinity purification step was performed using a Flex-Column 2.5x10 cm connected to a Van-Man vacuum manifold (Promega). Supernatant was loaded on 5 mL Ni²⁺ Sepharose (GE Healthcare Life Sciences) equilibrated with buffer A and mixed thoroughly with the resin. Vacuum of 15 psi was used to speed up removal of supernatant as well as wash out of unbound proteins (200 mL of buffer A). TrpAB complex was eluted with 25 mL buffer A supplemented with 500 mM imidazole pH 8.0. The eluate was concentrated to about 2 mL and loaded on a Superdex 200 16/70 size exclusion column (GE Healthcare Life Sciences) equilibrated with buffer A. Successful crystallization required the presence of two protein peaks, one containing the TrpAB complex with another containing excess of the TrpA subunit. Fractions containing TrpAB complex were collected and buffer A was replaced with crystallization buffer (150 mM KCl, 20 mM HEPES:NaOH pH 7.5, 1 mM PLP, 1 mM L-Ser, 1 mM TCEP) on Amicon 100 kDa cut-off concentrators (Millipore). The TrpAB complex was concentrated to ~36 mg/mL. The same procedure was applied to α G66V and β N185S mutant purification. During purification, sample exposure to light was reduced as much as feasible.

Mtb TrpAB *in vitro* kinetic assays. Prior to use, frozen, purified protein was dialyzed against buffer containing 20 mM HEPES (pH 8.0), 100 mM KCl, 40 μ M PLP, and 0.5 mM TCEP (TrpAB buffer). For most kinetic assays, 100 nM TrpAB was used. IC₅₀ against the β reaction was determined using 50 nM TrpAB and rates under saturating BRD4592 (Fig. 2.13) were determined using 500 nM TrpAB. TrpAB concentration was calculated based on the weight of the TrpAB dimer.

In the fluorescence-based assay, TrpAB was prepared in TrpAB buffer with 0.5 mM glyceraldehyde-3-phosphate dehydrogenase (GAPDH), 2.5 mM NAD⁺ and 0.015 M sodium pyrophosphate (pH 8.5) with 0.03 M sodium arsenate^{128,156}. Substrates were added to the wells of a black 96-well plate with a clear, flat bottom and enzyme in buffer was added to start the reaction. Reaction progress was monitored by NADH fluorescence (excitation 340 nm, emission 460 nm).

In the liquid chromatograph-mass spectrometry (LC-MS) based assay, TrpAB was prepared in TrpAB buffer. After 5-10 minutes incubation, reactions were quenched using 3 volumes 0.1% formic acid in methanol followed by storage at 4°C for two hours. Samples were then centrifuged and an aliquot of the supernatant was diluted 1:1 with water. 3.75 μ L of this final solution was injected. L-Trp and indole were detected by UPLC-MS (Waters). Compounds were quantitated by SIR on a SQ mass spectrometer by negative electrospray ionization. The SIR method was set for L-Trp at 203.4 m/z and for indole at 116.3 m/z. Mobile phase A consisted of 0.1% ammonium hydroxide in water, while mobile phase B consisted of 0.1% ammonium hydroxide in acetonitrile. The gradient ran from 2% to 95% mobile phase B over 2.65 minutes at 0.9 mL/minute. An Acquity BEH C18, 1.7 μ m 2.1x50 mm column was used with column temperature maintained at 65°C.

V_{\max} , K_M , and k_{cat} values were determined using non-linear fitting based on Michaelis-Menten kinetics in GraphPad Prism. BRD4592 inhibition data was analyzed using non-linear enzyme inhibition equations in GraphPad Prism. For BRD4592 versus L-Ser (with saturating IGP), the a mixed-type inhibition model fit the data best ($R^2 = 0.9841$) whereas for BRD4592 versus IGP (with saturation [L-Ser]), the mixed and uncompetitive inhibition models fit equally well ($R^2 = 0.9883$). The lines in a double reciprocal plot of 1/Rate versus 1/[IGP] (Fig. 2d) are nearly parallel and using this analysis method, α values are < 0.00001 , making BRD4592 effectively uncompetitive versus IGP.

Isothermal calorimetry. Isothermal calorimetry was performed using a MicroCal Auto-iTC200. 250 μM BRD4592 was injected into a cell containing 45 μM Mtb TrpAB in TrpAB buffer. Buffer, DMSO and L-Ser concentrations were matched between the syringe (containing the compound) and the cell (containing the protein) to ensure all observed effects were due only to the compound. BRD4592 was added in forty 1 μL injections at 25°C with reference power set to 10 $\mu\text{Cal/sec}$. Results were analyzed using Origin software.

ANS binding assay. 8-anilino-1-naphthalene sulfonic acid (ANS) (20 μM) was incubated in a quartz cuvette with Mtb TrpAB (10 μM) in TrpAB buffer with or without L-Ser (20 mM) and without added PLP. To ensure ANS and TrpAB concentrations remained constant, concentrated BRD4592 was prepared in TrpAB buffer with ANS (20 μM) and TrpAB (10 μM) with or without L-Ser (20 mM) and titrated into the cuvette. The fluorescence spectrum of ANS was measured using a spectramax M5 to excite at 380 nm and read

emission from 400 – 600 nm. The change in fluorescence emission at 480 nm was used to calculate the $K_d^{apparent}$ of BRD4592 by fitting to a hyperbolic equation (eq 2.1)¹²².

$$\Delta F = (F_i - F_n)[BRD4592]/(K_d^{apparent} + [BRD4592]) \quad (2.1)$$

Static UV-Vis absorbance spectra. Static UV-Vis absorbance spectra were measured on a Cary 4000. L-Ser was titrated into Mtb TrpAB (15 μ M) in TrpAB buffer without PLP, with or without BRD4592 (200 μ M) and the absorbance spectrum from 350 to 550 nm was collected. Binding of L-Ser to Mtb TrpAB was followed by changes in the absorbance at 412 nm, corresponding to the disappearance of the substrate-free species. Titration plots were fit to a hyperbolic equation (eq 2.2) to calculate $K_d^{apparent, L-Ser}$ ¹²². For L-Trp binding, the same experimental conditions were used, except binding was calculated based upon changing absorbance at 475 nm¹³¹.

$$\Delta A = (A_\infty - A_0)[L-Ser]/(K_d^{apparent, L-Ser} + [L-Ser]) \quad (2.2)$$

To assess the effect of indoline (2,3-dihydro-1H-indole) on the absorbance spectrum, 30 mM indoline was added to 15 μ M Mtb TrpAB with 20 mM L-Ser in TrpAB buffer without PLP and the absorbance spectrum from 350 nm to 550 nm was collected. 200 μ M BRD4592 was added and the absorbance spectrum was measured again.

Differential Scanning Calorimetry (DSC). Mtb TrpAB (0.5 mg/mL) was diluted in TrpAB buffer and melted using a GE Healthcare Microcal VP Capillary DSC. Data was collected

from 20-110°C, with 200°C/hour scan rate and 8 sec. filtering period. Data was analyzed in Origin software. For experiments involving L-Ser, TrpAB was incubated with L-Ser for at least 2 hours prior to melting.

Crystallization & ligand soaking. Crystallization experiments were conducted using the sitting drop vapor-diffusion method with the help of the Mosquito liquid dispenser (TTP LabTech) in 96-well CrystalQuick plates (Greiner Bio-One), where 0.4 μ L of protein and 0.4 μ L of crystallization solution were mixed and the mixture was equilibrated against 135 μ L of corresponding well solution. Trials were performed at 4°C and 16°C using several protein-to-reservoir ratios (2:1, 1:1, 1:2) and commercially available screens. Crystals usually appeared the next day and continued growing and forming in more conditions with time. The crystals suitable for structure determination appeared in 5 to 90 days. Tests showed that some crystals contained the Mtb TrpB protein only. The best crystals of the Mtb TrpAB complex appeared at 16°C in the PEG/Ion/F6 condition (8% v/v tacsimate pH 8.0, 20% w/v PEG 3350) but initially diffracted to 4 Å only. Crystallization from the PEG/Ion/F6 condition was optimized by altering pH, precipitant concentrations and using two Additive Screens (Hampton Research and Jena Bioscience). Ultimately, the Additive Screen from Hampton at 16°C and 2:1 protein-to-reservoir ratio produced robust diffraction quality crystals which were also suitable for inhibitor soaking. Further improvement of the purification protocol also enabled obtainment of better quality crystals in the original screen condition. Crystallization plates were kept in dark.

Crystals of the Mtb TrpAB complex in the open conformation ($\alpha^O\beta^O$) were obtained from PEG/Ion/F6 with additive B4 (8% v/v tacsimate pH 8.0, 20% w/v PEG3350, 0.1 M

KCl). For data collection at 100 K, the crystals were cryoprotected with mother liquor supplemented with 17% (v/v) ethylene glycol. The structure in the closed conformation ($\alpha^O\beta^C$) was obtained from crystals grown with additive G1 (8% v/v tacsimate pH 8.0, 20% w/v PEG3350, 3% w/v trimethylamine *N*-oxide dihydrate) and soaked for 3-5 min in the mother liquor with 80 mM CsCl, 30 mM L-Ser and 17% (v/v) ethylene glycol for cryoprotection.

The structure of the TrpAB complex with BRD4592 in the open conformation ($\alpha^O\beta^O$ -BRD4592) was obtained from crystals from the initial condition PEG/Ion/F6 which were soaked with 10 mM BRD4592 and 15% v/v ethylene glycol for 2-3 min. For the $\alpha^O\beta^C$ -BRD4592 structure in closed conformation, the TrpAB complex was co-crystallized with the BRD4592 inhibitor in PEG/Ion/F6 conditions with additive A1 (8% v/v tacsimate pH 8.0, 20% w/v PEG3350, 10 mM BaCl₂, 1 mM BRD4592) and crystal was soaked with 100 mM CsCl and 50 mM L-Ser for 2-3 min followed by cryoprotection with 16% (v/v) ethylene glycol.

The structure of the α G66V mutant in the open conformation (α G66V β^O) was obtained from crystals grown in the original condition PEG/Ion/F6 and cryoprotected with 20% v/v ethylene glycol.

Data collection. Prior to data collection at 100 K, all cryoprotected crystals were flash-cooled in liquid nitrogen. The x-ray diffraction experiments were carried out at 0.9793 Å wavelength at the Structural Biology Center 19-ID beamline at the Advanced Photon Source, Argonne National Laboratory. The diffraction images for $\alpha^O\beta^O$, $\alpha^O\beta^O$ -BRD4592, $\alpha^O\beta^C$ -BRD4592 and α G66V β^O were recorded on the ADSC Q315r detector while those

for $\alpha^O\beta^C$ were recorded on the Pilatus3 6M detector. The datasets were processed with the HKL3000 suite¹⁵⁷. Intensities were converted to structure factor amplitudes in the Ctruncate program^{158,159} from the CCP4 package¹⁶⁰.

Structure solution and refinement. The $\alpha^O\beta^O$ structure was solved by molecular replacement in Phaser¹⁶¹ with the *Salmonella enterica* homolog (PDB code 1KFJ) as a search template. Following autobuilding in PHENIX¹⁶², the final model was obtained through alternating manual rebuilding in COOT¹⁶³ and maximum-likelihood refinement in PHENIX and Refmac^{160,164}. Similarly, the subsequent structures were manually corrected in real space and crystallographically refined in Refmac. The refinement protocol included optimization of TLS parameters with 1 group per protein chain. The atomic coordinates and structure factors have been deposited in the Protein Data Bank under accession codes 5TCF ($\alpha^O\beta^O$), 5TCG ($\alpha^O\beta^C$), 5TCI ($\alpha^O\beta^O$ -BRD4592), 5TCJ ($\alpha^O\beta^C$ -BRD4592), 5TCH ($\alpha G66V^O\beta^O$). For these structures, 98.1, 97.9, 97.7, 97.9, and 98.1% of residues fall into favored regions of the Ramachandran plot, with 3, 4, 4, 4, and 3 residues being outliers, respectively.

Structure analysis. Superpositions were performed using the SSM algorithm¹⁶⁵, as implemented in CCP4¹⁶⁰. For analysis of atomic displacement parameters, a separate refinement run in Refmac was performed with no TLS. The resulting model was used for further calculations in PHENIX¹⁶². Cavity volumes were calculated in SPACEBALL¹⁶⁶, with probe radius of 1.42 Å, grid size of 0.3 Å in all directions and one rotation. Alternative conformations were removed for calculations. Analysis of contacts between BRD4592

and the protein was performed in UCSF Chimera, with default parameters¹⁶⁷. Structural figures were prepared in UCSF Chimera and The PyMOL Molecular Graphics System, Version 1.6 Schrödinger, LLC.

Jump dilutions. TrpAB (1 μ M) in buffer with or without L-Ser was incubated with or without BRD4592 (1.5 μ M) for 30 minutes at RT. The mixture was diluted 100-fold with buffer containing IGP for a final reaction mixture with 10 nM TrpAB, 0.5 mM L-Ser, 30 μ M IGP and 15 nM BRD4592. The reaction was incubated for 60 minutes to allow production of measurable levels of L-Trp and activity was measured using LC-MS detection of L-Trp. As a control, TrpAB that was not pretreated with BRD4592 was treated with BRD4592 upon addition of IGP to start the reaction.

Liquid Chromatography-Mass Spectrometry (LC-MS). Mtb TrpAB (0.2 mg/mL) was incubated with BRD4592 (250 μ M) or DMSO for 2-3 hours at room temperature. TrpAB protein intact mass was determined using LC-ESI-MS (QExactive; ThermoFisher). Briefly, 10 μ L of protein (0.1 mg/mL) was injected onto a 3.5 μ m 2.1x100 mm Zorbax 300SB-C8 column (Agilent Technologies) in 85% aqueous (0.1% formic acid/water) and 15% organic (0.1% formic acid/acetonitrile) phases. The protein was eluted using a linear gradient from 15% to 75% organic phase over 10 minutes. The mass spectrometer settings were as follows: positive mode, full-MS scan range (800-2100 m/z), resolution: 70,000, AGC target: 3e6, maximum inject time: 200 ms, microscans: 3, sheath gas flow rate: 35, aux gas flow rate: 5, sweep gas flow rate: 0, spray voltage: 3.5 kV, capillary temp: 340 °C, S-

lens RF level: 90, aux gas heater temp: 35°C. Collected spectra were deconvoluted using the ReSpect algorithm (Protein Deconvolution 2.0; Thermo Scientific).

**Chapter 3: Exploring central metabolism as a therapeutic
target: Mycobacterial responses to amino acid starvation**

Attributions

****Marked portions**** of this chapter were prepared as a manuscript by S. Wellington *et al.* for submission to *Nature Chemical Biology* and reformatted for this dissertation. A. Clatworthy, N. Sidiqqi, S. Combs, and S. Minami were collaborators on zebrafish and murine studies.

Chapter 3: Exploring central metabolism as a therapeutic target: Mycobacterial responses to amino acid starvation

Abstract

Mycobacterium tuberculosis (Mtb) is a highly successful intracellular pathogen with disease progression marked by the formation of dense clusters of immune cells called granulomas. The host environment within cells and within granulomas is limited in oxygen and certain nutrients, presenting very stressful conditions to infecting bacilli. While little is known about the exact nutrients available during infection, Mtb is able to scavenge some metabolites, such as tryptophan (L-Trp), from the host. Here, we use chemical tools to investigate the mycobacterial requirements for amino acid biosynthesis in various environments. We previously discovered BRD4592 to be a selective inhibitor of mycobacterial tryptophan synthase (TrpAB), which is the enzyme responsible for the final steps in L-Trp biosynthesis. Using BRD4592 as well as genetic tools, we found that **TrpAB is required for the survival of Mtb and *Mycobacterium marinum* during *in vivo* infection and that this requirement may be independent of an adaptive immune response.** We also took advantage of two inhibitors of branched-chain amino acid synthesis to compare the mycobacterial response to L-Trp starvation to the response to branched-chain amino acid starvation. Interestingly, both starvations induced an apparent stringent response in mycobacteria, but the response is not protective as the bacilli ultimately die. Altogether, this work supports the therapeutic efficacy of inhibiting proteins that are required *in vivo*, despite their apparent dispensability under *in vitro* conditions, and creates a foundation for understanding the mechanisms underlying these requirements for survival.

Section 3.1. Background

Current antibiotics target a narrow range of processes, primarily inhibiting various enzymes involved in macromolecular synthesis^{14,15}. Though full of promise, central metabolism has historically been very challenging to inhibit¹⁵. **Biosynthetic pathways in central metabolism are robust in that they must be able to maintain function in diverse environments even while the requirement for the pathway for survival varies across conditions^{15,91}. Many enzymes in central metabolism become essential only under certain conditions and we are only just beginning to uncover which functions are required for survival during the different stages of an *Mycobacterium tuberculosis* (Mtb) infection.** For example, when considering targeting amino acid biosynthesis, it becomes apparent that fluctuating *in vivo* concentrations of metabolites and substrates may affect the essentiality of any given enzyme. **Recently, the concept of conditional essentiality – that the requirement for a gene or pathway is highly dependent on the specific physiological setting¹⁶⁸⁻¹⁷⁰ – has fundamentally challenged the criteria for drug-discovery target validation and advanced the field from a reliance on data generated from growth in rich laboratory media to growth in minimal media and ultimately, to *in vivo* studies.

This is especially important for L-tryptophan (L-Trp) biosynthesis as it tends to be exquisitely regulated in most microorganisms, with the activity of the pathway depending upon the environment¹²⁰.** Little is known about how or if L-Trp biosynthesis is regulated at the transcriptional level in Mtb, but enzymes in the pathway are inhibited by L-Trp²⁶, indicating some level of post-translational feedback inhibition. Additionally, **Mtb has been previously reported to scavenge L-Trp from the host, and recent reports have argued that L-Trp biosynthesis becomes essential only in the context of adaptive immune

responses, once CD4⁺ T cells produce interferon- γ (IFN γ), which in turn induces indoleamine 2,3-dioxygenase (IDO) expression and subsequent degradation of host pools of L-Trp²⁶.** Thus, it is unclear if L-Trp biosynthesis is required in the early stages of infection.

Further, while starvation of some amino acids is bactericidal for Mtb, starvation of others results in a static response^{97,98}. Deletions of genes responsible for L-Trp biosynthesis⁹⁷ or for branched-chain amino acid biosynthesis are both bactericidal for mycobacteria⁹⁶ while deletion of enzymes involved in proline biosynthesis produce a static response⁹⁷. Our discovery of BRD4592 (Fig. 3.1a, Chapter 2), a highly specific inhibitor of mycobacterial tryptophan synthase (TrpAB), allows us to probe the requirement for TrpAB in various environments and the bactericidal response to L-Trp starvation. Here, we studied TrpAB in Mtb and in *M. marinum* (Mm) and *M. smegmatis* (MSm), which are both sensitive to BRD4592 (Chapter 2) due to the high level of conservation of TrpAB amongst the mycobacteria (85.87 and 79.01 percent identity, respectively, for TrpA compared to Mtb TrpA). **We provide genetic evidence that TrpAB is indeed required for the survival of Mtb in macrophages and in mice, and show that BRD4592 is effective in targeting TrpAB in a whole organism model of mycobacterial infection using *Danio rerio* (zebrafish). Our data also suggest that the requirement for L-Trp biosynthesis during *in vivo* infection is likely not dependent on T cells, which differs from what has been previously suggested²⁹.**

We went on to probe the mycobacterial response to branched-chain amino acid starvation using sulfometuron methyl (SMM) (Fig. 3.1a), an herbicide previously shown to inhibit acetohydroxy acid synthase (AHAS)⁴⁶, and norvaline (Fig. 3.1a), an inhibitor of

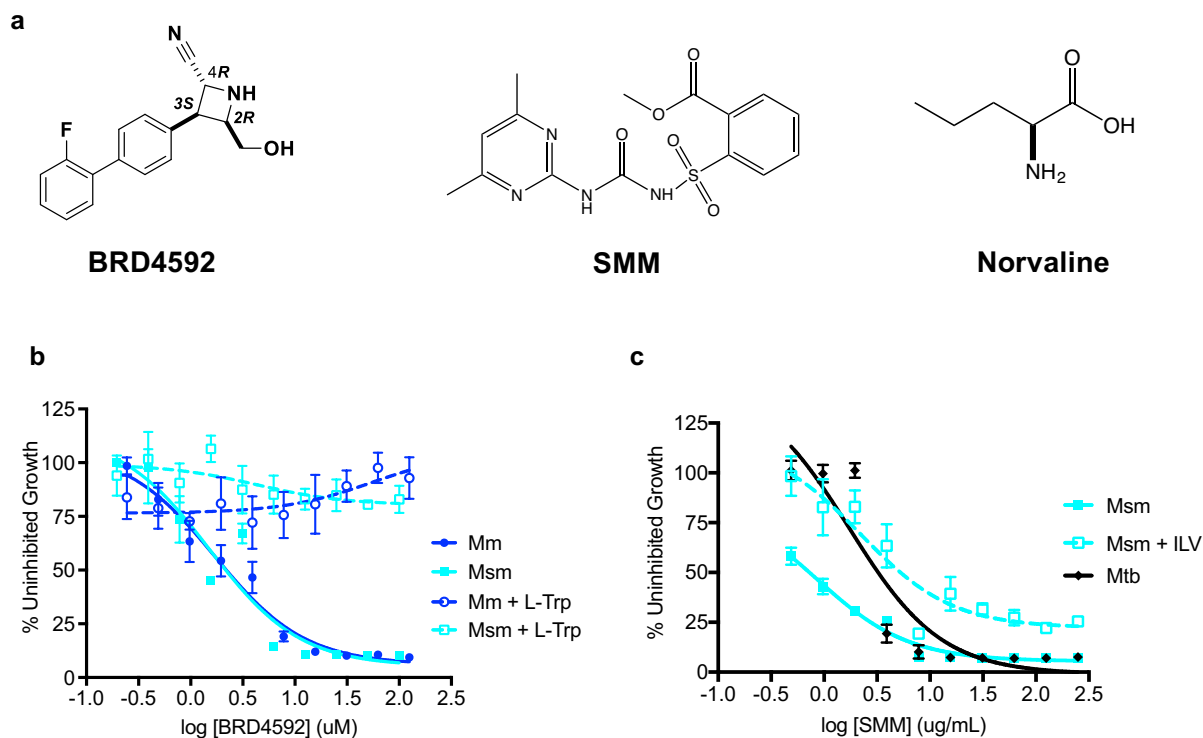


Figure 3.1. Structure and activity of amino acid synthesis inhibitors. (a) BRD4592, SMM, and norvaline chemical structures. **(b)** Activity of BRD4592 against *M. marinum* (Mm) and *M. smegmatis* (Msm) with and without L-Trp supplementation. BRD4592 is an inhibitor of L-Trp biosynthesis that can be overcome by supplementation of L-Trp (1 mM) in the growth media. **(c)** Activity of SMM against Mtb and Msm. SMM is an inhibitor of branched-chain amino acid synthesis and can be overcome by supplementation of L-Ile, L-Leu, and L-Val (1 mM each; ILV) in the growth media.

L-leucine (L-Leu) and L-isoleucine (L-Ile) tRNA aminoacylation^{171,172}. We found that starvation of either L-Trp or branched-chain amino acids induces a transcriptional response consistent with activation of the stringent response. However, inhibition of branched-chain amino acid synthesis or tRNA charging results in the upregulation of genes encoding the enzymes responsible for branched-chain amino acid synthesis while inhibition of TrpAB has no apparent effect on the expression of L-Trp biosynthetic genes. Interestingly, though an apparent stringent response is induced, it is not protective in the context of L-Trp starvation. Comparing these responses to the mycobacterial response to starvation of other amino acids, such as L-Pro, will provide insights into the mechanisms underlying the essentiality of various amino acid biosynthetic enzymes and may serve as a basis for understanding the essentiality of and utility of targeting enzymes in central metabolism more generally.

Section 3.2. Results

****Mtb TrpAB is essential in vivo.** BRD4592 is potent *in vitro*, and its inhibition is not overcome by increases in substrate concentration, making it an attractive inhibitor for *in vivo* applications. However, the ability to render the inhibitor ineffective against whole Mtb cells in environments with sufficient levels of L-Trp raises questions about TrpAB's essentiality under relevant *in vivo* conditions. Though other enzymes in the Mtb L-Trp biosynthetic pathway have previously been studied^{26,97}, the *in vivo* essentiality of Mtb TrpAB has not been assessed. Recent reports have suggested that Mtb can scavenge L-Trp from the host. However, these studies also show that CD4⁺ T cell-produced F γ Ny activates the host enzyme IDO, which degrades host pools of L-Trp, suggesting bacterial

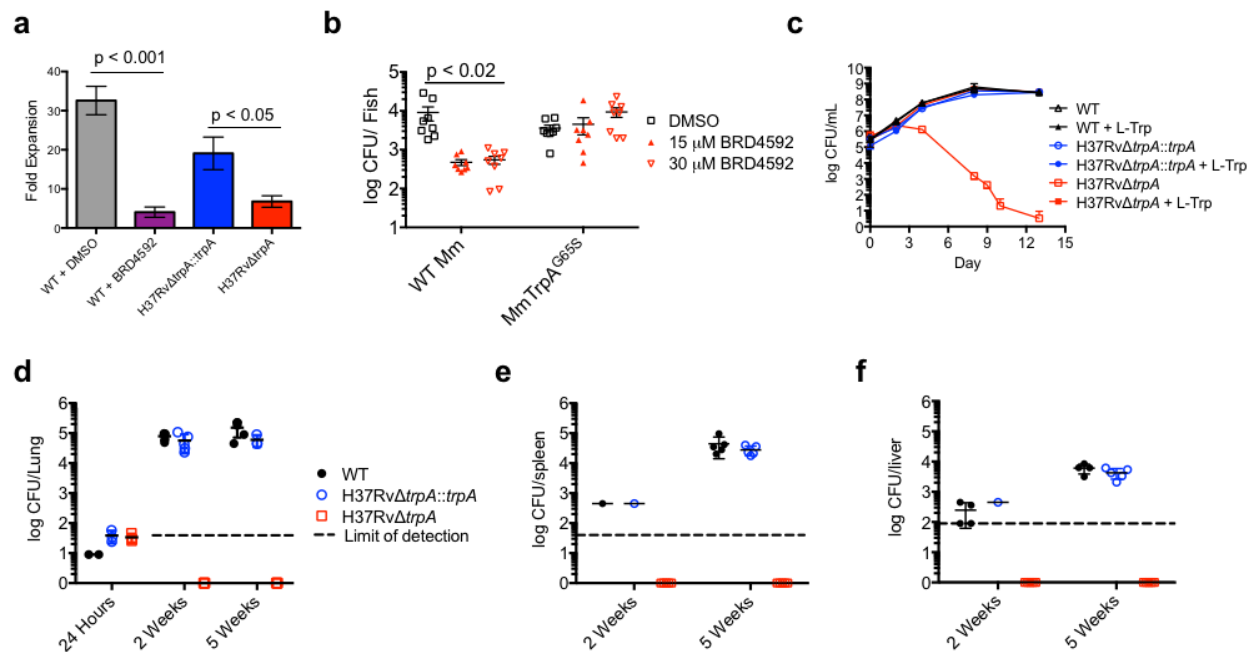


Figure 3.2. TrpAB is required for survival of Mtb in various conditions. (a) Fold expansion in J774 macrophages (Day 3 CFU/Day 0 CFU) of H37RvΔtrpA, H37RvΔtrpA::trpA, DMSO-treated WT (control) and BRD4592-treated WT Mtb. The deletion mutant and BRD4592-treated WT Mtb are attenuated. Significance is determined by an unpaired two-tailed t-test. (data are mean ± s.e.m. for four biological replicates and are representative of three independent experiments). (b) Effect of BRD4592 on *M. marinum* in zebrafish embryos/larvae following 5 days of treatment. Growth of wild-type *M. marinum* (WT Mm) is restricted by BRD4592, while a BRD4592-resistant mutant (MmTrpA^{G65S}) is unaffected by the compound. (data are representative of two independent experiments. n = 8 fish per condition; significance is determined by two-way ANOVA and Turkey's multiple comparison test). (c) Growth of wild-type Mtb (WT), H37RvΔtrpA, and H37Rv trpA::trpA in rich media with and without L-Trp supplementation shows the deletion mutant requires L-Trp for survival. (data are mean ± s.d. for three biological replicates and are representative of three independent experiments). (d) Survival of WT Mtb, H37RvΔtrpA, and H37RvΔtrpA::trpA, in C57BL/6 mouse lungs. At both the two-week and five-week time points, H37RvΔtrpA is severely attenuated, with no bacteria recovered (limit of detection = 1 CFU at 24 hr and 45 CFU at week 2 and 5). CFU/organ is plotted for spleen (e) and liver (f). As in the lungs, H37RvΔtrpA was below the limit of detection in spleen and liver (45 CFU and 90 CFU, respectively). (n = 3 mice per strain at 24 hours and n = 5 mice per strain at 2 and 5 weeks).

L-Trp biosynthetic machinery is essential due to the action of an adaptive immune response²⁶. Of note, these studies used tail vein injection to administer Mtb to mice rather than aerosol infection, which is the more natural mode of Mtb delivery and results in slower onset of adaptive immunity.

We first used BRD4592 to assess the essentiality of TrpAB beyond axenic culture using Mtb infection of macrophages. Treatment of WT Mtb-infected macrophages with BRD4592 restricts Mtb growth 8-fold compared to a DMSO control (Fig. 3.2a). Next, we turned to a whole organism model, using Mm infection of *Danio rerio* (zebrafish) embryos, a natural host-pathogen pair. We found that after 5 days of treatment, BRD4592 restricts Mm growth in zebrafish by about 1.5 logs compared to DMSO-treated controls (Fig. 3.2b), demonstrating the requirement for TrpAB in an *in vivo* setting. Furthermore, when we infected zebrafish with a BRD4592-resistant strain of Mm harboring a mutation in *trpA* (MmTrpA^{G65S}; Mm α 65 is equivalent to Mtb α 66) we found that the mutant was not affected by BRD4592 treatment (Fig. 3.2b). This demonstrates that the effect of BRD4592 is indeed due to the compound's activity against TrpAB. Interestingly, because the adaptive immune system has not yet matured in zebrafish at this early stage of development, this infection model has no T cells at the time of infection (2 days post fertilization (dpf)), with mature T cells leaving the thymus only at 6 dpf^{173,174}.

While we were unable to assess the efficacy of BRD4592 in mice due to the pharmacokinetic properties of the molecule (mouse liver microsome intrinsic clearance (CL_{int}) = 336.2 μ L/min/mg and hepatocyte CL_{int} = 47.2 μ L/min/ 10^6 cells), we sought to confirm the results of TrpAB essentiality in zebrafish using a genetic model in mammalian cells. We constructed a strain of Mtb with an in-frame clean deletion of *trpA* (H37Rv Δ *trpA*).

As expected, this strain requires L-Trp for growth *in vitro* (Fig. 3.2c). The profile of H37Rv $\Delta trpA$ viability loss when L-Trp is removed in axenic culture follows the same pattern as the cell death observed when WT cultures are treated with BRD4592 in that both treatment with BRD4592 and L-Trp starvation of the auxotroph result in a single round of replication followed by loss of Mtb CFU. H37Rv $\Delta trpA$ is also attenuated in macrophages (Fig. 3.2a), consistent with prior evidence of the essentiality of L-Trp biosynthesis in the intracellular milieu of macrophages^{26,97}. When H37Rv $\Delta trpA$ is complemented with an episomal copy of *trpA* (H37Rv $\Delta trpA::trpA$), growth in the absence of supplemented L-Trp and survival in macrophages is restored (Fig. 3.2a, c).

To assess the essentiality of Mtb TrpAB in a mammalian host, C57BL/6 mice were infected with aerosolized H37Rv $\Delta trpA$, H37Rv $\Delta trpA::trpA$, or WT Mtb. Mice were sacrificed at 24 hours, 2 weeks and 5 weeks post-infection. Importantly, at the 24-hour time point, equal numbers of H37Rv $\Delta trpA$ were recovered (~50 CFU/mouse) as for the WT strain, confirming all strains were delivered to the lungs (Fig. 3.2d). The $\Delta trpA$ mutant was severely attenuated at later infection time points and, in fact, was below the limit of detection in lung (45 CFU/lung), spleen (45 CFU/spleen), and liver (90 CFU/liver) at both week 2 and week 5 (Fig. 3.2d-f). In contrast, the WT and complemented strains grew to comparable levels of ~50,000 CFU/lung by week 2 and had disseminated to the liver and spleen by week 5 (Fig. 3.2d-f). As significant adaptive immune responses and IFN γ expression in the lungs are not observed until after 2 weeks post-infection in this well-characterized infection model¹⁷⁵, the inability to recover H37Rv $\Delta trpA$ bacteria at 2 weeks suggests that the L-Trp biosynthetic machinery is likely to be essential independent of the CD4⁺ T cell-mediated IFN γ response to deplete host L-Trp. Altogether, our findings

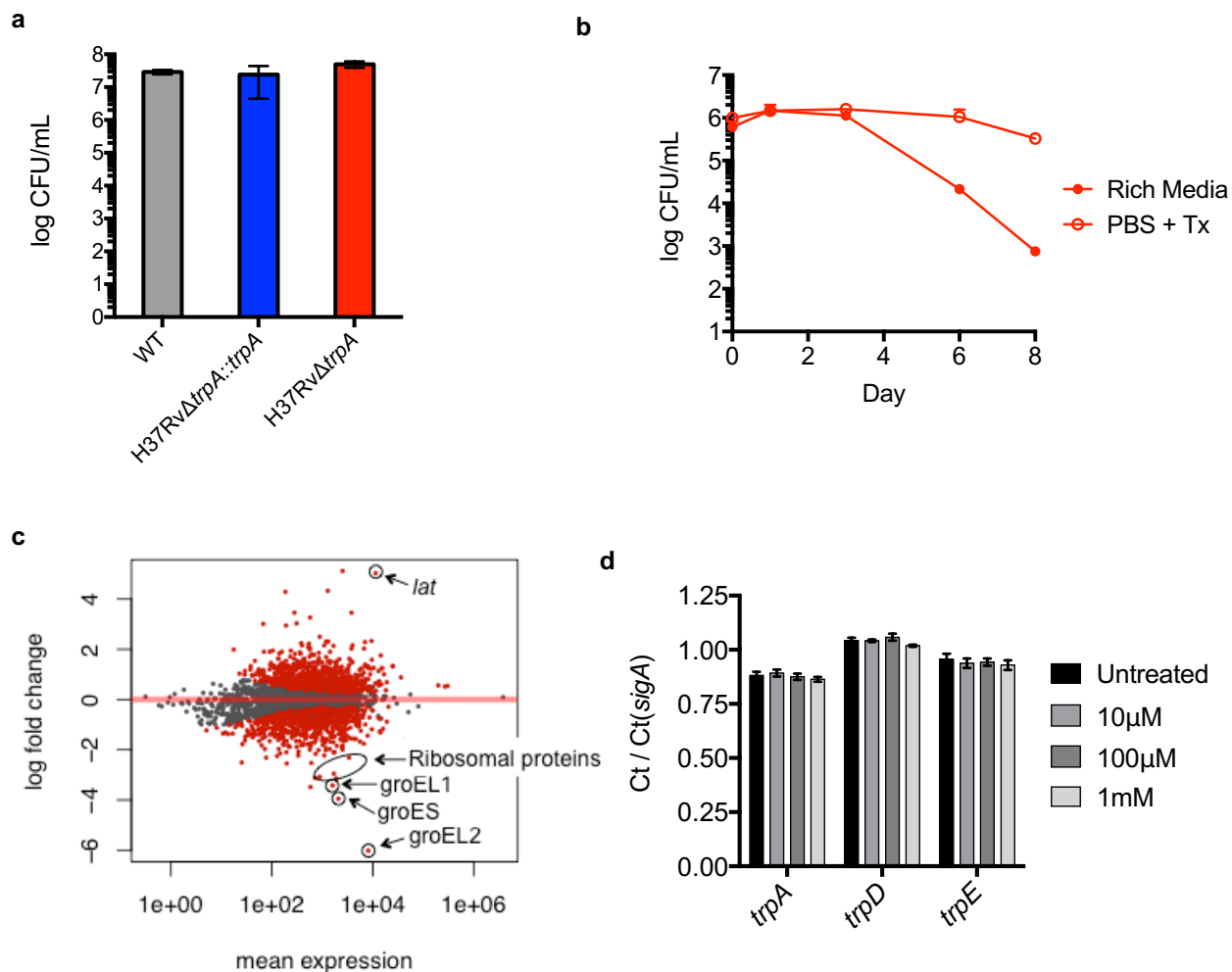


Figure 3.3 Mycobacterial response to L-Trp starvation. (a) Survival of WT Mtb (grey bar), H37RvΔtrpA (red bar), and H37RvΔtrpA::trpA (blue bar) starved in PBS/Tyloxopol for 42 days. When starved of all nutrients, all strains do not grow, but survive equally well. (b) CFU over time of H37RvΔtrpA when grown in rich media (red, closed circles) or when incubated in PBS/Tyloxopol (PBS + Tx; red open circles). When starved only of L-Trp, the auxotroph loses CFU over time. (c) log(2) fold change vs. mean abundance of genes in Mtb in response to 6 hours of treatment with 6 μM BRD4592 (2X MIC). Red dots represent genes that are significantly differentially expressed ($p < 0.05$) between DMSO- and compound-treated samples. The Mtb transcriptional response to longer treatment (24h) and to higher compound concentrations (31 μM) is similar. (d) RT-qPCR of L-Trp biosynthetic genes from Mtb grown in rich media supplemented with the indicated [L-Trp] for 48 hours. Cycle threshold (Ct) values are normalized to *sigA*. 1mM L-Trp is nearly 10-fold greater than the concentration of L-Trp required to support growth of an Mtb L-Trp auxotroph (H37RvΔtrpA) but results in no change in the expression of L-Trp biosynthetic genes in WT Mtb.

demonstrate that L-Trp biosynthesis is required for mycobacteria during *in vivo* infection, and that TrpAB inhibitors, such as BRD4592, can be highly effective *in vivo*.**

Probing the bactericidal response to L-Trp starvation. Though starvation of L-Trp is bactericidal for Mtb in rich media, we and others have observed that when Mtb is starved, either in PBS (Fig. 3.3a, b) or in water⁹⁷, deletion of L-Trp biosynthetic genes no longer results in a loss of CFU and is instead static, which is indistinguishable from the effect of total nutrient starvation on WT Mtb. Therefore, we hypothesized that cell death from L-Trp starvation may be due to the absence of a stress response that is activated and protective during total nutrient deprivation. The RelA-mediated stringent response is activated in several bacteria, including mycobacteria, in response to amino acid starvation or inhibition of tRNA-aminoacylation^{171,172}. This response is not only protective against amino acid starvation, but also confers some level of antibiotic tolerance to *Pseudomonas aeruginosa* biofilms¹⁷⁶. However, it was not known if L-Trp starvation induces the stringent response in mycobacteria.

In order to understand the response of mycobacteria to L-Trp starvation, we performed RNA-Seq on Mtb treated with BRD4592 for 3 or 6 hours – importantly, this time point was chosen such that the treated and control bacteria were in the same phase of growth and comparisons of the two groups measure the effect of the compound rather than effects due to growth phase. Surprisingly, we found that inhibition of TrpAB by BRD4592 resulted in transcriptional changes consistent with activation of the stringent response (Fig. 3.3c). Genes involved in protein synthesis and folding were downregulated^{171,177} and *lat*, a gene known to be upregulated in Msm during the stringent

response¹⁷⁸, was one of the most highly upregulated genes. In order to determine if we could use the faster-growing Msm as a model to further study amino acid starvation, we also performed RNA-Seq on Msm treated with BRD4592 and found the transcriptional response to be similar (Fig. 3.4d). Notably, L-Trp biosynthetic genes appear to be constitutively expressed *in vitro* and were not differentially regulated in response to BRD4592 treatment in either mycobacteria (Fig. 3.4d). We and others have also found that L-Trp biosynthetic genes are not downregulated in Mtb in response to L-Trp supplementation in the growth media⁹⁷ (Fig. 3.3d). Although mycobacteria respond to L-Trp starvation in a manner consistent with the stringent response, in this case, it is not protective against cell death.

Mycobacterial response to starvation of branched-chain amino acids. Norvaline has been shown to induce the stringent response in Msm¹⁷² even though it does not effectively inhibit bacterial growth. Even at 5 mg/mL, norvaline, only slightly delayed Mtb growth (Fig. 3.4a). The transcriptional response of Mtb treated with norvaline, was consistent with induction of a stringent response with genes involved in translation down regulated (Fig. 3.4d). Unlike L-Trp starvation, however, norvaline treatment resulted in the upregulation of genes involved in branched-chain amino acid synthesis.

SMM is an herbicide known to inhibit acetohydroxy acid synthase (AHAS), which is an enzyme required for branched-chain amino acid synthesis. SMM has previously been shown to inhibit AHAS in Mtb⁴⁶ and inhibits the growth of both Mtb and Msm (Fig. 3.1c). This inhibition is overcome by addition of L-Leu, L-Ile, and L-Val to the growth medium (Fig. 3.1c). Deletion of *ilvB1* and subsequent branched-chain amino acid

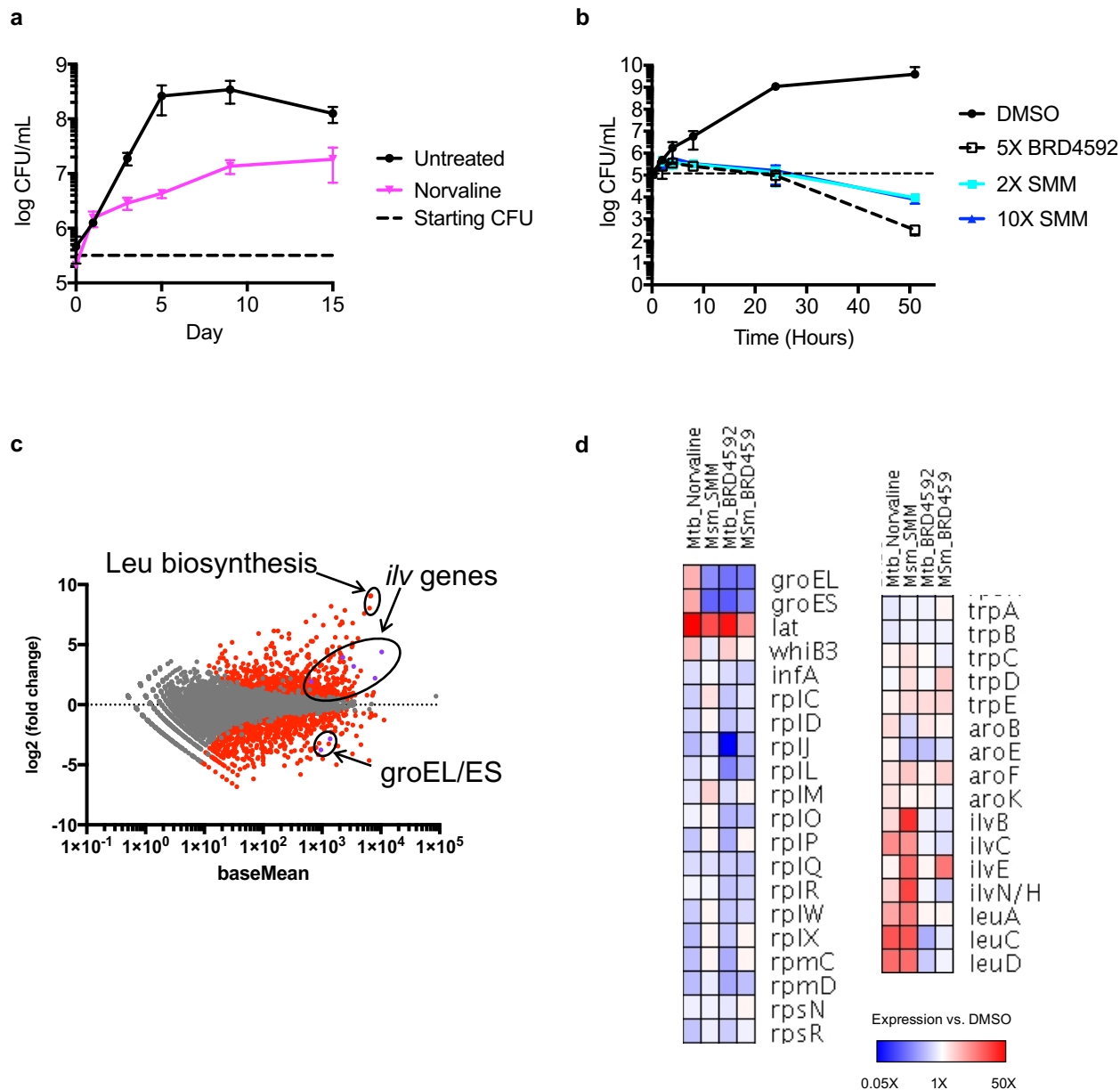


Figure 3.4. Mycobacterial response to branched-chain amino acid starvation. (a) Mtb growth when treated with norvaline (5 mg/mL). (b) Msm survival when treated with SMM (16 μ g/mL or 75 μ g/mL for 50 hours). (c) Msm transcriptional response to 20 minutes of treatment with 16 μ g/mL SMM (2X MIC). Red dots represent genes that are significantly differentially expressed ($p < 0.05$) between DMSO and compound-treated samples. Genes involved in the synthesis of branched-chain amino acids and in protein folding are shown as purple dots. (d) Heat map colored according to change in expression of genes compared to DMSO-controls in Mtb or Msm treated with Norvaline (5 mg/mL), SMM (16 μ g/mL) or BRD4592 (6 μ M) for 6 hours (Mtb) or 20 minutes (Msm). Genes involved in translation and protein folding are downregulated. Norvaline and SMM treatment result in increased expression of genes involved in branched chain amino acid biosynthesis while treatment with BRD4592 has no effect on aromatic amino acid biosynthesis.

starvation results in loss of viability in Mtb⁹⁶, however SMM treatment reduced Msm CFU only after a prolonged treatment (Fig. 3.4b). Like norvaline treatment, SMM treatment of Msm resulted in a transcriptional response consistent with induction of the stringent response and in upregulation of genes involved in branched-chain amino acid synthesis, including *ilvB* (Fig. 3.4c, d). The two most highly upregulated genes in SMM-treated Msm (>500 fold-change), MSMEG_2288 and MSMEG_1008, are both hypothetical with gene ontology suggesting L-Lue biosynthesis activity. Perhaps the upregulation of genes responsible for branched-chain amino acid biosynthesis accounts for the relatively static response of mycobacteria to treatment with norvaline and SMM.

Section 3.3. Discussion

Chemical genetics, or the use of small molecules to probe the function of a biological system, is a powerful tool for understanding processes required for bacterial survival and virulence^{179,180}. Probes, such as BRD4592 and SMM are useful tools for exploring the requirements for L-Trp and brached-chain amino acid biosynthesis, respectively, in mycobacteria throughout the course of an infection and across various environments. They also can be used to understand the basis for the response of mycobacteria to various amino acid starvations.

******Here, in an *in vivo* model of mycobacterial infection, we show that BRD4592 is effective against Mm in zebrafish embryos/larvae and that this efficacy is due to the compound's inhibition of TrpAB. As the infection is carried out over the first 7 days of development and T cells are not detectable outside the thymus until 6 dpf¹⁷⁴, it is less likely T cells are important in restricting Mm infection in this context. IFN γ , however, is

known to be present in embryos and important for defense against infection many days prior to full T cell maturation¹⁸¹. Thus, IFN γ may still be responsible for TrpAB essentiality in this infection model. Furthermore, TrpAB is required for Mtb growth in our macrophage infection model, which lacks T cells, and via aerosol infection of mice with H37Rv $\Delta trpA$, we find that TrpAB is required for Mtb survival in mammals before an adaptive immune response would be mounted. Thus, we suggest that TrpAB essentiality can be independent of adaptive host immunity, which would be important in the setting of Mtb with HIV co-infection. Given recent work showing the importance of CD4⁺ T cell-produced IFN γ in depleting host L-Trp and restricting Mtb growth²⁶, we would expect TrpAB to be even more essential when coupled with the activity of the adaptive immune system. It is possible that IFN γ produced by innate immune responses results in this requirement for L-Trp biosynthesis in earlier stages of infection and we cannot fully rule out T cell involvement in our models. Nevertheless, these data demonstrate the requirement for TrpAB for survival during infection and the effectiveness of allosteric inhibition for targeting TrpAB during *in vivo* infection as a model for targeting central metabolic enzymes more generally.**

Through this work, we became interested in understanding why starvation of L-Trp results in a bactericidal response, rather than growth cessation. This is especially interesting as starvation of all nutrients results in a static response in both wild type Mtb and our *trpA* deletion mutant and single starvation of certain other amino acids also results in a static response^{97,98}. Though inhibition of L-Trp or of branched-chain amino acid synthesis activate an apparent stringent response, it appears to be non-protective in that the bacilli still die. It will be important to directly measure the stringent response alarmone

guanosine 3',5'-bispyrophosphate ((p)ppGpp) to confirm the role of the stringent response during these amino acid starvations in mycobacteria. Interestingly, mycobacteria seem unable to respond to increased or decreased concentrations of L-Trp by differentially regulating L-Trp biosynthetic genes. Branched-chain amino acid starvation, on the other hand, resulted in the upregulation of amino acid biosynthetic genes, perhaps accounting for the relative insensitivity of mycobacteria to chemical inhibitors of branched-chain amino acid processes. By comparing these results to the effects of other single-amino acid starvations such as L-Leu and L-Pro, which result in a static response^{97,98}, and L-His, which is bactericidal⁹⁷, we seek to identify patterns underlying Mtb's response to various amino acid starvations and define general mechanisms behind the static or cidal responses to these starvations. Ultimately, understanding which enzymes in central metabolism are required for survival and why, which will facilitate expansion into new therapeutic targets.

Section 3.4. Materials and methods

Chemicals. Unless otherwise noted, all chemicals were purchased from commercial suppliers. BRD4592 was synthesized as described in Chapter 2.

Bacterial strains and growth conditions. *M. tuberculosis* H37Rv (Mtb) and *M. marinum* were grown in Middlebrook 7H9 supplemented with OADC (Middlebrook Oleic Albumin Dextrose Catalase Growth Supplement), 0.2% glycerol and 0.05% Tween-80. *M. smegmatis* (mc²155) was grown in Middlebrook 7H9 supplemented with ADC (Middlebrook Albumin Dextrose Catalase Supplement).

Nutrient starvation media consisted of Phosphate-buffered saline with 0.05% tyloxopol. Cultures were grown to log-phase, then washed three times in starvation media prior to incubation in the starvation media⁷.

*****trpA* deletion strain (H37RvΔ*trpA*) construction.** In the Mtb tryptophan synthesis operon, *trpA* overlaps *trpB* upstream and *lgt* downstream by a single nucleotide. The *trpA* deletion strain was constructed by replacing the native operon with *trpB* engineered to overlap *lgt* in the same manner that *trpA* overlaps each gene. Gibson assembly was used to stitch together *trpB* and *lgt* into the suicide vector pJG1100¹⁸². The plasmid was transformed into Mtb and selected for using hygromycin (50 µg/mL) and kanamycin (15 µg/mL). Recombination to eliminate *trpA* as well as the plasmid backbone was selected for by plating on sucrose. Resulting clones were selected into liquid media and spotted on standard agar and agar containing L-Trp, hygromycin, or kanamycin. Clones that grew only on agar with L-Trp were expanded. PCR of the region around *trpA* followed by

Sanger sequencing confirmed the clean deletion of *trpA*. The deletion strain was complemented with pUV3583c constitutively expressing *trpA*. All medias used for deletion strain construction contained 1 mM L-Trp.

MICs and survival curves. Bacteria were grown to mid-log phase, then added to 96 well plates at OD₆₀₀ = 0.025 and grown in the presence of varying [BRD4592] for 2 weeks. Growth was assessed by reading OD₆₀₀. The minimal inhibitory concentration, MIC₉₀, was defined as the minimum concentration that inhibited growth by 90% relative to a DMSO control. For growth curves, Mtb was grown to mid-log phase and diluted to OD₆₀₀ = 0.0025 in inkwells containing the indicated amounts of compound in triplicate. Aliquots were plated on 7H10 agar to determine colony forming units (CFU) at the time points indicated.

Macrophage infection model. Wild-type Mtb H37Rv, or H37RvΔ*trpA* or its complement (H37RvΔ*trpA*::*trpA*) were used to infect J774 macrophages (ATCC) using a previously published assay¹⁸³. Briefly, Mtb was added to macrophages at a multiplicity of infection of 1 and incubated for 4 hours at which point extracellular bacteria were washed away and fresh media with or without drug was added to the wells containing macrophages. Infections were incubated for 3 days after which macrophages were lysed with Triton-X 100 (0.5%) and surviving bacteria were plated for CFU. Cell lines were verified to be free of mycoplasma contamination using the ATCC universal mycoplasma detection kit.

Mouse infections. Female C57BL/6 mice were obtained from Jackson Laboratory. Mice were infected with 10^5 CFU/mL aerosolized WT *Mtb* H37Rv, H37Rv Δ *trpA* or H37Rv Δ *trpA::trpA*. At 24 hours post-infection, 3 mice were sacrificed per *Mtb* strain and lungs were harvested and plated for CFU. At 14 days and 35 days post-infection 5 mice were sacrificed per *Mtb* strain and lung, liver, and spleen were harvested and plated for CFU. The protocols, personnel, and animals used were approved and monitored by the Institutional Animal Care and Use Committee. The animal facilities are AALAC accredited. Sample size was selected using OpenEpi, Version 3, open source calculator—SSCohort¹⁸⁴ with the following parameters: 1-alpha = 95, 1-beta = 80, unexposed/exposed = 1, percent of unexposed with outcome = 0.1, percent of exposed with outcome = 99.

Zebrafish infections. BRD4592-resistant *M. marinum* colonies were isolated from wild-type *M. marinum* carrying a plasmid for constitutive GFP expression and kanamycin resistance. Single cell suspensions of *M. marinum* were prepared for infection by washing mid log-phase bacteria twice in PBS/Tween-80 (0.05%), then sonicating in a water-bath sonicator (VWR Scientific, B2500A-MT) for five 1-minute cycles with 30 seconds in between. Cultures were then pelleted and resuspended 50-fold concentrated. The concentrated culture was centrifuged at 500 rpm for 5 minutes to remove large clumps of bacteria. The supernatant was filtered through a 5- μ m filter to isolate single bacteria. Optical density of the final culture was measured and cultures were diluted or concentrated to a final concentration of ~ 300 CFU/nL. Aliquots of the single-cell preparation were frozen at -80°C and thawed immediately prior to infections. Zebrafish

embryos to be used for infections were treated with bleach (~0.005%) as previously described¹⁸⁵ 24 hours post fertilization (hpf) to minimize contamination of embryos with non-mycobacterial species derived from the fish facility prior to infection. Forty-eight-hour post-fertilization zebrafish embryos were inoculated intravenously with ~500 CFU *M. marinum* in the duct of Cuvier³⁷. Infected embryos were treated with DMSO or BRD4592 for 5 days and were then euthanized, washed once in PBS, and homogenized in 0.1% Triton X-100 with 5 mm stainless steel beads in three 2-minute cycles of 40 Hz using a TissueLyser bead mill (Qiagen). Homogenates were vortexed well between bead mill cycles and just prior to plating on 7H10 agar supplemented with 15 µg/ml kanamycin to enumerate colonizing *M. marinum*.**

RNA-Seq. Mtb or Msm were grown to log-phase in standard rich 7H9 media and then diluted to OD = 0.4 in pre-warmed 7H9 media containing the indicated amount of compound or DMSO. Cultures (10 mL) were treated in duplicate. At indicated time points, cultures were pelleted and resuspended in TRIzol. Pellets were frozen at -80°C at least overnight, then thawed and lysed using three 1-minute cycles of bead beating. RNA was extracted using Direct-zol RNA MiniPrep kits. RNAtag-Seq libraries were constructed using published methods¹⁸⁶ and sequenced using Illumina HiSeq or NextSeq. Sequencing data was analyzed using published methods¹⁸⁶ and to determine differential expression, both replicates of compound-treated samples were compared to the two DMSO treated samples within the same time point using DESeq.

qPCR. The following primers were used for *sigA* 5' CGTCTGGGATGAAGACGAGT and 5' CTTGCCGATCTGTTTGAGGT. For *trpA* the following primers were used: 5' GAATCCGGTTGCGACATTAT and 5' GGCTAACGTATCCCGGACTC. For *trpD*, 5' CCCACCGTGTTCAATCTTCT and 5' CGTGTACCACCAGCACACTG. For *trpE*, 5' GCACCGTCGAAGAATATGGT and 5' GTTACCCGCAGAATTCCGGTA. Primers were confirmed to be specific and result in linear amplification using gDNA controls.

Samples were treated with L-Trp at indicated concentrations and RNA was extracted as described above. cDNA was synthesized using Superscript III Reverse Transcriptase (ThermoFisher) and the protocol for random hexamers and GC-rich templates. qPCR was performed using Platinum SYBR Green qPCR mix with ROX (ThermoFisher). A 7300 Real-Time PCR system (Applied Biosystems) was used with the following settings: stage 1: 50°C, 2 minutes; stage 2: 95°C, 10 minutes; stage 3: 95°C 0.25 minutes, 55°C 1 minute, 40 cycles; stage 4: 95°C 0.25 minutes, 60°C 1 minute, 95°C 0.25 minutes, 60°C 0.25 minutes. Cycle threshold was calculated for three independent replicates and normalized to the house-keeping gene *sigA*.

Chapter 4: New compounds against non-replicating

Mycobacterium tuberculosis

Attributions

****Marked portions**** of this chapter were published as a manuscript by S. Grant & S. Wellington, *et al.* titled “Baeyer-Villiger Monooxygenases EthA and MymA are Required for Activation of Replicating and Non-replicating *Mycobacterium tuberculosis* Inhibitors” in Cell Chemical Biology volume 23, issue 6, pages 666-677.

The high-throughput screen that identified compounds studied in this chapter was conducted by S. Grant as published in the following manuscript: Grant, S., *et al.* Identification of Novel Inhibitors of Nonreplicating *Mycobacterium tuberculosis* Using a Carbon Starvation Model. *ACS Chem. Biol.* **8**(10), 2224-34 (2013). Tomohiko Kawate synthesized or otherwise purchased all small molecules studied in this chapter. James Gomez and Emma Frank conducted initial research on TK010-016R.

Chapter 4: New compounds against non-replicating *Mycobacterium tuberculosis*

Abstract

Despite the availability of effective treatments, *Mycobacterium tuberculosis* (Mtb) kills 1-2 million people per year. With lengthy treatment times and an increasing prevalence of antibiotic resistance, there is a significant need for new antitubercular therapeutics. Within the host, infection is likely comprised of a heterogeneous population of bacteria, including a subpopulation of non-replicating, phenotypically drug-resistant bacilli thought to contribute to the lengthy treatment time. To discover chemical inhibitors of this non-replicating state, we recently completed a high-throughput screen against carbon-starved Mtb. We identified several active compounds, including an aminothiazole that binds nickel and cobalt and disrupts metal ion homeostasis in Mtb, as well as several compounds that act like prodrugs, requiring oxidation by Baeyer-Villiger monooxygenases (BVMOs) for activity. **Two molecules require BVMO EthA (Rv3854c) for activation and the third molecule requires the BVMO MymA (Rv3083). While EthA is known to activate the antitubercular drug ethionamide, this is the first description of MymA as an activating enzyme of a prodrug. Further, we found that MymA also plays a role in activating ethionamide, with loss of MymA function resulting in ethionamide resistant Mtb. These findings suggest overlap in function and specificity of the BVMOs in Mtb**, highlight the propensity to discover prodrugs through whole-cell screening against Mtb, and provide probes for understanding the carbon-starved non-replicating state in Mtb.

Section 4.1. Background

** Infection with the bacterium *Mycobacterium tuberculosis* (Mtb) remains a major global health problem, with an estimated 9.0 million new infections and 1.5 million deaths occurring in 2013¹⁸⁷. While active tuberculosis (TB) infection is curable, successful treatment requires a complex treatment regimen over at least six months. In the case of infection with a drug-resistant Mtb strain, the treatment course is typically longer and less likely to be successful¹⁸⁸. Treating clinically asymptomatic or latent infection, in which the host immune system restricts Mtb growth but does not eradicate infection, also requires a prolonged course of antibiotic therapy: either multi-drug therapy for 3 months or monotherapy for as long as 9 months¹⁸⁸.

During TB infection, a subpopulation of Mtb bacteria likely exists in a non-replicating or slowly replicating state, refractory to many antibiotics^{189,190}. The presence of non-replicating bacteria within the host is thought to contribute to the need for prolonged drug therapy for active and latent TB infection¹⁹¹. The majority of anti-tuberculosis drugs used clinically are ineffective against carbon-starved non-replicating bacteria, with the notable exceptions of bedaquiline, which targets ATP synthase, and clofazimine, an antibiotic approved for the treatment of leprosy, which is reduced by the enzyme NDH-2 within the electron transport chain and produces toxic ROS upon oxidation^{192,193}. Recent studies demonstrate that including bedaquiline and clofazimine in antitubercular regimens in a murine model of tuberculosis improves treatment outcomes and in addition, a clofazimine-containing 12-month regimen successfully treated 89% of MDR-TB cases¹⁹⁴. These data suggest that including antibiotics with activity against non-

replicating bacteria may shorten the duration of antibiotic therapy for both active and latent tuberculosis infection.

We recently identified novel inhibitors of the non-replicating state, using carbon starvation as a model for non-replicating Mtb⁷.** In this report, we describe an aminothiazole that binds nickel and cobalt, as well as **3 molecules that act like prodrugs in that they require oxidation by monooxygenases for activity. EthA, a Baeyer-Villiger monooxygenase (BVMO) required for the activation of the antitubercular drug ethionamide and the second-line antibiotics thiacetazone and isoxyl¹⁹⁵⁻¹⁹⁷, is required for the activity of two of the small molecules. MymA (Rv3083), also a BVMO¹⁹⁸, is required to activate the third molecule. Further, we show that MymA can additionally activate ethionamide and that loss of MymA function confers some resistance to ethionamide. We suggest that EthA and MymA both function as activating enzymes within the cell, activating ethionamide as well as newly identified sulfur-containing compounds. Our experiences suggest that the abundance of oxidizing enzymes in Mtb may favor the discovery of prodrugs that require oxidation.** Additionally, for all compounds, target identification will lead to a better understanding of the vulnerabilities of the carbon-starved state and the processes required for survival in this state.

Section 4.2. Results

Characterization of a metal-binding aminothiazole. Our previous screen identified a potent aminothiazole, TK010-016R (*N*-(3-methylpyridin-2-yl)-4-(pyridin-2-yl)thiazol-2-amine) (Fig 4.1a), with activity against replicating (MIC₉₀ = 2 µM) and carbon-starved Mtb (MBC₉₀ = 2 µM). TK010-016R is bactericidal, rapidly reducing the colony forming units (CFU) of cultures treated with compound (Fig. 4.1b). Extensive synthesis and testing of

analogues indicated that the nitrogen of the pyridine on position 4 of the thiazole ring is critical for activity and a nucleophilic group is required on the N² substituent, with a pyridal group resulting in the highest level of activity. Overall, an arrangement of four nitrogen atoms around the center of the molecule or three nitrogen atoms along with another nucleophilic group is required for potent activity. Together, these results suggested that activity may be dependent on the ability of the compound to effectively chelate cations.

In order to test this hypothesis, we co-treated Mtb with TK010-016R and various cations, with cations added to the growth media at the highest non-toxic concentration possible. We found that nickel and cobalt each rescue Mtb from the effects of TK010-016R (Fig. 4.1c). This rescue is dose-dependent with lower concentrations of Ni²⁺ or Co²⁺ resulting in less rescue.

The aminothiazole perturbs metal-responsive genes. In order to better understand the mechanism of TK010-016R and its interaction with nickel, we performed RNA-Seq on cells treated with the aminothiazole or co-treated with the aminothiazole and nickel. In cultures treated with TK010-016R for 3 hours, 129 genes were upregulated and 6 genes were down regulated (Fig. 4.2a). Of the upregulated genes, 46 (36%) are repressed by the iron-sensitive regulator IdeR or by iron via another mechanism¹⁹⁹⁻²⁰¹. The most highly upregulated genes include those encoding for the Mtb siderophore mycobactin while down regulated genes include iron-storage proteins such as BfrB. Several upregulated genes (18 genes, 14%) are also known to be induced by copper and 67 are responsive to oxidative stress^{202,203}. There is significant overlap in the set of genes responsive to nickel or copper and those responsive to oxidative stress. When co-treated with nickel,

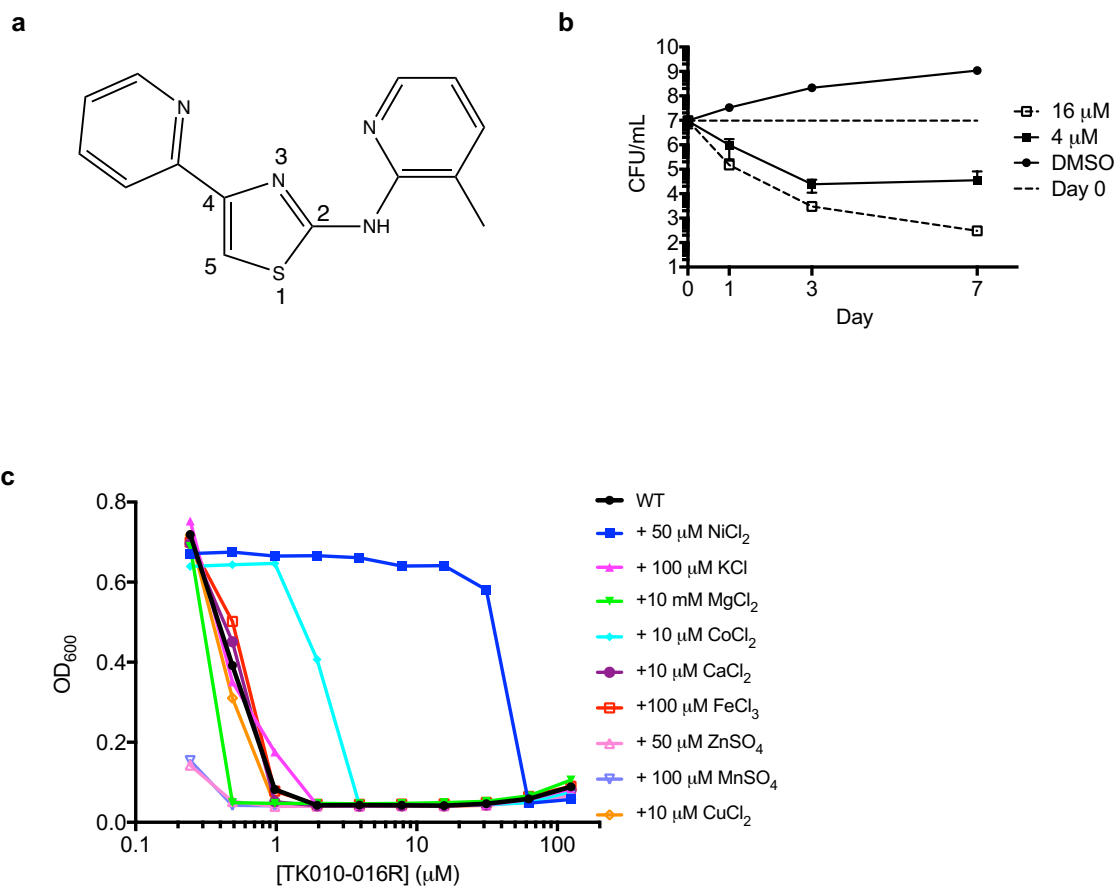


Figure 4.1. Activity of an aminothiazole that binds metal ions. (a) Chemical structure of TK010-016R. **(b)** Activity of TK010-016R against replicating *Mtb*. Points show mean \pm s.d. for three replicates. **(c)** Activity of TK010-016R when *Mtb* is co-treated with compound and metal ions. Nickel and cobalt both rescue *Mtb* from the effects of the compound.

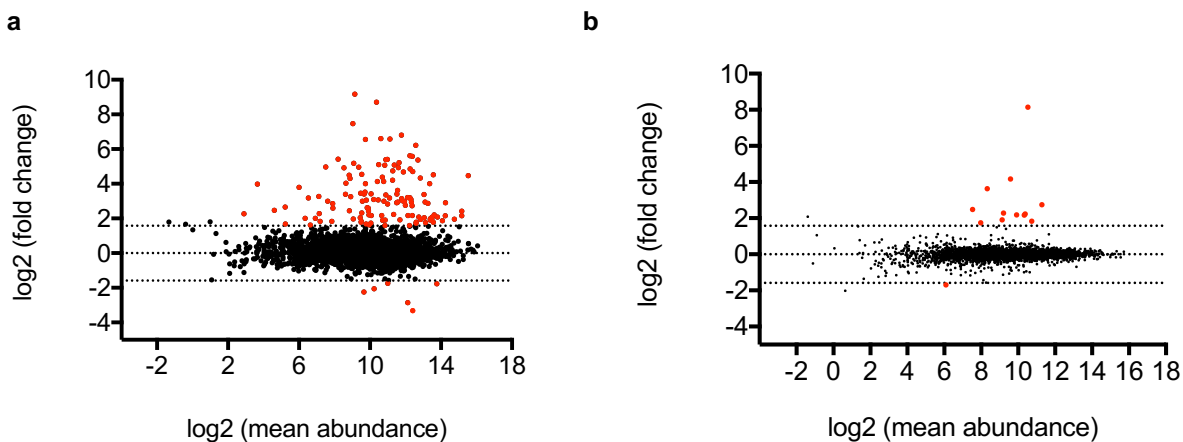


Figure 4.2. Mycobacterial response to TK010-016R. (a) Transcriptional response of Mtb to treatment with TK010-016R (4 μ M) for 3 hours. Genes that are differentially regulated (compared to DMSO controls) with greater than or equal to a three-fold change in expression level and $p < 0.05$ are shown in red. Several genes are differentially regulated compared to DMSO-treated controls, including genes known to be responsive to iron, copper, and oxidative stress. (b) Transcriptional response of Mtb to co-treatment with TK010-016R (4 μ M) and nickel (50 μ M). When co-treated with nickel, there are very few genes differentially regulated in response to TK010-016R.

Mtb did not have a large response to TK010-016R, with only 13 genes differentially regulated (Fig. 4.2b).

Identification of non-toxic analogues of TK010-016R. TK010-016R is toxic to hepG2 cells, however this toxicity is not rescued by nickel or cobalt (Fig. 4.3a), suggesting that activity against Mtb may be separable from activity against mammalian cells. Extensive testing of chemical analogs of TK010-016R allowed us to identify two compounds, TK012-144A (5-methyl-2-(6-methylpyridin-2-yl)-*N*-(pyrimidin-4-yl)thieno[2,3-*d*]pyrimidin-4-amine) and CB7867360 (*N*-(2,4-dimethoxyphenyl)-4-(pyridin-2-yl)thiazol-2-amine) (Fig 4.3c), that retained activity against replicating and non-replicating Mtb while displaying significantly less toxicity to hepG2 cells (Fig. 4.3b). The MIC₉₀ against replicating Mtb is 8 µM and 16 µM for TK012-144A and CB786730, respectively. Against non-replicating Mtb, the MBC₉₀ is 16 µM and 8 µM, respectively. The activity of both compounds remains sensitive to metal ion concentration. However their profiles differed somewhat from TK010-016R. TK012-144A is rescued by nickel (10X increase in MIC), and sensitized by copper (10X decrease in MIC) while CB7867360 is only slightly rescued by nickel (4X increase in MIC) and is sensitized by cobalt and zinc (Fig. 4.3d).

Mycobacterial response to non-toxic analogues. We again turned to RNA-Seq to gain insight into the mechanism of TK012-144A and CB7867360. Similarly to TK010-016R, treatment with TK012-144A induced mycobactin biosynthetic genes and copper-responsive genes (Fig. 4.3e). The response, however, contains fewer-iron sensitive genes with copper-responsive genes comprising a greater proportion of the induced

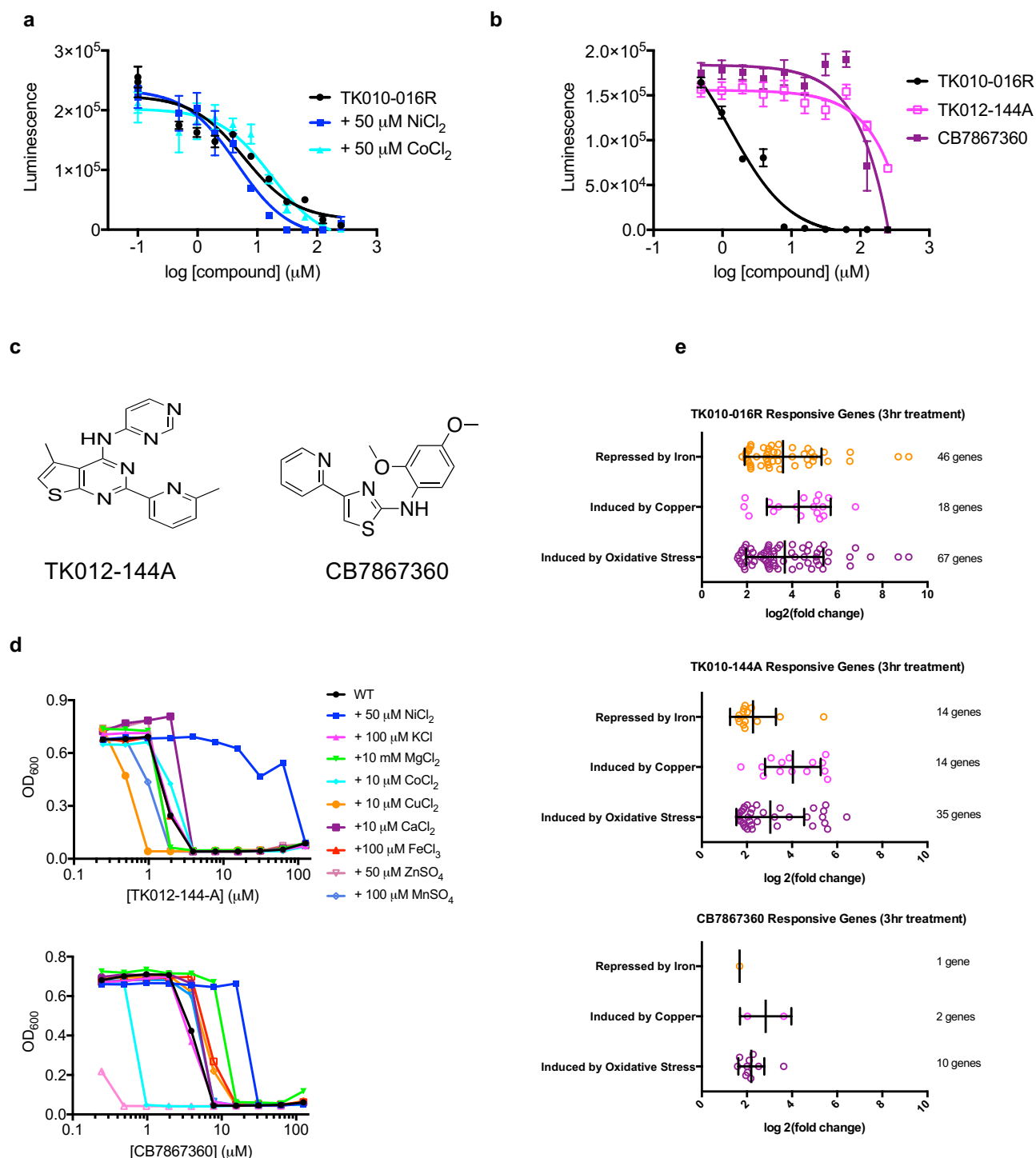


Figure 4.3. Non-toxic analogs of TK010-016R. (a) Effect of TK010-016R on hepG2 cells. (b) Activity of analogues against hepG2 cells. (c) Chemical structures of TK010-016R with reduced toxicity to hepG2 cells. (d) Effect of metal ions on analogue activity against Mtb. (e) Summary of genes upregulated in Mtb in response to treatment with metal-binding compounds.

genes (14/63 genes, 22%). The transcriptional response to CB7867360 was minimal, with only 17 genes upregulated and 2 genes downregulated, and little overlap with the response to the other two compounds. Though TK010-016R and TK012-144A clearly affect metal ion sensing or homeostasis, the mechanism by which the compounds exert their effect remains unclear.

Attempts to isolate resistant mutants by plating Mtb on agar containing compound failed each of the three compounds. Though colonies occasionally grew on compound, they either failed to grow when selected in liquid media or did not demonstrate resistance when MIC was re-tested. This outcome, while potentially promising for the future utility of the compounds as probes or clinical candidates, complicates attempts to understand the mechanisms of the compounds. Future work is focused on measuring the effects of the compounds on Mtb intracellular metal ion concentration and on the development of affinity probes for the compounds.

Our investigation into the mechanisms of three other compounds identified through our initial screen reveals another common outcome of selecting for resistant mutants: the identification of resistance-conferring mutations in activating enzymes rather than in targets themselves.

****Sequencing of resistant mutants for target identification.** We had previously identified 3 small molecules with replicating and non-replicating activity against Mtb: 3-(*m*-tolyl)-5-((1-piperidiny)carbonylmethyl)thio-1,2,4-thiadiazole (**1**), *N*-(4-chlorophenyl)-5-(1-methyl-5-(trifluoromethyl)-1*H*-pyrazol-3-yl)thiophene-2-carboxamide (**2**), and 2-((2-(1,3-dioxan-2-yl)ethyl)thio)-5-phenyl-1,3,4-oxadiazole (**3**) (Fig. 4.4a). We sought to

understand their mechanisms of action by generating resistant mutants followed by whole genome sequencing^{19,34,35,40}. Independent resistant mutants were generated in parallel using 4 parent clones and resistance confirmed prior to whole genome sequencing using Illumina based technology (Fig. 4.5a-c).

EthA is required for activity of compounds 1 and 2. For two compounds, thiadiazole 1 and thiophene-pyrazole 2, mutations in the *ethA* gene were identified in each of the four independent resistant clones sequenced (Fig. 4.5a-c and Table 4.1). All contained frameshift or missense mutations leading to loss of function mutations in *ethA*. Consistent with there being loss of function mutations in *ethA*, the mutant strains displayed varying levels of ethionamide resistance compared to the wild-type strain (Fig. 4.4b and Fig. 4.5d, e). The resistant mutant strains generated against one compound were cross-resistant to the other (Fig. 4.4c, d). When complemented with an episomal copy of wild-type *ethA* under the control of a constitutive promoter, the resistant strains regained sensitivity to ethionamide, 1 and 2 (Fig. 4.4e-g). While EthA has previously been reported to oxidize the thioamide group in small molecules such as ethionamide and thioureas in thiacetazone and isoxyl, and was recently reported to oxidize a thiophene that inhibits the CTP Synthetase PyrG, the role of EthA in oxidizing other sulfur containing compounds such as thioether 1 suggests a wider substrate preference than previously reported²⁰⁴.

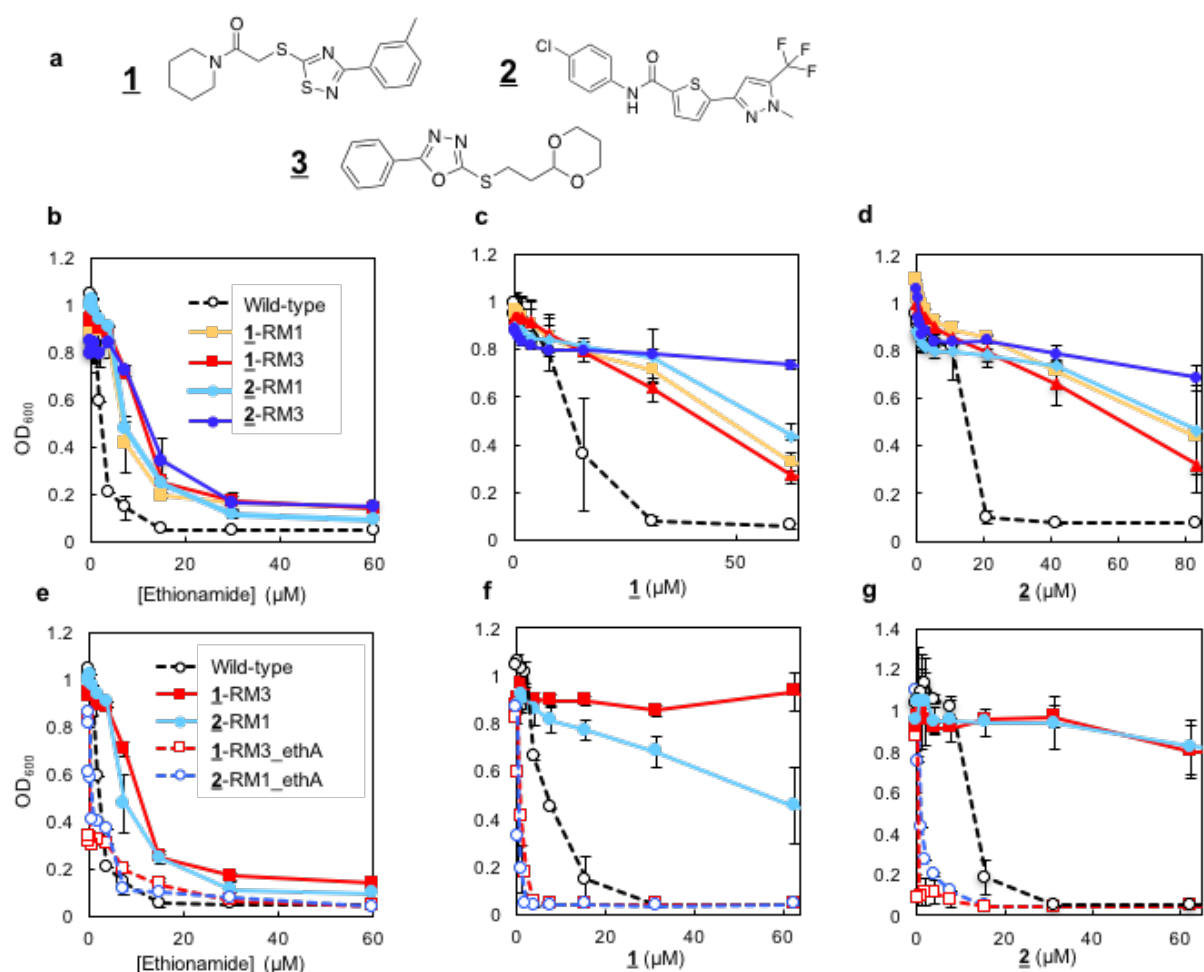


Figure 4.4. Resistance to compounds 1 and 2 is conferred by mutations in *ethA*. (a) Structures for compounds 1, 2 and 3. (b-d) Dose response curves for 1-RM1 (orange) and 1-RM3 (red), 2-RM1 (light blue) and 2-RM3 (dark blue) and wild-type Mtb (open black circles) against ethionamide (b), 1 (c) and 2 (d). (e-g) Dose response curves for wild-type Mtb (open black circles), 1-RM3 with (red open squares) and without (red closed squares) episomal complementation with *ethA*, and a 2-RM1 with (blue open squares) and without (blue closed squares) episomal complementation with *ethA* against ethionamide (e), 1 (f) and 2 (g).

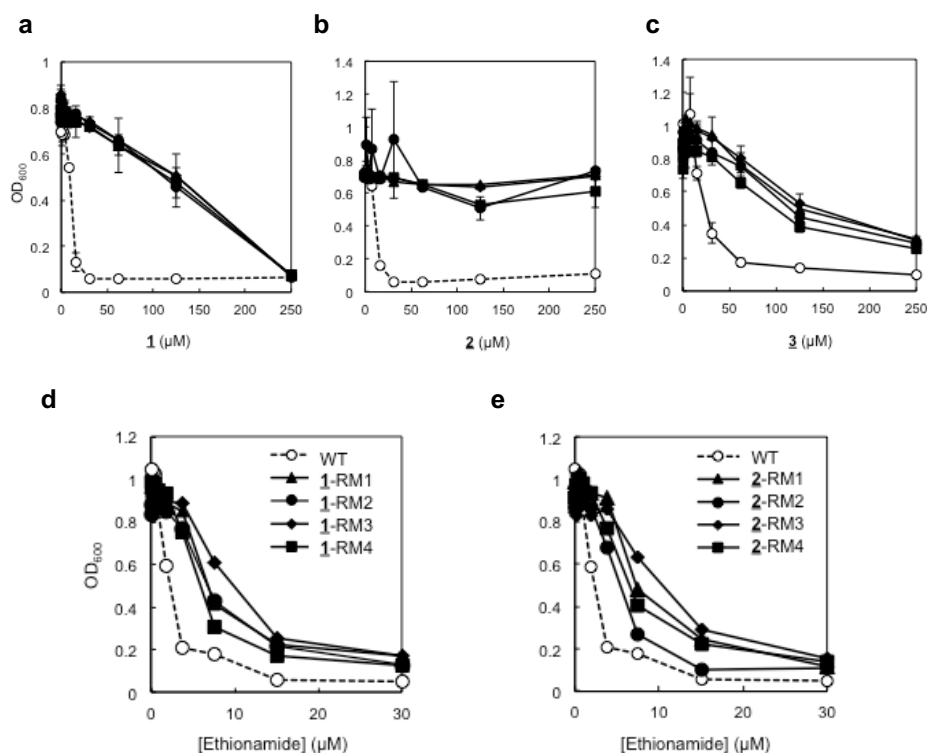


Figure 4.5. Dose-response curves for mutants with resistance to compounds 1 (a), 2 (b), 3 (c). (d,e) Dose response curves for ethionamide against the 8 *ethA* mutants. Open circles represent wild-type (WT) Mtb and black shapes represent four independent generated resistant mutants. Points represent the average of quadruplicates and error bars show standard deviation. The experiments were repeated three times.

Table 4.1. Strains and plasmids

Strains			
Strain	Genotype	Allele characterization	Source
Wild-type (WT)	H37Rv		
<u>1</u> -RM1	ethA-	<i>ethA</i> E36Q	WT selected with <u>1</u>
<u>1</u> -RM2	ethA-	<i>ethA</i> Frameshift +g AA436	WT selected with <u>1</u>
<u>1</u> -RM3	ethA-	<i>ethA</i> W69R	WT selected with <u>1</u>
<u>1</u> -RM4	ethA-	<i>ethA</i> W240stop	WT selected with <u>1</u>
<u>2</u> -RM1	ethA-	<i>ethA</i> Frameshift –c AA156	WT selected with <u>2</u>
<u>2</u> -RM2	ethA-	<i>ethA</i> P447T	WT selected with <u>2</u>
<u>2</u> -RM3	ethA-	<i>ethA</i> Frameshift –a AA133	WT selected with <u>2</u>
<u>2</u> -RM4	ethA-	<i>ethA</i> C131stop	WT selected with <u>2</u>
<u>3</u> -RM1	mymA-	13kB deletion RV3079c-Rv3089	WT selected with <u>3</u>
<u>3</u> -RM2	mymA-	<i>virS</i> E285Q	WT selected with <u>3</u>
<u>3</u> -RM3	mymA-	<i>virS</i> E285Q	WT selected with <u>3</u>
<u>3</u> -RM4	mymA-	Frameshift +cAA318	WT selected with <u>3</u>
Rv3083::TN		3448753	This study
RV3084::TN		3450033	This study
Rv3085::TN		3451750	This study
Rv3086::TN		3452413	This study
Rv3087::TN		3452961	This study
Rv3088::TN		3454690	This study
Rv3089::TN		3455999	This study
Rv3854c::TN		4327379	This study
Rv1393c::TN		1569366	This study
Rv0565c::TN		657361	This study
Rv3049c::TN		3411023	This study
SG1	ethA- mymA-	<i>ethA</i> S138A <i>mymA</i> 13kbΔ Rv3079c-Rv3089	<u>3</u> -RM1 selected with ethionamide
SG2	ethA- mymA-	<i>ethA</i> W45C <i>mymA</i> 13kbΔ Rv3079c-Rv3089	<u>3</u> -RM1 selected with ethionamide
SG3	ethA- mymA-	<i>ethA</i> -cAA302 <i>mymA</i> 13kbΔ Rv3079c-Rv3089	<u>3</u> -RM1 selected with ethionamide
<u>1</u> -RM3_OE_ethA		<u>1</u> -RM3 harboring pRS3Δtet_Rv3854	This study
<u>2</u> -RM1_ethA		<u>2</u> -RM1 harboring pRS3Δtet_Rv3854	This study
<u>3</u> -RM1_VirS		<u>3</u> -RM1 harboring pMV762_VirS	This study
<u>3</u> -RM4_VirS		<u>3</u> -RM4 harboring pMV762_VirS	This study
WT_mymA		H37Rv harboring pUVR3_Rv3083	This study
Rv3083c::TN_mymA		Rv3083c::TN harboring pUVR3_Rv3083	This study
<u>3</u> -RM1_mymA		<u>3</u> -RM1 harboring pUVR3_Rv3083	This study
<u>3</u> -RM_ethA		<u>3</u> -RM1 harboring pUVR3Δtet_Rv3854	This study
SG1_ethA		SG1 harboring pUVR3Δtet_Rv3854	This study

Table 4.1 Continued

SG1_ethA		SG1 strain harboring pUVRS3_Rv3083	This study
Plasmids			
pUVRS3	pUV15 <i>tet</i> ORm derivative with HA tag		
pMV762_VirS	pMV762 derivative expressing VirS		
pUVRS3_Rv3083c	pUVRS3 derivative expression Rv3083c (inducible)		
pUVRS3Δ <i>tet</i> _Rv3854	pUVRS3 derivative with <i>tetR</i> deleted and subsequent constitutive expression of Rv3854		

To determine whether EthA is also required for the activity of these two compounds against non-replicating cells, we tested the activity of **1** and **2** against carbon starved wild-type Mtb and one of the *ethA* mutants (**2**-RM3). We found that both small molecules exhibited significantly less activity against the *ethA* mutant strain compared to wild-type under carbon starvation conditions, suggesting that activation by EthA is also required for the non-replicating activity (Fig. 4.6a, b). The *ethA* mutation does not provide complete protection against these molecules, however, suggesting that there may be an additional mechanism for activation, or alternatively, that the reduced parent molecule may have some activity on non-replicating bacteria.

For thiadiazole **1** we hypothesized that EthA may oxidize the sulfide to a sulfoxide. To test this hypothesis, we synthesized the sulfoxide analog, **4** (Fig. 4.6c). When tested against replicating wild-type Mtb, the MIC₉₀ (minimum inhibitory concentration, measured by outgrowth of bacteria) of **4** is the same as that of the parent molecule **1** (Fig. 4.6d). When tested against two of the *ethA* mutants that are resistant to **1**, the MICs of the sulfoxide **4** were the same for both the *ethA* resistant mutant and the wild-type strain, consistent with the hypothesis that EthA is no longer required for activation of **4** (Fig. 4.6e). We then tested the sulfoxide **4** against a carbon starved *ethA* mutant (**2**-RM3) and found that the starvation MBC₉₀ (minimal bactericidal concentration, measured by plating for colony forming units following treatment with compound) was the same for the wild-type and *ethA* mutant strain, in contrast to **1** which had reduced starvation activity in the *ethA* mutant strain (Fig. 4.6f). The similar efficacies of **1** and **4** against non-replicating cells suggest that the reduced parent molecule does not have significant activity under

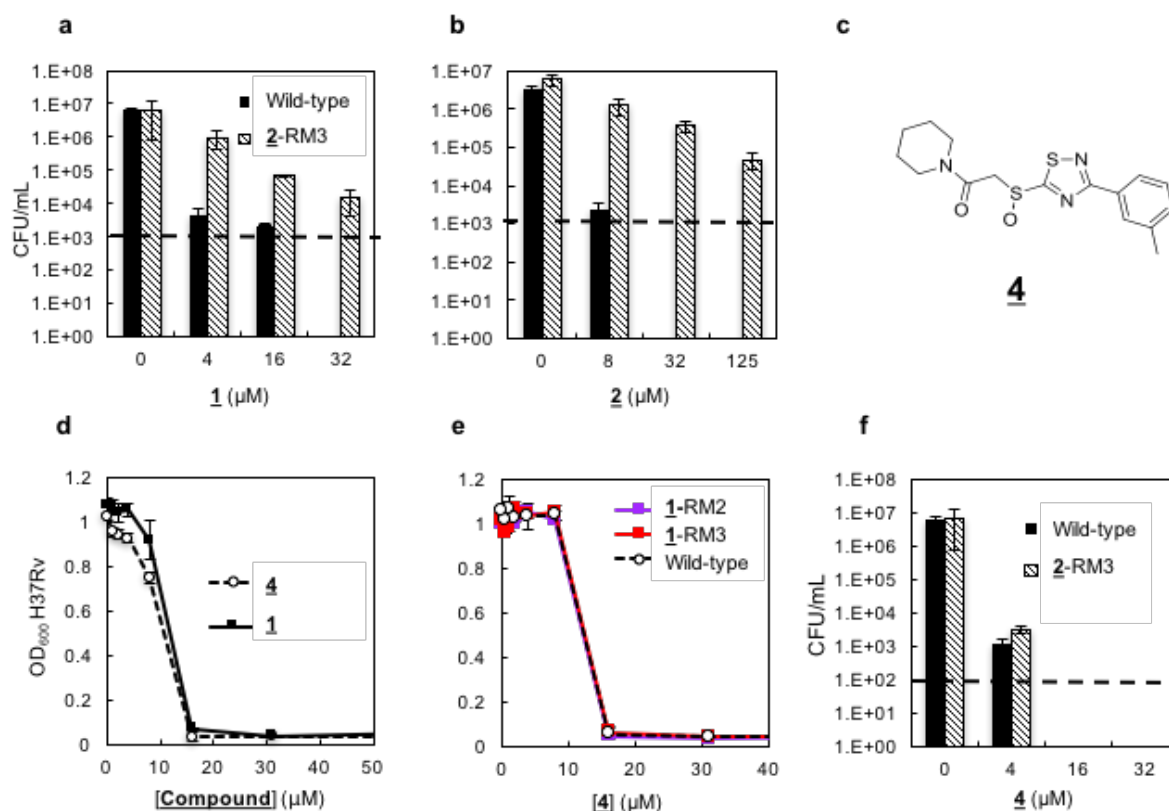


Figure 4.6. Resistance under non-replicating conditions is also conferred by loss of function mutations in *ethA*. (a,b) Wild-type Mtb (black bars) or an *ethA* mutant (**2**-RM3, hatched bars) was starved for 5 weeks in 7H9/Tx media and then treated for 14 days with compound at the indicated doses. Dashed lines indicate limit of detection. (c) Structure of **4**. (d) Dose response curves for **1** and **4** versus wild-type Mtb. (e) Dose response curves for **4** versus wild-type Mtb (open black circles) and two *ethA* mutants (purple, red squares). (f) The analog **4** was tested against carbon starved wild-type Mtb (black bars) or an *ethA* mutant (**2**-RM3, hatched bars). Treatment duration was 2 weeks.

non-replicating conditions. Thus, the residual 1 mediated killing observed in the carbon starved *ethA* mutant (Fig. 4.6a) likely reflects the presence of an additional mechanism for compound activation within the cell. Together these data suggest that EthA oxidizes compound 1 to the sulfoxide analog 4, which is the active form of this small molecule under replicating and non-replicating conditions, and further, that there may be multiple mechanisms to activate the molecule within the cell.

MymA is required for thiooxadiazole 3 activity. For the thiooxadiazole 3, we isolated four independent resistant clones which all contained mutations involving the gene *virS* (Fig. 4.5c, Table 4.1). VirS, an AraC/XylS transcription factor, regulates an operon (*mymA* operon) located downstream from *virS*, in a divergent orientation (Fig. 4.7a)²⁰⁵. The *mymA* operon has been reported to be upregulated under acidic stress and *virS* mutants exhibit altered mycolic acid composition and cell wall ultrastructure^{205,206}. One of the resistant mutants (3-RM1) was found to have a 13 kB deletion spanning the entire *mymA* operon as well as *virS* and *pknK*, the gene encoding a serine/threonine protein kinase located upstream of *virS*. Two resistant mutants contained an identical SNP at position 285 (3-RM2 and 3-RM3) in *virS*, and the fourth mutation contained a frameshift mutation in the 3'-end of *virS* (3-RM4) (Table 4.1). The fact that resistance is conferred when *virS* and the *mymA* operon are deleted indicates that VirS cannot be the direct target of the thiooxadiazole.

We complemented two of the resistant mutants, the deletion mutant (3-RM1) and the frameshift mutant (3-RM4), with a wild-type episomal copy of *virS* under the control of the *groEL* promoter. In the frameshift mutant 3-RM4, complementation with wild-type

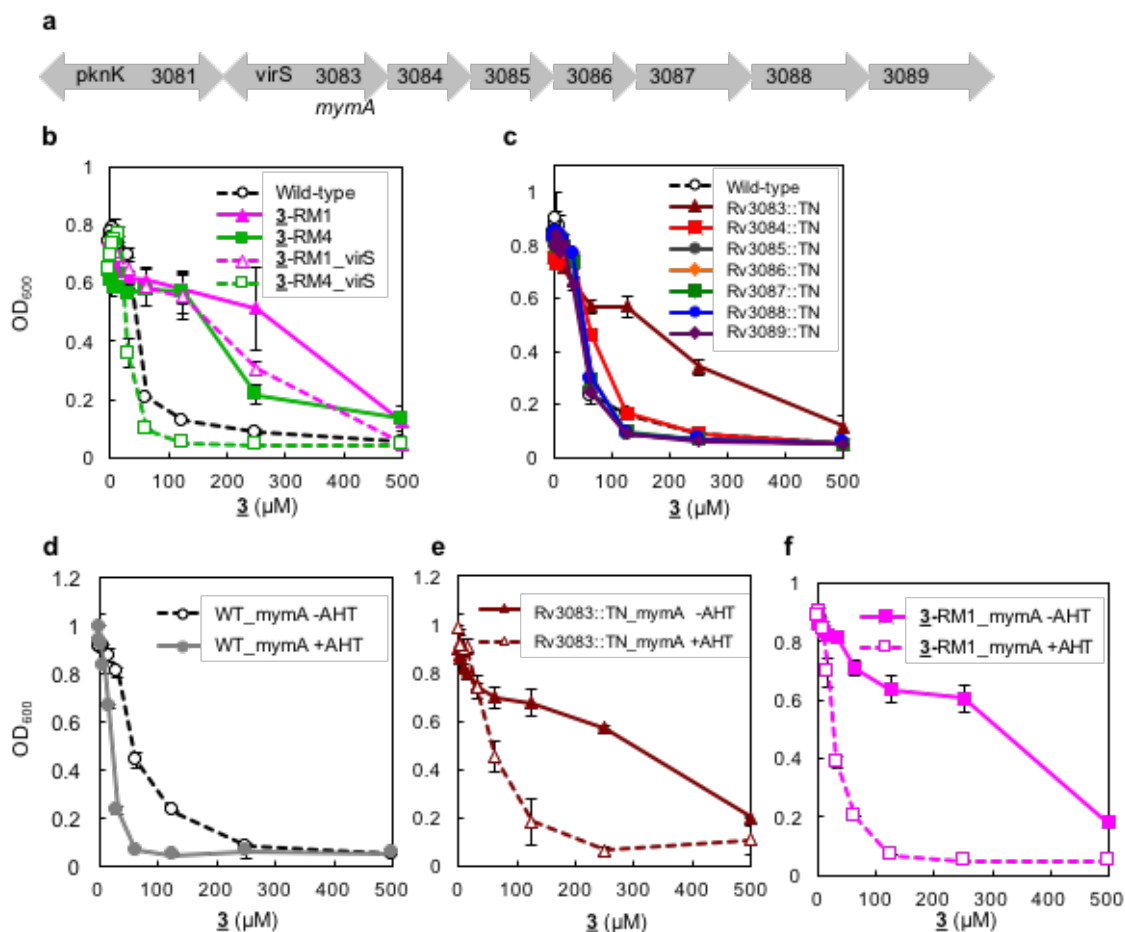


Figure 4.7. The monooxygenase encoded by *mymA* activates compound **3.** (a) The structure of the *mymA* operon. *VirS* is a transcription factor located upstream from the *mymA* operon in a divergent orientation. (b) Dose response curves for wild-type Mtb (open black circles), **3**-RM1 (pink triangles), **3**-RM4 (green squares) and **3**-RM1 and **3**-RM4 complemented with an episomal copy of *virS* (open triangles and squares) versus **3**. (c) Dose response curves for transposon mutants in the *mymA* operon versus **3**. (d) Dose response curves for wild-type Mtb containing an inducible episomal copy of *mymA*, either induced (gray circle) with anhydrotetracycline (AHT) or uninduced (open circle), versus **3**. (e) Dose response curves for the Rv3083c::TN_ *mymA*, either induced with AHT (open triangles) or uninduced (closed triangles) versus **3**. (f) Dose response curves for the *virS* deletion mutant containing an inducible copy of *mymA*, either induced with AHT (open squares) or uninduced (closed squares), versus **3**.

virS restored sensitivity to thiooxadiazole **3**. However, in the deletion mutant **3**-RM1, complementation of *virS* failed to restore sensitivity (Fig. 4.7b). These results led us to hypothesize that the loss of function mutations in *virS* may confer resistance via its impact on expression of genes in the *mymA* operon.

To test this hypothesis, we measured the sensitivity to thiooxadiazole **3** of a set of mutants in which each of the genes of the *mymA* operon (Rv3083-3089) was disrupted by a transposon insertion (Fig. 4.7c). We found that disruption of *mymA* (Rv3083) uniquely confers resistance to the thiooxadiazole **3**, suggesting that *mymA* is required for thiooxadiazole **3** activity (Fig. 4.7c). When we overexpressed *mymA* in three strains: wild-type, the *mymA* transposon mutant (Rv3083c::Tn) and **3**-RM1, we observed the restoration of sensitivity to **3** in each of these strains when *mymA* expression was induced with anhydrotetracycline (AHT) compared to uninduced controls (Fig. 4.7d-f). This result suggests that resistance to **3** in all of the mutants is due to loss of function of MymA.

Optimization of the thiooxadiazole scaffold for replicating and non-replicating activity. We next performed chemistry on thiooxadiazole **3** to optimize both replicating and non-replicating activity. We found that compounds with S-2-pyridylmethyl substitution improve activity against non-replicating bacteria (**3**, **3A** vs **3B~3G**, Table 4.2) and the presence of a halogen or small substituent (methyl or methoxy) at the *para* position of phenyl group at 5-position of oxadiazole improves activity against replicating phase (**3B** vs **3C~3G**). The three most active molecules, **3F**, **3E**, and **3C**, have an MIC₉₀ against replicating bacteria of 16µM (Fig. 4.8a). When tested against non-replicating bacteria the compounds remain active; **3F** has an MBC₉₀ against non-replicating, carbon-starved

Table 4.2. Activity of compounds and analogs against replicating wild-type (WT) Mtb and a *mymA* mutant as well as against WT carbon-starved Mtb

	Structure	MIC ₉₀ (μM) vs WT replicating bacteria	MIC ₉₀ (μM) vs WT starved bacteria	MIC ₉₀ (μM) vs replicating <i>mymA</i> mutant
<u>1</u>		16 - 32	< 4*	16
<u>2</u>		20	< 8*	32
<u>3</u>		125	62	500
<u>4</u>		16	< 4*	
<u>5</u>		> 125		
<u>6</u>		> 125		
<u>7</u>		125	< 2*	125
<u>3A</u>		125	62	500
<u>3B</u>		125	31	250
<u>3C</u>		16	16	31
<u>3D</u>		62	16	>500
<u>3E</u>		16	16	31
<u>3F</u>		16	8-16	62
<u>3G</u>		31	16	250

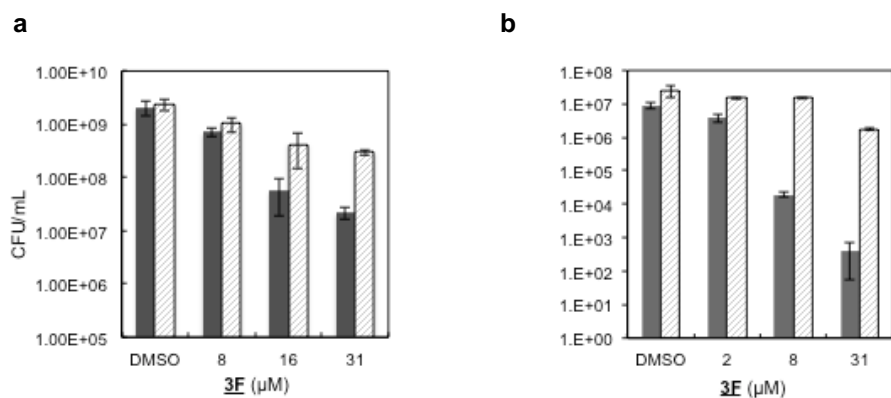


Figure 4.8. Activity of analog 3F in replicating and carbon-starved *Mtb*. The analog 3F was tested against mid-log phase (**A**) or carbon-starved (**B**) wild-type (gray bars) and *mymA* deletion mutant (3-RM1) (dashed bars) strains at the indicated concentrations for 14 days. The bacteria were then serially diluted and plated for enumeration by CFU. Bars represent the average of three technical replicates and error bars represent the standard deviation.

bacteria of 8µM (Fig. 4.8b). Thus, this molecule is active against replicating *Mtb* as well as non-replicating *Mtb*. We confirmed that loss of function mutations in MymA confer resistance to **3F** under both replicating and non-replicating conditions, similar to the original thiooxadiazole **3** (Fig. 4.8a,b). MymA is therefore required for **3** and **3F** activity under both replicating and non-replicating conditions. **3F** was selected for these experiments it has the greatest dependence on MymA for activity.

MymA activates thiooxadiazole 3. Given that MymA is required for thiooxadiazole **3** activity, we hypothesized that MymA, previously described as a Baeyer-Villiger monooxygenase similar to EthA, may be functioning as an activating enzyme of a prodrug by oxidizing thiooxadiazole **3**^{196,198}. As oxadiazolones have previously been reported to have activity against replicating wild-type *Mtb*, as determined by an Alamar blue inhibition assay^{207,208}, we hypothesized that MymA may be converting the thiooxadiazole **3** into the corresponding oxadiazolone **5** (Fig. 4.9). When we tested oxadiazolone **5** as well as an additional oxadiazolone **6** against wild-type *Mtb* H37Rv, however, we found that the oxadiazolones had significantly less activity against replicating bacteria than the parent thiooxadiazole **3** (Fig. 4.9b). Alternatively, MymA could oxidize the thioether to its corresponding sulfoxide. We thus synthesized the corresponding sulfoxide, **7**, (Fig. 4.9a) for one of the thiooxadiazoles(**3A**) and found that the sulfoxide **7** displayed similar efficacy against wild-type H37Rv as the parent **3A** (Fig. 4.9c). In addition, it was equally active against the *virS* deletion mutant and the *mymA* transposon mutant, consistent with the hypothesis that MymA is required for activation of **3A** by oxidizing it to the sulfoxide (Fig. 4.9c).

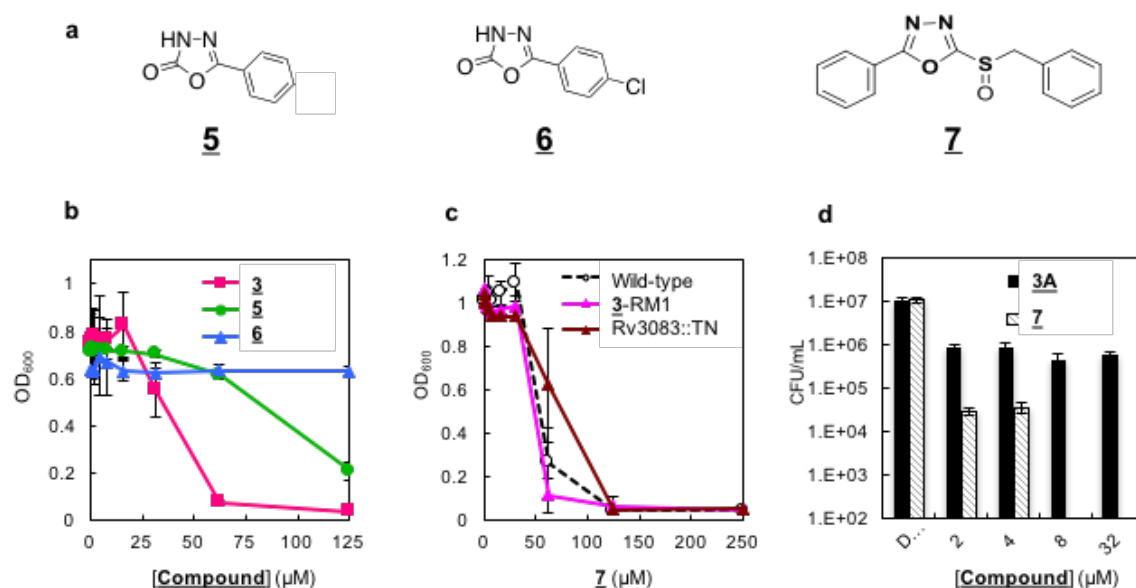


Fig. 4.9. Activity of oxidized 3 analogs. **A)** The structures of analogs 5-7. See also Figure S3 **B)** Dose response curves for analogs 3, 5, and 6 against wild-type replicating Mtb. **C)** Dose response curves for analog 7 against wild-type (open black circles), the *mymA* transposon mutant (red triangles) and the *mymA* deletion mutant (pink triangles). **D)** The activity of analog 7 (hatched) and analog 3A (solid) versus carbon-starved wild-type Mtb at the indicated doses. The bacteria were treated for 14 days, then serially diluted and enumerated by CFU.

To confirm MymA's ability to oxidize **3A**, we directly tested the activity of recombinant MymA on **3A** *in vitro* and observed, by LC-MS, the formation of a product with a molecular weight and retention time consistent with that of the corresponding sulfoxide **7** and sulfone (Fig. 4.10). The oxidized product, **7** is also a substrate for MymA *in vitro* as we observed conversion to the sulfone in a MymA dependent manner (Fig. 4.10). The sulfone then degrades to lower molecular weight products. Though **7** is a substrate for MymA *in vitro*, its activity in whole cells does not depend on MymA (Fig. 4.9c, d), suggesting that **7** must act on its target *in vivo* before MymA can oxidize it further.

We next tested the thiooxadiazole **3A** and the sulfoxide **7** in wild-type H37Rv carbon starved Mtb to compare the non-replicating activity of the thioether and sulfoxide analogs (Fig. 4.9d). We found that the sulfoxide **7** demonstrates greater activity than the thioether **3A** under non-replicating conditions. The superior activity of **7** against non-replicating bacteria compared to **3A** could arise if MymA is less active in carbon-starved cells than in replicating cells, thereby preventing the conversion of **3A** to the active entity **7**. Together these data suggest that the sulfoxide is the active form of the compound under both replicating and non-replicating conditions and that it might be a preferable candidate to the parent thioether for any further development against TB.

Evidence for MymA activation of ethionamide. Previous work has suggested the presence of 6 Baeyer-Villiger monooxygenases in Mtb, with EthA being the most characterized because of its known role in activating the prodrug ethionamide. Of these 6 monooxygenases, *mymA* and *ethA* share the greatest sequence homology^{196,198}. In light of the finding that MymA activates **3** through oxidation, we sought to test whether

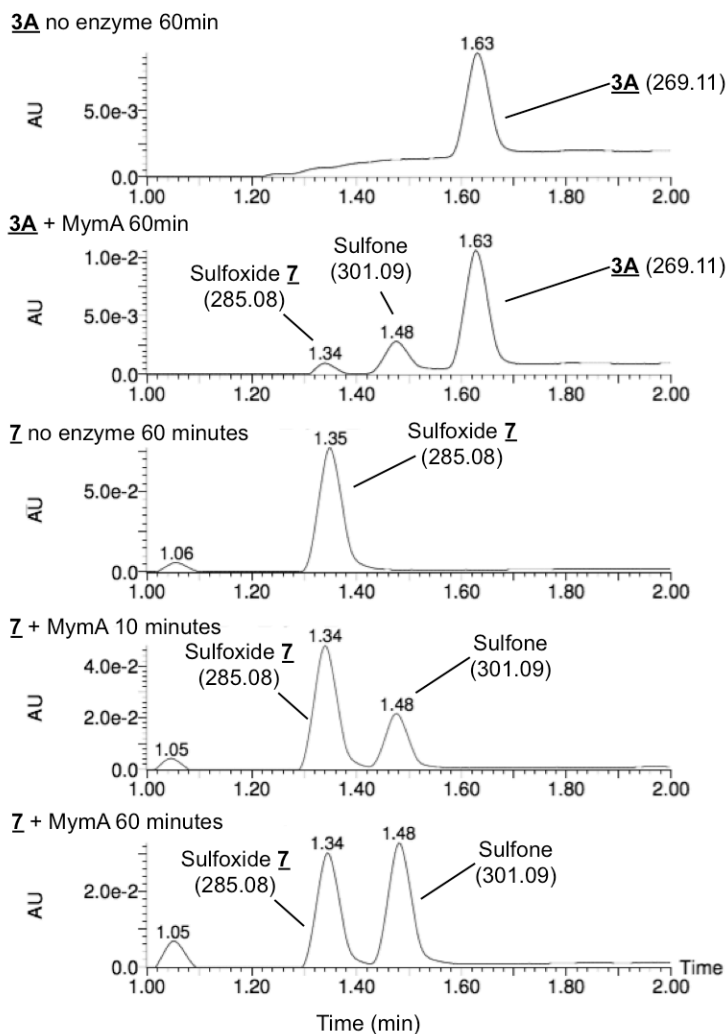


Figure 4.10. MymA biochemical activity. **3A** or **7** were incubated with MymA or in reaction buffer without MymA for the indicated time. The reaction mixture was directly injected onto Liquid Chromatography-Mass Spectrometry (LC-MS) for identification of substrates and products. Absorbance traces from the LC are shown. Peaks are labeled with the corresponding small molecule, with m/z listed in parenthesis. **3A** (m/z = 269.11, retention time = 1.63 minutes) is converted to the sulfoxide **7** (m/z = 285.08, retention time = 1.34) and to the sulfone (m/z = 301.09, retention time = 1.48) in a MymA-dependent manner. **7** is also a substrate for MymA and is converted into a product with retention time and weight consistent with the sulfone before breaking down. The sulfone is unstable when synthesized chemically and seems unstable in these conditions as well. **7** appears to be oxidized more rapidly than **3A** under these conditions.

MymA might also activate ethionamide. We first tested whether loss of function mutations in *mymA* confer resistance to ethionamide. Indeed, we found that loss of MymA function in 3-RM1 or Rv3083::Tn confers comparable levels of resistance to ethionamide as loss of EthA function in 2-RM3 or a mutant containing transposon disruption of *ethA* (Rv3854c::Tn) (Fig. 4.11a). We found that loss of function of MymA (3-RM1) also confers low-level resistance to 1 and 2, though not as high level as observed with EthA loss of function mutations (Fig. 4.11b,c). We then overexpressed *mymA* using an inducible promoter in wild-type Mtb H37Rv and observed a two-fold decrease in the MIC₉₀ for ethionamide, further suggesting that MymA can activate ethionamide (Fig. 4.11d). When we overexpressed *mymA* using an inducible promoter in 3-RM1, we similarly observed a decrease in the MIC₉₀ for ethionamide (Fig 4.11e). Given this finding, we tested transposon mutants in three other BVMOs, Rv1393c, Rv0565c, and Rv3049c, and found that loss of any of these genes does not confer resistance to ethionamide *in vitro* (Fig. 4.11f).

In order to test the complementary roles of EthA and MymA in oxidizing the prodrug ethionamide, we attempted to select for resistant mutants with mutations in both *mymA* and *ethA*. We plated the *mymA* deletion mutant (3-RM1) on high concentrations of ethionamide (500 μ M) with a selection frequency for resistance of approximately 1 in 10⁸ colonies. Three independent clones (SG1-3) were selected from different plates for confirmation of resistance. When tested against ethionamide, these strains exhibited significantly higher levels of resistance to ethionamide (IC₅₀ > 50 μ M; wild-type IC₅₀ = 2.2 μ M) than the original strains carrying only a *mymA* deletion (IC₅₀ = 10.1 μ M) or only a loss of function mutation in *ethA* mutant strains (IC₅₀ = 12.5 μ M) (Fig. 4.12a, b). In addition,

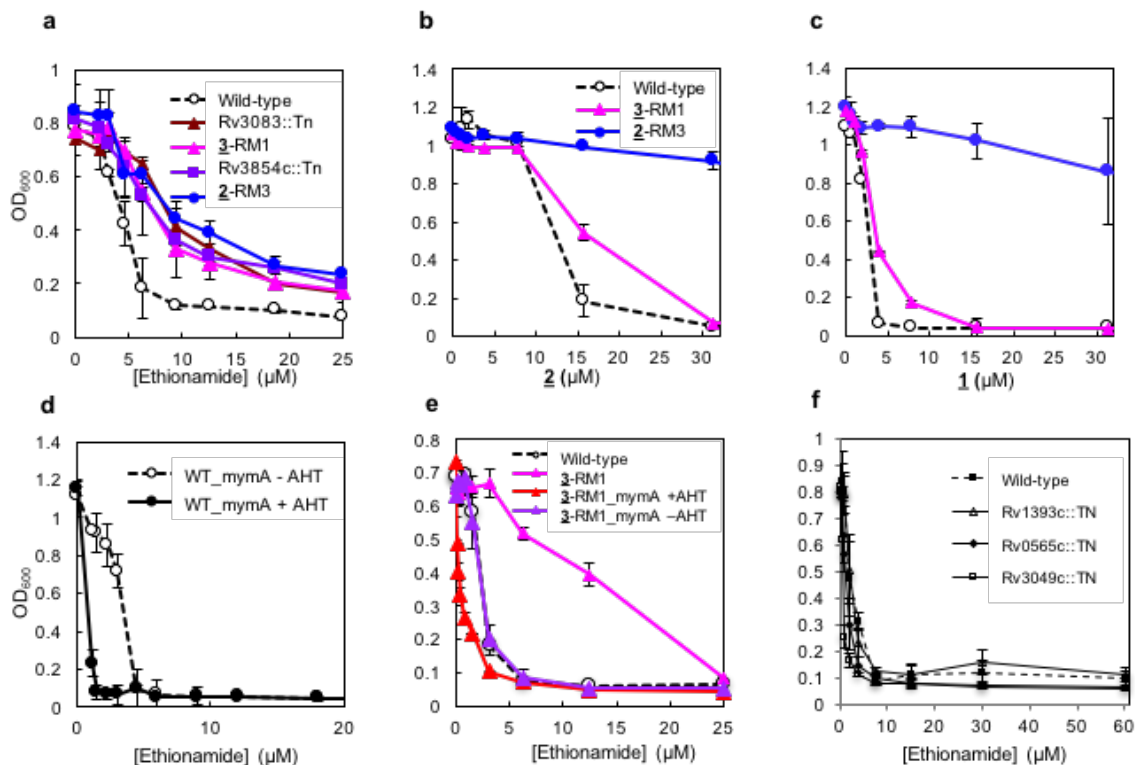


Figure 4.11. MymA and EthA can both activate ethionamide. (a) Dose response curves for ethionamide against wild-type (black open circles), the *mymA* transposon mutant (red triangles), the 3 deletion mutant (pink triangles), the *ethA* transposon mutant (purple squares) and 2-RM3 (blue circles) strains. (b,c) Dose response curves for the 3 deletion mutant (pink triangles) and 2-RM3 (blue circles) strains versus 2 (b) and 1 (c). (d) Dose response curve for wild-type Mtb uninduced (open black circles) and induced (black circles) *mymA* overexpression versus ethionamide. (e) Dose response curve for wild-type (open black circles), 3-RM1 (pink triangles), 3-RM1_mymA induced with AHT (red triangles) or uninduced (purple triangles) versus ethionamide. (f) Activity of ethionamide against replicating Mtb Baeyer-Villiger Monooxygenase transposon mutants. Dose response curves for WT, Rv1393c::TN, Rv0565c::TN, Rv3049c::TN against ethionamide. Points represent the average of quadruplicates and error bars represent standard deviation with the experiment repeated twice.

while the parent *mymA* mutant 3-RM1 did not exhibit resistance to thiacetazone, the 3-RM1 clones selected for high level ethionamide resistance also exhibited resistance to thiacetazone (Fig. 4.12c). As thiacetazone is an antitubercular drug that requires activation by EthA, this observed resistance suggested loss of EthA function in the mutants. Subsequent whole genome sequencing indeed confirmed new mutations in *ethA* in these strains with high level of resistance to ethionamide, in addition to the parental *mymA* deletion (Table 4.1). We then complemented these mutants with episomal copies of *mymA* or *ethA* and found that episomal copies of *mymA* or *ethA* restored sensitivity to ethionamide (Fig. 4.12d, e). Together these data suggest that both EthA and MymA can activate ethionamide in an additive manner, thus representing a novel mechanism for ethionamide activation and resistance.

Selection for loss of function of *mymA* in clinical strains. A review of recently published whole genome sequencing data for clinical *Mtb* strains²⁰⁹ suggests a potential role for MymA *in vivo*. The landscape of resistance to ethionamide *in vivo* is very complex. Many resistance loci have been identified for ethionamide, including *ethA*, *ndh*, *mshA*, and the *inhA* promoter, and yet there are still clinical isolates resistant to ethionamide that do not harbor mutations in any of these known loci²¹⁰. Furthermore, not all strains containing *ethA* loss of function mutations achieve levels of clinical resistance. For example, in the Casali *et al.* dataset, 29 of 83 strains harboring *ethA* loss of function mutations (35%) are classified as sensitive to ethionamide (Table 4.3), which would be consistent with our laboratory findings that an *ethA* mutation alone, is not sufficient to confer high level ethionamide resistance. In contrast, the two strains in their data set that

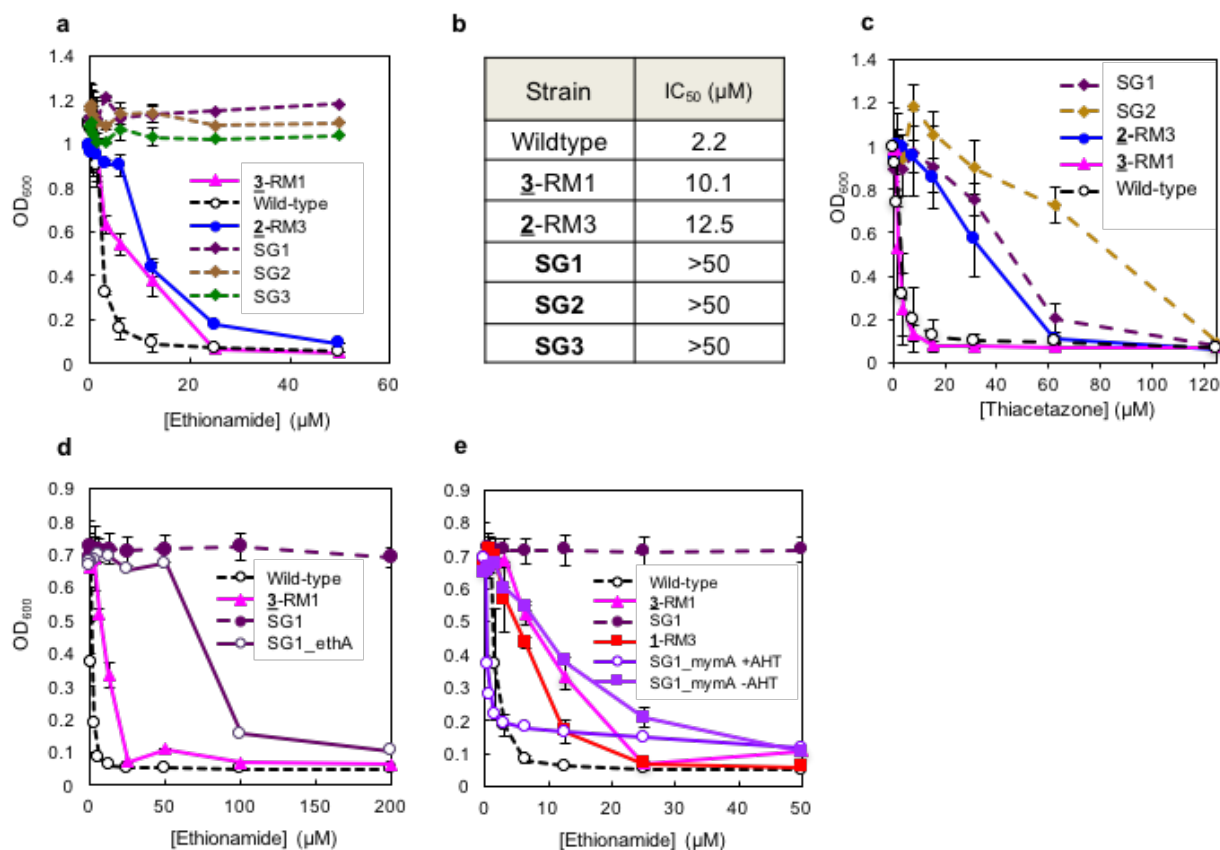


Figure 4.12. The SG1 double mutant exhibits high levels of ethionamide resistance. (a) Dose response curves for SG1 (purple), SG2 (brown), SG3 (green), 2-RM3 (blue), 3-RM1 (pink), and wild-type Mtb (black open circles) versus ethionamide. **(b)** Activity of ethionamide against wild-type Mtb, the original resistant mutants and the *mymA/ethA* double mutants. IC₅₀ is reported as a more relevant metric of activity due to the long tail of slight growth at higher concentrations of ethionamide that would make accurate determination of an MIC₉₀ challenging. **(c)** Dose response curves for thiacetazone against Mtb. Points represent the average of quadruplicates with the experiment repeated twice. **(d,e)** *mymA/ethA* double mutants complemented with *ethA* (d) and *mymA* (e).

carry both *ethA* and *mymA* mutations are indeed classified as clinically ethionamide resistant.

Analysis of this dataset identified 105 strains with 15 unique *mymA* loss of function mutations (nonsense or frameshift mutations). Of this set of >1000 clinical strains, *mymA* had more unique loss of function mutations than nearly all other TB genes, ranking 10th; *ethA*, *pncA*, and *gidB* loss of function, which are associated with resistance to ethionamide, pyrazinamide, and streptomycin, ranked 2nd, 6th, and 15th on the list, respectively (Table 4.4). Unique *mymA* loss of function mutations are, therefore, as frequent as other known loss of function resistance mechanisms, and are more frequent than 99.7% of all Mtb genes, suggesting that there is indeed selective pressure to inactivate *mymA*. In this list, another monooxygenase, Rv0565c ranks 25th (Table 4.4). In fact, others have also observed that this gene is frequently mutated in clinical samples, but it has yet to be linked to a specific phenotype *in vitro*²¹¹.**

Table 4.3. Occurrences of *mymA*, *ethA*, and *inhA* promoter mutations in the Casali *et al.* dataset of whole genome sequencing of Mtb clinical isolates

<i>mymA</i> allele	<i>ethA</i> allele	<i>inhA</i> promoter allele	Number of strains Ethionamide sensitive	Number of strains Ethionamide Resistant	Total
WT	WT	WT	203	78	
WT	WT	SNP	7	32	
LOF	WT	WT	19	10	
LOF	WT	SNP	0	0	
WT	LOF	WT	29	54	
WT	LOF	SNP	2	3	
LOF	LOF	WT	0	2	
LOF	LOF	SNP	0	0	
			260	179	439

Table 4.4. Number of unique loss of function mutations occurring in the genes of clinical Mtb strains. The genomes of over 1000 clinical isolates of Mtb from the Casali, et al. data set were analyzed for loss of function mutations. Genes are ordered by number of unique loss of function mutations. Loss of MymA function ranks 10th on this list, making this loss of function more frequent than 99.7% of all Mtb genes.

Gene Number	Number of unique loss of function mutations	Gene name
RVBD_3508	27	PE-PGRS family protein PE_PGRS54
RVBD_3854c	23	monooxygenase EthA
RVBD_3347c	23	PPE family protein PPE55
RVBD_0878c	23	PPE family protein PPE13
RVBD_2048c	19	polyketide synthase Pks12
RVBD_2043c	18	pyrazinamidase/nicotinamidase PncA
RVBD_0355c	17	PPE family protein PPE8
RVBD_1450c	17	PE-PGRS family protein PE_PGRS27
RVBD_3350c	17	PPE family protein PPE56
RVBD_3083	15	oxidoreductase
RVBD_3514	13	PE-PGRS family protein PE_PGRS57
RVBD_3879c	13	ESX-1 secretion-associated protein EspK
RVBD_0278c	12	PE-PGRS family protein PE_PGRS3
RVBD_3894c	12	ESX-2 secretion system protein EccC2
RVBD_3919c	12	glucose-inhibited division protein B Gid
RVBD_3800c	12	polyketide synthase Pks13
RVBD_0094c	12	hypothetical protein
RVBD_2187	11	long-chain-fatty-acid-CoA ligase FadD15
RVBD_1248c	11	2-oxoglutarate decarboxylase
RVBD_1588c	11	13E12 repeat family protein
RVBD_3466	10	hypothetical protein
RVBD_1527c	10	polyketide synthase Pks5
RVBD_0834c	10	PE-PGRS family protein PE_PGRS14
RVBD_0565c	10	monooxygenase
RVBD_0761c	10	NAD-dependent zinc-type alcohol dehydrogenase
RVBD_1384	10	carbamoyl-phosphate synthase large chain CarB
RVBD_0872c	10	PE-PGRS family protein PE_PGRS15
RVBD_0032	10	8-amino-7-oxononanoate synthase BioF2
RVBD_0860	10	fatty oxidation protein FadB

Section 4.3. Discussion

Given the challenges in finding novel antibiotics that can penetrate the cell wall of bacteria, recent efforts have shifted toward taking a whole cell screening approach to antibiotic discovery. With this shift has come the challenge of target identification of active candidates. Our discovery of TK010-016R, which has activity that is sensitive to metal ion concentration in both replicating and non-replicating cells, reveals that metal ion homeostasis may be a vulnerable process in Mtb. Our work implicates nickel, cobalt, iron and copper in the mechanism of the aminothiazole screening hit as well as its analogues. Interestingly, previous work in *Escherichia coli* has shown that in anoxic conditions, Cu^{2+} toxicity is increased by both Co^{2+} and Ni^{2+} while Ni^{2+} toxicity is reduced by the presence of Fe^{2+} ²¹². This work also suggested that Fe^{2+} may interfere with copper homeostasis systems in *E. coli* ²¹². That these metal ions and regulatory systems can influence each other suggests TK010-016R and its analogues may act via a specific mechanism that ultimately affects several metal ions and their homeostasis.

Whole genome resequencing of resistant mutants has become a dominant approach to identify the targets of Mtb inhibitors identified using whole-cell screens. Using this approach to attempt to determine the targets of replicating and non-replicating Mtb inhibitors that we had previously identified, we have encountered a high frequency of cases in which mutations in activating enzymes were found or in which we were unable to evolve high-level resistance. **It has been suggested that resistance generation coupled with whole genome resequencing may bias towards identifying targets that can easily accommodate mutations while preserving protein function¹⁹. This work illustrates

an additional drawback to this approach, specifically the frequency of mutations encountered in activating enzymes rather than in the actual mechanistic target.

Unlike most of the antibiotics against conventional, rapidly growing bacterial species, a disproportionate number of the antibiotics currently used to treat TB infection are prodrugs, which require metabolism by a bacterial enzyme before having a bactericidal effect. Examples include isoniazid, oxidized by the catalase-peroxidase KatG; pyrazinamide, activated by *pncA* encoded pyrazinamidase; and ethionamide, activated by the BVMO EthA¹⁹⁶. It is unclear why so many antibiotics used to treat tuberculosis are prodrugs. One hypothesis is that this phenomenon may be linked to the large number of oxidases encoded in the Mtb genome²¹³ with at least 49 genes annotated as monooxygenases, oxidoreductases or cytochrome P450 oxygenases¹⁹⁶ that may be required for the bacterium to survive in an environment of increased oxidative stress. Among the 49 oxygenases, Mtb encodes 6 monooxygenases that contain the BVMO motif¹⁹⁸. While the presence of BVMOs is not uncommon among prokaryotes, with approximately 50% of sequenced microbial genomes containing a BVMO gene, only a few microorganisms contain multiple BVMOs, primarily actinomyces and mycobacteria²¹⁴. Each BVMO typically has a preference for a certain class of compounds and the multiplicity of BVMOs within mycobacteria may increase the diversity of molecules that can be oxidized within the cell²¹⁵.

In this work, we characterized 3 new molecules with activity against both replicating and non-replicating Mtb, that behave like prodrugs in requiring a monooxygenase for activity. For two small molecules, thiadiazole **1** and thiophene-pyrazole **2**, we found evidence that activation by EthA, a BVMO previously described as

activating the antitubercular prodrugs ethionamide, isoxyl and thiacetazone, is required for both replicating and non-replicating activity. These molecules do not contain the thioamide or thiourea groups previously described as EthA substrates²⁰⁴, suggesting that the diversity of molecules that can be activated by EthA is greater than previously described. For the third small molecule thiooxadiazole **3**, we found that MymA, a BVMO not previously described as an activating enzyme, is required to oxidize **3** to the corresponding sulfoxide for its replicating and non-replicating activity. We confirmed its enzymatic activity using purified MymA and LC-MS to detect the oxidized products. This is the first example of a compound with antitubercular activity activated by the MymA BVMO.

Surprisingly, our results indicate that MymA can also activate ethionamide and that loss of MymA function confers resistance comparable to loss of EthA function. Loss of MymA function therefore represents a novel ethionamide resistance mechanism observed *in vitro*. *ethA* was originally determined to be the ethionamide resistance locus due to the observation that overexpression of EthR, a repressor of EthA, confers resistance to ethionamide *in vitro* while overexpression of EthA sensitizes to ethionamide^{196,216}. Furthermore, recombinant EthA has been shown to activate ethionamide *in vitro*²¹⁷ and EthA loss of function has been associated with clinical resistance to ethionamide^{196,218}. To our knowledge, however, there is no study on ethionamide sensitivity in a mutant with EthA loss of function compared directly to a parent strain with the same genetic background. In this work, we find that compared to the levels of resistance reported for clinical EthA loss of function mutants²¹⁸, loss of function of EthA alone, or MymA alone, only confers lower levels of resistance. Loss of function in *both*

EthA and MymA were required for high levels of ethionamide resistance. This observation indicates some redundancy in function and substrate specificity for these two BVMOs and suggests that other mutations, in addition to those in *ethA*, are required for high-level resistance to ethionamide.

Analysis of whole genome sequencing data from clinical isolates²⁰⁹ shows that unique *mymA* loss of function mutations are more frequent than in 99.7% of all Mtb genes and at least as common as other loss of function mutations associated with resistance to drugs. These findings suggest that *mymA* loss of function mutations are under selective pressure *in vivo*. We were unable to definitively link *mymA* mutations with an ethionamide resistant phenotype in the absence of access to these particular strains, potentially because *mymA* loss of function mutations confer only low-level resistance to ethionamide while loss of function of both MymA and EthA are required to confer the much higher levels of resistance that are detected by conventional, clinical MIC testing. Such additional experiments however may be warranted, given recent interest in developing genotype-based diagnostics for drug resistance in tuberculosis.

In addition to highlighting the complex mechanisms of compound activation present in Mtb, this work demonstrates that three molecules that we have identified with antitubercular activity and that contain a sulfur (thioether or thiophene) group require activation by a BVMO. At a time when whole-cell high-throughput screening is being utilized to identify new leads against Mtb, this finding suggests that the selection of sulfur containing compounds may bias lead selection towards a prodrug mechanism and a relatively high frequency of resistance development. Considerations for further

development of these compounds should prioritize synthesis and testing of the oxidized forms, with preferential focus on the oxidized forms of such compounds if proven active.

In summary, in this work we highlight the high propensity for thiol-containing substrates to be oxidized in a promiscuous manner by the large number of Mtb BVMOs, thereby activating the prodrugs. Not only do we show the ability of EthA to activate a broader range of substrates than previously described, but we also identify a new BVMO, MymA, that is capable of activating prodrugs. Further, we demonstrate that MymA plays a role in activating the known tubercular drug ethionamide. Surprisingly, loss of function mutations in MymA or EthA confer comparable levels of resistance. EthA and MymA thus have previously unrecognized overlap in their substrates, including the redundant ability to activate ethionamide. Loss of function of MymA represents a novel mechanism for ethionamide resistance and together, loss of function of MymA and EthA confer higher levels of resistance to ethionamide. The greater significance of *mymA* mutations in affording clinical resistance to ethionamide, in conjunction with *ethA* mutations, will need to be evaluated as greater numbers of Mtb genomes become available with rigorous ethionamide resistance testing and MIC measurements.**

Section 4.4. Materials and Methods

Bacterial strains and growth conditions. *M. smegmatis* mc²155 was grown at 37 at 37°C in Middlebrook 7H9 broth supplemented with ADS (Albumin Dextrose Saline). **Mtb H37Rv was grown at 37°C in Middlebrook 7H9 broth supplemented with 10% OADC (oleic acid-albumin-dextrose complex), 0.2% glycerol and 0.05% Tween-80 or on Middlebrook 7H10 plates supplemented with 10% OADC, 0.5% glycerol, and 0.05% Tween-80. Carbon starved bacteria were prepared as previously described⁷. The plasmid used to overexpress *ethA* in Mtb was pUVRS3Δtet (a derivative of pUV15tetORm with the tet repressor deleted for constitutive expression). The inducible plasmid pUVRS3 (a derivative of pUV15tetORm) was used for *mymA* overexpression and pMV762 was used to overexpress *virS* under the control of the *groEL* promoter^{219,220}. Inducible constructs were pre-induced with 50 ng/mL anhydrotetracycline for 24 hours prior to determination of dose response curves.

Chemistry. Unless otherwise noted, reagents and solvents and were obtained from commercial suppliers and were used without further purification. Column chromatography was performed using EMD silica gel 60 (230-400 mesh). ¹H-NMR (300 MHz) and ¹³C-NMR (75 MHz) spectra were recorded on a Bruker instrument (XWIN-NMR) and chemical shifts are reported in parts per million (ppm, δ) downfield from tetramethylsilane (TMS) or residual solvent peak. Coupling constants (*J*) are reported in Hz. Spin multiplicities are described as s (singlet), brs (broad singlet), d (doublet), t (triplet), q (quartet), and m (multiplet). LCMS analysis was conducted on a Agilent Poroshell 120 EC-C18 column (30 mm × 3.0 mm i.d.) eluting with 0.01% formic acid in water (solvent A) and 0.01% in

acetonitrile (solvent B) at a flow rate of 1.75 mL/min, using the following gradient: 0.0 min ~ 0.03 min, 5%B; 0.03 min ~ 1.78 min, 5~95%B; 1.78 min ~ 2.28 min, 95%B; 2.28 min ~ 2.30 min, 95~5%B; 2.30 min ~ 2.50 min, 5%B. The mass spectra were recorded in electrospray positive and/or negative ion modes (ESI+ and ESI-) on a Waters ZQ mass spectrometer. Purity of the compounds was assessed from chromatogram (UV₂₅₄) and was >95%. Ethionamide, compounds **1**, **2**, **3**, **3A** and **5** were obtained from commercial suppliers.

Generation of resistant mutants. The agar MIC was determined for each compound by plating bacteria on agar containing a dose response of compound in a 96 well plate format. The MIC was defined as the lowest concentration resulting in inhibition of bacterial growth. Resistant mutants were generated by plating 1×10^9 bacteria on agar containing 2X, 4X and 10X the agar MIC using four independently derived wild-type clones. Colonies were inoculated into liquid media containing 2X the liquid MIC of the compound. These cultures were retested in a liquid MIC assay to confirm resistance and then used to generate genomic DNA for whole genomic sequencing.

Determination of dose response curves, MIC₉₀s and MBC₉₀s. Bacteria were grown to mid-log phase and plated in 96 well plates at OD₆₀₀ = 0.025 in the presence of a dose response of small molecule inhibitors for 2 weeks, and growth was assessed by reading the OD₆₀₀. The minimal inhibitory concentration, MIC₉₀, was defined as the minimum concentration that inhibited growth by 90% relative to the DMSO control. For all dose response curves the points represent the average and error bars represent the standard

deviation of technical quadruplicates. All dose response curves were repeated 2 (minimum) to 4 times.

To determine starvation MBC_{90} , carbon-starved bacteria were diluted to $OD_{600} = .05$ in starvation media as previously described and incubated in the presence of small molecule inhibitors for 2 weeks⁷. Surviving bacteria were enumerated by plating for CFUs and minimal bactericidal concentration, MBC_{90} was defined as the minimum concentration at which CFU of treated bacteria was 10% (or less) that of untreated bacteria. CFU experiments were conducted using three technical replicates and repeated a minimum of 2 times.

Analysis of clinical strain sequencing data.

Sequence data for clinical strains was downloaded from NCBI (BioProject PRJEB2138). Reads were mapped onto a reference strain of H37Rv (GenBank accession number CP003248.2) using BWA version 0.5.9 (PMID: 19451168). Variants were identified using Pilon version 1.5 (PMID: 25409509) and variant effects were determined using VCF annotator (<http://sourceforge.net/projects/vcfannotator/>). Gene sequences were then evaluated for nonsense mutations and small indels (≤ 10 bp) causing frameshifts.

Transposon Library: TraSH pools²²¹ were thawed, diluted and plated on 7H10 agar with kanamycin. Individual colonies were picked into 96 well 2 mL assay blocks (Corning #3960). Blocks were incubated at 37°C until pellets were visible at the bottom of the wells. Wells were resuspended and aliquots split into 2 96 well plate replicates (Corning #3770).

One replicate was heated to 80°C for 2 hours and then removed from the BSL3 for sequencing. The first PCR reaction used a transposon specific primer paired with a universal primer, and the second PCR reaction used a different transposon specific primer paired with the same universal primer. The PCR product was then sequenced and the data obtained for each clone outside of the transposon was aligned to the genome. In the event of multiple alignments, e-values and proximity to the start of the read were considered when selecting the best alignment. Each clone used in the work was sequenced at least twice for confirmation of transposon location.

Purification of MymA and *in vitro* activation. His-tagged *mymA* was overexpressed in *E. coli* B834 cells using a pET28 vector. Cells were grown at 37°C to an OD of 0.4-0.6, chilled on ice for 15 minutes, and then induced with 0.5 mM isopropyl β -D-1-thiogalactopyranoside (IPTG) and grown at 18°C overnight. Cells were pelleted and frozen at -80°C until lysis. Cells were lysed chemically using lysis buffer consisting of 50mM Tris (pH 7.4), 300 mM NaCl, 1% triton-X, 6 mM imidazole, 25 U/mL benzonase, 500 μ g/mL lysozyme, 1 Roche complete protease inhibitor tablet, and 1x bug buster extraction reagent and incubation at 4°C for 1 hour. Following lysis, insoluble material was pelleted at 20,000g for 20 minutes. Protein was then purified using a GE Healthcare HisTrap HP column. After applying supernatant to the column, the column was washed with 5 volumes binding buffer (50 mM Tris (pH 7.4), 300 mM NaCl, 20 mM imidazole), then 2 volumes elution buffer (50 mM Tris (pH 7.4), 300 mM NaCl) with increasing concentrations of imidazole (50mM, 100mM, 200mM, 250mM, and 500mM). Fractions 4 and 5 were combined and concentrated, then dialyzed against 50mM Tris (pH 7.4) and 100mM KCl.

3A or **7** (150 μ M) were incubated with purified MymA (1.5 μ M) at room temperature in reaction buffer containing 0.2 mM NADPH, 100 mM KCl, and 50 mM Tris (pH 7.4)^{195,197}. The reaction was allowed to progress for indicated amounts of time, and then the reaction mixture was directly injected on LC-MS.

Determination of MIC₉₀ against starved bacteria using luciferase. An inducible firefly luciferase expression plasmid (kanamycin selection) was constructed using an ATc inducible system as described previously²¹⁹. Compounds (20 μ L) were arrayed into 96 well plates as a dose response curve using 2-fold serial dilutions. ATc (50 ng/mL) was added to a carbon-starved H37Rv culture containing the inducible firefly luciferase plasmid and 80 μ L was dispersed into assay plates. After 5 days, the cells were lysed with the addition of 20 μ L of Cell Culture Lysis 5 \times Reagent (Promega Corporation) and 5 mixing cycles (full volume aspirate and dispense). After 10 minutes 100 μ L of luciferase was reagent added and luminescence immediately measured (Luciferase Assay System, Promega Corporation). Data was analyzed as described previously⁷.**

HepG2 cytotoxicity assays. HepG2 cells were cultured in Dulbecco's modified Eagle's medium (with 4.5g/L glucose, L-Glutamine, and Pyruvate) supplemented with 10% fetal bovine serum at 37C, 5% CO₂, in a humidified atmosphere. To test cytotoxicity, HepG2 cells were seeded in 96-well plates at 10,000 cells in 100 μ L media per well. After seeding, cells were allowed to recover overnight, then 2 μ L per well diluted compound was added. Cells were incubated for 48h with compound, at which point cells were lysed with 50 μ L complete CellTiter-Glo Reagent (Promega) diluted 1:2 in 1x

Phosphate Buffered Saline. The reagents and cells were allowed to equilibrate to room temperature prior to addition of reagent to the cells. Plates were incubated for 10 minutes at room temperature to allow the luminescence signal to stabilize, then luminescence was read at an integration of 100 ms/well using a SpectraMax M5 plate reader. Cytotoxicity was determined by comparing signal from cells treated with compound to cells treated with DMSO only. Each compound was tested in at least 3 and up to 4 replicates.

RNA-Seq. RNA extraction, library construction, sequencing and analysis were completed as reported in Chapter 3. All mycobacteria were grown in standard rich 7H9 media. Designation of genes as responsive to copper, iron, or oxidative stress was based on literature reports.

Chapter 5: Summary and Perspectives

Section 5.1. Summary of findings

The discovery of antitubercular compounds with novel targets is greatly needed to combat the growing epidemic. The predominant goals of new antitubercular drug discovery are (1) combating multi- and extensively drug-resistant infections and (2) shortening treatment duration². While numerous functions have been characterized as essential for *Mycobacterium tuberculosis* (Mtb) survival in various conditions, very few are inhibited by current drugs. Further, *in vivo*, Mtb is likely to exist in various states, including a subpopulation of non-replicating, phenotypically drug-resistant bacilli⁴. It is thought that by developing inhibitors active against this non-replicating state, treatment duration may be decreased, which will improve patient compliance and decrease the emergence of drug resistance. In order to identify novel inhibitors of Mtb, we conducted a screen against replicating Mtb¹⁹ using new libraries of inhibitors (*i.e.* a library of synthetic compounds developed at the Broad Institute) and a screen against non-replicating, carbon-starved Mtb⁷.

Of the several compounds identified in these efforts, this dissertation focuses on three sets of small molecules: (1) an azetidine with activity against replicating Mtb; (2) an aminothiazole with activity against both replicating and non-replicating Mtb; and (3) a set of sulfur-containing compounds which we discovered to act as prodrugs against both replicating and non-replicating Mtb.

We first report the characterization of BRD4592, an azetidine with stereo-specific activity against replicating Mtb (Chapter 2). We found that BRD4592 potently inhibits mycobacterial tryptophan synthase by binding an allosteric site at the protein-protein interface. BRD4592 has a unique and complex mechanism of action, stabilizing several

substrate- and product-bound conformations of the enzyme. Importantly, it has historically been challenging to develop potent inhibitors of enzymes in central metabolism because their active sites tend to be shallow and hydrophilic - a poor starting point for drug development¹⁵. We suggest that allosteric inhibition, and especially uncompetitive inhibition, may be a powerful strategy for generating more potent inhibitors of metabolic enzymes. Further, our results that indicate highly dynamic metabolic enzymes with multiple subunits and natural allosteric regulation may be prime targets for the development of such inhibitors.

Because Mtb is capable of scavenging tryptophan²⁶, BRD4592 is rendered ineffective against whole Mtb cells by exogenous tryptophan. It was therefore important to assess the efficacy of BRD4592 *in vivo*. Though enzymes upstream in the Mtb tryptophan biosynthesis pathway have been previously characterized^{26,97}, BRD4592 is the first small molecule described to inhibit tryptophan synthase. Previous reports have suggested that tryptophan biosynthesis is only essential in the context of an adaptive immune response when host CD4 T cell-produced interferon- γ (IFN γ) induces the expression of indoleamine 2,3-dioxygenase (IDO), which degrades tryptophan²⁶. We find that BRD4592 is effective against *Mycobacterium marinum* in zebrafish embryos - an infection model lacking mature T cells (Chapter 3). Further, we find that Mtb lacking *trpA* is attenuated in macrophage culture independent of T cells and attenuated in mice prior to the time at which adaptive immune response are expected to play a role. We, therefore, suggest that tryptophan synthase is essential for mycobacteria *in vivo* even before an adaptive immune response is mounted. This is perhaps due to IFN γ produced by the innate immune system.

Our studies of BRD4592 and tryptophan synthase highlight how little is known about the metabolic environment *in vivo*, which processes are required for Mtb survival at various stages of infection, and why they are required. Tryptophan starvation produces a bactericidal effect in Mtb, yet starvation of other amino acids, such as proline and leucine, results in a static response^{97,98}. We became very interested in understanding why Mtb responds differently to various amino acid starvations. Using BRD4592 as a chemical probe along with two inhibitors of branched-chain amino acid processes, we studied the mycobacterial response to amino acid starvation. While both amino acid starvations result in the induction of an apparent stringent response, starvation of tryptophan has no effect on the expression of tryptophan biosynthetic genes while starvation of branched-chain amino acids results in the upregulation of branched-chain amino acid biosynthetic genes. This difference may account for the relative insensitivity of mycobacteria to branched-chain amino acid inhibitors. Comparisons of these responses to the responses to other amino acid starvations will provide insight into the mechanisms underlying the effects of starvation on Mtb survival.

We go on to study the mechanisms of four compounds found to kill carbon-starved, non-replicating Mtb (Chapter 4). One compound, TK010-016R, binds nickel and cobalt and disrupts metal ion homeostasis, resulting in the upregulation of iron scavenging genes and the downregulation of copper-sensitive genes. Though we have yet to identify the precise mechanism through which TK010-016R exerts its effects on Mtb cells, our discovery suggests that metal ion homeostasis may be a vulnerable process in replicating and non-replicating cells.

The final three compounds we studied each contain a sulfur atom. By isolating resistant mutants, we found that two of the compounds require EthA, an enzyme known to activate the antitubercular drug ethionamide, for activity while the third compound requires MymA, a monooxygenase related to EthA. We show that MymA acts on both our newly discovered compound as well as ethionamide, demonstrating that MymA can, in fact, function as an activating enzyme of prodrugs. We further find that MymA loss of function is common in clinical strains, suggesting it may affect ethionamide sensitivity clinically. Together, these findings highlight the propensity of whole-cell screening followed by target identification via selection for resistance to uncover prodrugs. Though we have gained insight into the fate of these compounds inside Mtb cells and identified a novel activating enzyme, we have not yet identified the molecular mechanisms of these compounds. Target identification for these compounds is complicated as standard techniques, *i.e.* resistance generation and affinity chromatography, have limited utility for prodrugs. Further research on the mechanisms of these three compounds and of the metal-binding aminothiazole will provide insights into vulnerable targets in carbon-starved Mtb.

Section 5.2. Conclusions and future directions

With ever advancing technology, high-throughput screening has come to significantly outpace target deconvolution. Though we are adept at identifying active compounds, the drug discovery field faces significant challenges prioritizing hits and identifying the molecular mechanisms of those hits. Compounding these challenges, recent high-throughput screening efforts against Mtb have uncovered new chemical

scaffolds that inhibit the same small set of proteins, namely MmpL3 and DprE1^{12,19,35}. Though target-based whole-cell screening alleviates some of these issues, hit compounds still require target verification and optimization after their discovery. Further, we know little about which functions are required for Mtb survival *in vivo*, rather than for survival in axenic culture, or about why those functions are essential. This limits the ability of researchers to perform such directed screens.

Various groups are beginning to develop higher throughput methods of target identification using microscopy²²² and RNA-Seq²²³. Such methods have the potential to allow for rapid target identification. We are also exploring methods for prioritizing hit compounds that are likely to have novel targets, such as early testing to exclude DprE1 and MmpL3 inhibitors from further study. Rapid and effective target identification will result in an increasing number of chemical probes which we can then use to understand the mechanisms underlying Mtb's response to various perturbations and the impact disruption of these processes has on Mtb survival *in vivo*.

The work presented in this dissertation highlights methods currently employed for target deconvolution as well as successes (the identification of a specific probe of tryptophan synthase and the identification of a new activating enzyme in Mtb) and limitations of current techniques (the propensity to uncover prodrugs and the difficulty of target identification when the isolation of resistant mutants is unsuccessful). Several fruitful avenues of research have emerged from this work. Using BRD4592, a specific tryptophan synthase inhibitor, we are actively pursuing research to understand why tryptophan starvation is bactericidal for Mtb when certain other amino acid starvations are bacteriostatic. We believe that such knowledge will lead to a better understanding of

which functions serve as the most effective targets *in vivo*. Additionally, future research to identify the molecular mechanisms of compounds active against non-replicating Mtb will provide important information about the requirements for survival in this state as well as vulnerable processes that may serve as drug targets. Collectively, these questions of basic microbiology are critical to advancing the drug discovery field and countering the Mtb epidemic.

References

- 1 WHO. Global tuberculosis report 2015. (World Health Organization, Geneva, Switzerland, 2015).
- 2 Zumla, A., Nahid, P. & Cole, S. T. Advances in the development of new tuberculosis drugs and treatment regimens. *Nat. Rev. Drug Discov.* **12**, 388-404 (2013).
- 3 Cosma, C. L., Sherman, David R. & Ramkrishnan, L. The Secret Lives of Pathogenic Mycobacteria. *Annu. Rev. Microbiol.* **57**, 641-676 (2003).
- 4 Chao, M. C., Rubin E.J. Letting Sleeping dos Lie: Does Dormancy Play a Role in Tuberculosis? *Annu. Rev. Microbiol.* **64**, 293-311 (2010).
- 5 Warner, D. F. & Mizrahi, V. Tuberculosis Chemotherapy: the Influence of Bacillary Stress and Damage Response Pathways on Drug Efficacy. *Clin. Microbiol. Rev.* **19**, 558-570 (2006).
- 6 Esmail, H., Barry III, C. E. & Wilkinson, R. J. Understanding latent tuberculosis: the key to improved diagnostic and novel treatment strategies. *Drug Discov. Today* **17**, 514-521 (2012).
- 7 Grant, S. S. *et al.* Identification of Novel Inhibitors of Nonreplicating Mycobacterium tuberculosis Using a Carbon Starvation Model. *ACS Chem. Biol.* **8**, 2224-2234 (2013).
- 8 Keren, I., Minami, S., Rubin, Eric J. & Lewis, K. Characterization and Transcriptome Analysis of *Mycobacterium tuberculosis* persists. *mBio* **2**, e00100-00111 (2011).
- 9 Katsuno, K. *et al.* Hit and lead criteria in drug discovery for infectious diseases of the developing world. *Nat. Rev. Drug Discov.* **14**, 751-758 (2015).
- 10 Mak, P. A. *et al.* A High-Throughput Screen To Identify Inhibitors of ATP Homeostasis in Non-replicating Mycobacterium tuberculosis. *ACS Chem. Biol.* **7**, 1190-1197 (2012).
- 11 Gold, B., Warriar, T. & Nathan, C. in *Mycobacteria Protocols* (eds Tanya Parish & M. David Roberts) 293-315 (Springer New York, 2015).
- 12 Christophe, T. *et al.* High Content Screening Identifies Decaprenyl-Phosphoribose 2' Epimerase as a Target for Intracellular Antimycobacterial Inhibitors. *PLoS Pathog.* **5**, e1000645 (2009).
- 13 VanderVen, B. C. *et al.* Novel Inhibitors of Cholesterol Degradation in *Mycobacterium tuberculosis* Reveal How the Bacterium's Metabolism Is Constrained by the Intracellular Environment. *PLoS Pathog.* **11**, e1004679 (2015).

- 14 Payne, D. J., Gwynn, M. N., Holmes, D. J. & Pompliano, D. L. Drugs for bad bugs: confronting the challenges of antibacterial discovery. *Nat. Rev. Drug Discov.* **6**, 29-40 (2007).
- 15 Murima, P., McKinney, J. D. & Pethe, K. Targeting Bacterial Central Metabolism for Drug Development. *Chem. Biol.* **21**, 1423-1432 (2014).
- 16 Abrahams, G. L. *et al.* Pathway-Selective Sensitization of Mycobacterium tuberculosis for Target-Based Whole-Cell Screening. *Chem. Biol.* **19**, 844-854 (2012).
- 17 Debnath, J. *et al.* Discovery of Selective Menaquinone Biosynthesis Inhibitors against Mycobacterium tuberculosis. *J. Med. Chem.* **55**, 3739-3755 (2012).
- 18 Mdluli, K., Kaneko, T. & Upton, A. The Tuberculosis Drug Discovery and Development Pipeline and Emerging Drug Targets. *Cold Spring Harb. Perspect. Med.* **5**, a021154 (2015).
- 19 Stanley, S. A. *et al.* Identification of Novel Inhibitors of *M. tuberculosis* Growth Using Whole Cell Based High-Throughput Screening. *ACS Chem. Biol.* **7**, 1377-1384 (2012).
- 20 Pethe, K. *et al.* Discovery of Q203, a potent clinical candidate for the treatment of tuberculosis. *Nat. Med.* **19**, 1157-1160 (2013).
- 21 Lu, X., Zhang, H., Tonge, P. J. & Tan, D. S. Mechanism-based inhibitors of MenE, an acyl-CoA synthetase involved in bacterial menaquinone biosynthesis. *Bioorg. Med. Chem. Lett* **18**, 5963-5966 (2008).
- 22 Kozic, J. *et al.* Synthesis and in vitro antimycobacterial and isocitrate lyase inhibition properties of novel 2-methoxy-2'-hydroxybenzanilides, their thioxo analogues and benzoxazoles. *Eur. J. Med. Chem.* **56**, 108-119 (2012).
- 23 Krieger, Inna V. *et al.* Structure-Guided Discovery of Phenyl-diketo Acids as Potent Inhibitors of M. tuberculosis Malate Synthase. *Chem. Biol.* **19**, 1556-1567 (2012).
- 24 Ferreras, J. A., Ryu, J.-S., Di Lello, F., Tan, D. S. & Quadri, L. E. N. Small-molecule inhibition of siderophore biosynthesis in Mycobacterium tuberculosis and Yersinia pestis. *Nat. Chem. Biol.* **1**, 29-32 (2005).
- 25 Manos-Turvey, A. *et al.* Inhibition Studies of Mycobacterium tuberculosis Salicylate Synthase (MbtI). *ChemMedChem* **5**, 1067-1079 (2010).
- 26 Zhang, Y. J. *et al.* Tryptophan Biosynthesis Protects Mycobacteria from CD4 T-Cell-Mediated Killing. *Cell* **155**, 1296-1308 (2013).

- 27 Hung, A. W. *et al.* Application of Fragment Growing and Fragment Linking to the Discovery of Inhibitors of Mycobacterium tuberculosis Pantothenate Synthetase. *Angew. Chem. Int. Ed.* **48**, 8452-8456 (2009).
- 28 Kumar, A. *et al.* A High-Throughput Screen against Pantothenate Synthetase (PanC) Identifies 3-Biphenyl-4-Cyanopyrrole-2-Carboxylic Acids as a New Class of Inhibitor with Activity against *Mycobacterium tuberculosis*. *PLoS ONE* **8**, e72786 (2013).
- 29 White, E. *et al.* A novel inhibitor of Mycobacterium tuberculosis pantothenate synthetase. *J. Biomol. Screen* **12**, 100-105 (2007).
- 30 Vasan, M. *et al.* Inhibitors of the Salicylate Synthase (MbtI) from Mycobacterium tuberculosis Discovered by High-Throughput Screening. *ChemMedChem* **5**, 2079-2087 (2010).
- 31 Tommasi, R., Brown, D. G., Walkup, G. K., Manchester, J. I. & Miller, A. A. ESKAPEing the labyrinth of antibacterial discovery. *Nat. Rev. Drug Discov.* **14**, 529-542 (2015).
- 32 Wilson, R. *et al.* Antituberculosis thiophenes define a requirement for Pks13 in mycolic acid biosynthesis. *Nat. Chem. Biol.* **9**, 499-506 (2013).
- 33 Moriera, W. *et al.* Target Mechanism-Based Whole-Cell Screening Identifies Bortezomib as an Inhibitor of Caseinolytic Protease in Mycobacteria. *mBio* **6**, e00253-00225 (2015).
- 34 Makarov, V. *et al.* Benzothiazinones kill Mycobacterium tuberculosis by blocking arabinan synthesis. *Science* **324**, 801-804 (2009).
- 35 Grzegorzewicz, A. E. *et al.* Inhibition of mycolic acid transport across the *Mycobacterium tuberculosis* plasma membrane. *Nat. Chem. Biol.* **8**, 334-341 (2012).
- 36 Yamaguchi, H. *et al.* Capuramycin, a new nucleoside antibiotic. Taxonomy, fermentation, isolation and characterization. *J. Antibiot.* **39**, 1047-1053 (1986).
- 37 Stanley, S. A. *et al.* Diarylcoumarins inhibit mycolic acid biosynthesis and kill Mycobacterium tuberculosis by targeting FadD32. *Proc. Natl Acad. Sci.* **110**, 11565-11570 (2013).
- 38 Shinabarger, D. L. *et al.* Mechanism of action of oxazolidinones: effects of linezolid and eperezolid on translation reactions. *Antimicrob. Agents and Chemother.* **41**, 2132-2136 (1997).
- 39 Lee, R. E. *et al.* Spectinamides: A New Class of Semisynthetic Anti-Tuberculosis Agents that Overcome Native Drug Efflux. *Nat. Med.* **20**, 152-158 (2014).

- 40 Andries, K. *et al.* A diarylquinoline drug active on the ATP synthase of *Mycobacterium tuberculosis*. *Science* **307**, 223-227 (2005).
- 41 Weinstein, E. A. *et al.* Inhibitors of type II NADH:menaquinone oxidoreductase represent a class of antitubercular drugs. *Proc. Natl Acad. Sci.* **102**, 4548-4553 (2005).
- 42 Stover, C. K. *et al.* A small-molecule nitroimidazopyran drug candidate for the treatment of tuberculosis. *Nature* **405**, 962-966 (2000).
- 43 Krátký, M. *et al.* Salicylanilide derivatives block *Mycobacterium tuberculosis* through inhibition of isocitrate lyase and methionine aminopeptidase. *Tuberculosis* **92**, 434-439 (2012).
- 44 Sriram, D. *et al.* 5-Nitro-2-furoic acid hydrazones: Design, synthesis and in vitro antimycobacterial evaluation against log and starved phase cultures. *Bioorg. Med. Chem. Lett* **20**, 4313-4316 (2010).
- 45 Sriram, D. *et al.* Synthesis and Antimycobacterial Evaluation of Novel Phthalazin-4-ylacetamides Against log- and Starved Phase Cultures. *Chem. Biol. Drug Des.* **75**, 381-391 (2010).
- 46 Patil, V. *et al.* Design and synthesis of triazolopyrimidine acylsulfonamides as novel anti-mycobacterial leads acting through inhibition of acetohydroxyacid synthase. *Bioorg. Med. Chem. Lett* **24**, 2222-2225 (2014).
- 47 Kirstein, J. *et al.* The antibiotic ADEP reprogrammes ClpP, switching it from a regulated to an uncontrolled process. *EMBO Mol Med.* **1**, 37-49 (2009).
- 48 Gavrish, E. *et al.* Lassomycin, a ribosomally synthesized cyclic peptide, kills *Mycobacterium tuberculosis* by targeting the ATP-dependent protease ClpC1P1P2. *Chem. Biol.* **21**, 509-518 (2014).
- 49 Schmitt, E. K. *et al.* The Natural Product Cyclomarin Kills *Mycobacterium Tuberculosis* by Targeting the ClpC1 Subunit of the Caseinolytic Protease. *Angew. Chem. Int. Ed.* **50**, 5889-5891 (2011).
- 50 Brown, L., Wolf, J. M., Prados-Rosales, R. & Casadevall, A. Through the wall: extracellular vesicles in Gram-positive bacteria, mycobacteria and fungi. *Nat. Rev. Microbiol.* **13**, 620-630 (2015).
- 51 Brecik, M. *et al.* DprE1 Is a Vulnerable Tuberculosis Drug Target Due to Its Cell Wall Localization. *ACS Chem. Biol.* **10**, 1631-1636 (2015).
- 52 Panda, M. *et al.* Discovery of Pyrazolopyridones as a Novel Class of Noncovalent DprE1 Inhibitor with Potent Anti-Mycobacterial Activity. *J. Med. Chem.* **57**, 4761-4771 (2014).

- 53 Neres, J. *et al.* 2-Carboxyquinoxalines Kill *Mycobacterium tuberculosis* through Noncovalent Inhibition of DprE1. *ACS Chem. Biol.* **10**, 705-714 (2015).
- 54 Naik, M. *et al.* 4-Aminoquinolone Piperidine Amides: Noncovalent Inhibitors of DprE1 with Long Residence Time and Potent Antimycobacterial Activity. *J. Med. Chem.* **57**, 5419-5434 (2014).
- 55 Zhang, Y., Wade, M. M., Scorpio, A., Zhang, H. & Sun, Z. Mode of action of pyrazinamide: disruption of *Mycobacterium tuberculosis* membrane transport and energetics by pyrazinoic acid. *J. Antimicrob. Chemother.* **52**, 790-795 (2003).
- 56 Zhang, Y., Shi, W., Zhang, W. & Mitchison, D. Mechanisms of Pyrazinamide Action and Resistance. *Microbiol Spectr.* **2**, 1-12 (2013).
- 57 Trefzer, C. *et al.* Benzothiazinones: Prodrugs That Covalently Modify the Decaprenylphosphoryl- β -d-ribose 2'-epimerase DprE1 of *Mycobacterium tuberculosis*. *J. Am. Chem. Soc.* **132**, 13663-13665 (2010).
- 58 Makarov, V. *et al.* Towards a new combination therapy for tuberculosis with next generation benzothiazinones. *EMBO Mol Med.* **6**, 372-383 (2014).
- 59 Tahlan, K. *et al.* SQ109 Targets MmpL3, a Membrane Transporter of Trehalose Monomycolate Involved in Mycolic Acid Donation to the Cell Wall Core of *Mycobacterium tuberculosis*. *Antimicrob. Agents Chemother.* **56**, 1797-1809 (2012).
- 60 La Rosa, V. *et al.* MmpL3 Is the Cellular Target of the Antitubercular Pyrrole Derivative BM212. *Antimicrob. Agents Chemother.* **56**, 324-331 (2012).
- 61 Lun, S. *et al.* Indoleamides are active against drug-resistant *Mycobacterium tuberculosis*. *Nat. Commun.* **4** (2013).
- 62 Rao, S. P. S. *et al.* Indolcarboxamide Is a Preclinical Candidate for Treating Multidrug-Resistant Tuberculosis. *Sci. Transl. Med.* **5**, 214ra168-214ra168 (2013).
- 63 Remuiñán, M. J. *et al.* Tetrahydropyrazolo[1,5-*a*]Pyrimidine-3-Carboxamide and *N*-Benzyl-6',7'-Dihydrospiro[Piperidine-4,4'-Thieno[3,2-*c*]Pyran] Analogues with Bactericidal Efficacy against *Mycobacterium tuberculosis* Targeting MmpL3. *PLoS ONE* **8**, e60933 (2013).
- 64 Ioerger, T. R. *et al.* Identification of New Drug Targets and Resistance Mechanisms in *Mycobacterium tuberculosis*. *PLoS ONE* **8**, e75245 (2013).
- 65 Li, K. *et al.* Multitarget Drug Discovery for Tuberculosis and Other Infectious Diseases. *J. Med. Chem.* **57**, 3126-3139 (2014).
- 66 Reddy, V. M., Einck, L. & Nacy, C. A. In Vitro Antimycobacterial Activities of Capuramycin Analogues. *Antimicrob. Agents and Chemother.* **52**, 719-721 (2008).

- 67 Siricilla, S., Mitachi, K., Skorupinska-Tudek, K., Swiezewska, E. & Kurosu, M. Biosynthesis of A Water-Soluble Lipid I Analogue and A Convenient Assay for Translocase I. *Anal. Biochem.* **461**, 36-45 (2014).
- 68 Nikonenko, B. *et al.* Therapeutic Efficacy of SQ641-NE against Mycobacterium tuberculosis. *Antimicrob. Agents and Chemother.* **58**, 587-589 (2014).
- 69 Manjunatha, U., Boshoff, H. I. M. & Barry, C. E. The mechanism of action of PA-824: Novel insights from transcriptional profiling. *Commun. Integr. Biol.* **2**, 215-218 (2009).
- 70 Schatz, A., Bugle, E. & Waksman, S. A. Streptomycin, a Substance Exhibiting Antibiotic Activity Against Gram-Positive and Gram-Negative Bacteria. *Exp. Biol. Med* **55**, 66-69 (1944).
- 71 Shaila, M. S., Gopinathan, K. P. & Ramakrishnan, T. Protein Synthesis in Mycobacterium tuberculosis H37Rv and the Effect of Streptomycin in Streptomycin-Susceptible and -Resistant Strains. *Antimicrob. Agents and Chemother.* **4**, 205-213 (1973).
- 72 Cynamon, M. H., Klemens, S. P., Sharpe, C. A. & Chase, S. Activities of Several Novel Oxazolidinones against Mycobacterium tuberculosis in a Murine Model. *Antimicrob. Agents and Chemother.* **43**, 1189-1191 (1999).
- 73 Williams, K. N. *et al.* Promising Antituberculosis Activity of the Oxazolidinone PNU-100480 Relative to That of Linezolid in a Murine Model. *Antimicrob. Agents and Chemother.* **53**, 1314-1319 (2009).
- 74 Fortún, J. *et al.* Linezolid for the treatment of multidrug-resistant tuberculosis. *J. Antimicrob. Chemother.* **56**, 180-185 (2005).
- 75 von der Lippe, B., Sandven, P. & Brubakk, O. Efficacy and safety of linezolid in multidrug resistant tuberculosis (MDR-TB)—a report of ten cases. *J. Infect.* **52**, 92-96 (2006).
- 76 Condos, R. *et al.* Case Series Report of a Linezolid-Containing Regimen for Extensively Drug-Resistant Tuberculosis*. *Chest* **134**, 187-192 (2008).
- 77 Lee, M. *et al.* Linezolid for Treatment of Chronic Extensively Drug-Resistant Tuberculosis. *N. Engl. J. Med.* **367**, 1508-1518 (2012).
- 78 Chang, K.-C. *et al.* Can Intermittent Dosing Optimize Prolonged Linezolid Treatment of Difficult Multidrug-Resistant Tuberculosis? *Antimicrob. Agents and Chemother.* **57**, 3445-3449 (2013).
- 79 Wallis, R. S. *et al.* Mycobactericidal Activity of Sutezolid (PNU-100480) in Sputum (EBA) and Blood (WBA) of Patients with Pulmonary Tuberculosis. *PLoS ONE* **9**, e94462 (2014).

- 80 Brigden, G., Hewison, C. & Varaine, F. New developments in the treatment of drug-resistant tuberculosis: clinical utility of bedaquiline and delamanid. *Infect. Drug Resist.* **8**, 367-378 (2015).
- 81 Black, P. A. *et al.* Energy Metabolism and Drug Efflux in *Mycobacterium tuberculosis*. *Antimicrob. Agents and Chemother.* **58**, 2491-2503 (2014).
- 82 Abrahams, K. A. *et al.* Identification of Novel Imidazo[1,2-a]pyridine Inhibitors Targeting *M. tuberculosis* QcrB. *PLoS ONE* **7**, e52951 (2013).
- 83 Qurient Co., L. (ed United States: Food and Drug Administration) (Brooklyn, Maryland, United States, 2015).
- 84 Advani, M. J., Siddiqui, I., Sharma, P. & Reddy, H. Activity of Trifluoperazine against Replicating, Non-Replicating and Drug Resistant *M. tuberculosis*. *PLoS ONE* **7**, e44245 (2012).
- 85 Diacon, A. H. *et al.* 14-day bactericidal activity of PA-824, bedaquiline, pyrazinamide, and moxifloxacin combinations: a randomised trial. *The Lancet* **380**, 986-993 (2012).
- 86 Koul, A. *et al.* Delayed bactericidal response of *Mycobacterium tuberculosis* to bedaquiline involves remodelling of bacterial metabolism. *Nat. Commun.* **5** (2014).
- 87 Ryan, N. J. & Lo, J. H. Delamanid: First Global Approval. *Drugs* **74**, 1041-1045 (2014).
- 88 Matsumoto, M. *et al.* OPC-67683, a Nitro-Dihydro-Imidazooxazole Derivative with Promising Action against Tuberculosis In Vitro and In Mice. *PLoS Med.* **3**, e466 (2006).
- 89 Singh, R. *et al.* PA-824 Kills Nonreplicating *Mycobacterium tuberculosis* by Intracellular NO Release. *Science* **322**, 1392-1395 (2008).
- 90 Brinster, S. *et al.* Type II fatty acid synthesis is not a suitable antibiotic target for Gram-positive pathogens. *Nature* **458**, 83-87 (2009).
- 91 Becker, D. *et al.* Robust *Salmonella* metabolism limits possibilities for new antimicrobials. *Nature* **440**, 303-307 (2006).
- 92 DeLaBarre, B., Hurov, J., Cianchetta, G., Murray, S. & Dang, L. Action at a Distance: Allostery and the Development of Drugs to Target Cancer Cell Metabolism. *Chem. Biol.* **21**, 1143-1161 (2014).
- 93 Höner Zu Bentrup, K., Miczak, A., Swenson, D. L. & Russell, D. G. Characterization of Activity and Expression of Isocitrate Lyase in *Mycobacterium avium* and *Mycobacterium tuberculosis*. *J. Bacteriol.* **181**, 7161-7167 (1999).

- 94 Munoz-Elias, E. J. & McKinney, J. D. Mycobacterium tuberculosis isocitrate lyases 1 and 2 are jointly required for in vivo growth and virulence. *Nat. Med.* **11**, 638-644 (2005).
- 95 Sharma, V. *et al.* Structure of isocitrate lyase, a persistence factor of Mycobacterium tuberculosis. *Nat. Struct. Biol.* **7**, 663-668 (2000).
- 96 Awasthy, D. *et al.* Inactivation of the *ilvB1* gene in *Mycobacterium tuberculosis* leads to branched-chain amino acid auxotrophy and attenuation of virulence in mice. *Microbiology* **155**, 2978–2987 (2009).
- 97 Parish, T. Starvation Survival Response of *Mycobacterium tuberculosis*. *J. Bacteriol.* **185**, 6702-6706 (2003).
- 98 Berney, M. *et al.* Essential roles of methionine and S-adenosylmethionine in the autarkic lifestyle of Mycobacterium tuberculosis. *Proc. Natl Acad. Sci.* **112**, 10008-10013 (2015).
- 99 Grandoni, J. A., Marta, P. T. & Schloss, J. V. Inhibitors of branched-chain amino acid biosynthesis as potential antituberculosis agents. *J. Antimicrob. Chemother.* **42**, 475-482 (1998).
- 100 Dias, M. V. B. *et al.* Molecular models of tryptophan synthase from Mycobacterium tuberculosis complexed with inhibitors. *Cell Biochem. Biophys* **44**, 375-384 (2006).
- 101 Ollinger, J., O'Malley, T., Kesicki, E. A., Odingo, J. & Parish, T. Validation of the Essential ClpP Protease in *Mycobacterium tuberculosis* as a Novel Drug Target. *J. Bacteriol.* **194**, 663-668 (2012).
- 102 Famulla, K. *et al.* Acyldepsipeptide antibiotics kill mycobacteria by preventing the physiological functions of the ClpP1P2 protease. *Mol. Microbiol.*, 194-209 (2016).
- 103 Yang, Y. *et al.* A discovery of novel Mycobacterium tuberculosis pantothenate synthetase inhibitors based on the molecular mechanism of actinomycin D inhibition. *Bioorg. Med. Chem. Lett* **21**, 3943-3946 (2011).
- 104 Evans, J. C. *et al.* Validation of CoaBC as a Bactericidal Target in the Coenzyme A Pathway of Mycobacterium tuberculosis. *ACS Infect. Dis.* **2**, 958-968 (2016).
- 105 Timm, J. *et al.* Differential expression of iron-, carbon-, and oxygen-responsive mycobacterial genes in the lungs of chronically infected mice and tuberculosis patients. *Proc. Natl Acad. Sci.* **100**, 14321-14326 (2003).
- 106 Lun, S. *et al.* Pharmacokinetic and In Vivo Efficacy Studies of the Mycobactin Biosynthesis Inhibitor Salicyl-AMS in Mice. *Antimicrob. Agents and Chemother.* **57**, 5138-5140 (2013).

- 107 Reddy, P. V. *et al.* Disruption of Mycobactin Biosynthesis Leads to Attenuation of *Mycobacterium tuberculosis* for Growth and Virulence. *J Infect Dis.* **208**, 1255-1265 (2013).
- 108 Neres, J. *et al.* Inhibition of Siderophore Biosynthesis in *Mycobacterium tuberculosis* with Nucleoside Bisubstrate Analogues: Structure–Activity Relationships of the Nucleobase Domain of 5'-O-[N-(Salicyl)sulfamoyl]adenosine. *J. Med. Chem.* **51**, 5349-5370 (2008).
- 109 Dawadi, S., Viswanathan, K., Boshoff, H. I., Barry, C. E. & Aldrich, C. C. Investigation and Conformational Analysis of Fluorinated Nucleoside Antibiotics Targeting Siderophore Biosynthesis. *J. Org. Chem* **80**, 4835-4850 (2015).
- 110 Nelson, K. M. *et al.* Synthesis and Pharmacokinetic Evaluation of Siderophore Biosynthesis Inhibitors for *Mycobacterium tuberculosis*. *J. Med. Chem.* **58**, 5459-5475 (2015).
- 111 Dawadi, S., Kawamura, S., Rubenstein, A., Remmel, R. & Aldrich, C. C. Synthesis and pharmacological evaluation of nucleoside prodrugs designed to target siderophore biosynthesis in *Mycobacterium tuberculosis*. *Bioorg. Med. Chem.* **24**, 1314-1321 (2016).
- 112 Payne, R. J., Kerbarh, O., Miguel, R. N., Abell, A. D. & Abell, C. Inhibition studies on salicylate synthase. *Org. Biomol. Chem.* **3**, 1825-1827 (2005).
- 113 Liu, Z., Liu, F. & Aldrich, C. C. Stereocontrolled Synthesis of a Potential Transition-State Inhibitor of the Salicylate Synthase MbtI from *Mycobacterium tuberculosis*. *J. Org. Chem* **80**, 6545-6552 (2015).
- 114 Kana, B. D., Karakousis, P. C., Parish, T. & Dick, T. Future target-based drug discovery for tuberculosis? *Tuberculosis* **94**, 551-556 (2014).
- 115 Shirude, P. S. *et al.* Azaindoles: Noncovalent DprE1 Inhibitors from Scaffold Morphing Efforts, Kill *Mycobacterium tuberculosis* and Are Efficacious in Vivo. *J. Med. Chem.* **56**, 9701-9708 (2013).
- 116 Dunn, M. F. Allosteric Regulation of Substrate Channeling and Catalysis in the Tryptophan Synthase Bienzyme Complex. *Arch. Biochem. Biophys.* **519**, 154-166 (2012).
- 117 Dunn, M. F. *et al.* The Tryptophan Synthase Bienzyme Complex Transfers Indole between the α - and β -Sites via a 25-30 Å Long Tunnel. *Biochemistry* **29**, 8598-8607 (1990).
- 118 Anderson, K. S., Miles, E. W. & Johnson, K. A. Serine Modulates Substrate Channeling in Tryptophan Synthase. *J. Biol. Chem.* **266**, 8020-8033 (1991).

- 119 Niks, D. *et al.* Allostery and Substrate Channeling in the Tryptophan Synthase Bienzyme Complex: Evidence for Two Subunit Conformations and Four Quaternary States. *Biochemistry* **52**, 6396-6411 (2013).
- 120 Merino, E., Jensen, R. A. & Yanofsky, C. Evolution of bacterial trp operons and their regulation. *Curr. Opin. Microbiol.* **11**, 78-86 (2008).
- 121 Akashi, H. & Gojobori, T. Metabolic efficiency and amino acid composition in the proteomes of *Escherichia coli* and *Bacillus subtilis*. *Proc. Natl Acad. Sci.* **99**, 3695-3700 (2002).
- 122 Ngo, H. *et al.* Synthesis and Characterization of Allosteric Probes of Substrate Channeling in the Tryptophan Synthase Bienzyme Complex. *Biochemistry* **46**, 7713-7727 (2007).
- 123 Lane, A. N. & Kirschner, K. The Catalytic Mechanism of Tryptophan Synthase from *Escherichia coli*: Kinetics and the Reaction of Indole with the Enzyme-L-Serine Complexes. *Eur. J. Biochem.* **129**, 571-582 (1983).
- 124 Ngo, H. *et al.* Allosteric Regulation of Substrate Channeling in Tryptophan Synthase: Modulation of the L-Serine Reaction in Stage I of the β -Reaction by α -Site Ligands. *Biochemistry* **46**, 7740-7753 (2007).
- 125 Hilario, E. *et al.* Visualizing the tunnel in tryptophan synthase with crystallography: Insights into a selective filter for accommodating indole and rejecting water. *Biochim. Biophys. Acta* **1864**, 268-279 (2016).
- 126 Marcaurelle, L. A. & *al.*, e. An aldol-based build/couple/pair strategy for the synthesis of medium- and large-sized rings: discovery of macrocyclic histone deacetylase inhibitors. *J. Am. Chem. Soc.* **132**, 16962-16979 (2010).
- 127 Burke, M. D. & Schreiber, S. L. A planning strategy for diversity oriented synthesis. *Angew. Chem. Int. Ed.* **43**, 46-58 (2004).
- 128 Creighton, T. E. A Steady-State Kinetic Investigation of the Reaction Mechanism of the Tryptophan Synthase of *Escherichia coli*. *Eur. J. Biochem.* **13**, 1-10 (1970).
- 129 Copeland, R. A. *Evaluation of Enzyme Inhibition in Drug Discovery*. 2 edn, (John Wiley & Sons, Inc., 2013).
- 130 Kirschner, K., Wiskocil, R. L., Foehn, M. & Rezeau, L. The Tryptophan Synthase from *Escherichia coli*. *Eur. J. Biochem.* **60**, 513-523 (1975).
- 131 Brzovic, P., Ngo, K. & Dunn, M. F. Allosteric Interactions Coordinate Catalytic Activity between Successive Metabolic Enzymes in the Tryptophan Synthase Bienzyme Complex. *Biochemistry* **31**, 3831-3839 (1992).

- 132 Copeland, R. A., Basavaparthuni, A., Moyer, M. & Porter Scott, M. Impact of enzyme concentration and residence time on apparent activity recovery in jump dilution analysis. *Anal. Biochem.* **416**, 206-210 (2011).
- 133 Blumenstein, L. *et al.* β Q114N and β T110V Mutations Reveal a Critically Important Role of the Substrate α -Carboxylate Site in the Reaction Specificity of Tryptophan Synthase. *Biochemistry* **46**, 14100-14116 (2007).
- 134 Weyand, M. & Schlichting, I. Crystal Structure of Wild-Type Tryptophan Synthase Complexed with the Natural Substrate Indole-3-glycerol Phosphate. *Biochemistry* **38**, 16469-16480 (1999).
- 135 Kulik, V. *et al.* On the Role of α Thr183 in the Allosteric Regulation and Catalytic Mechanism of Tryptophan Synthase. *J. Mol. Biol* **324**, 677-690 (2002).
- 136 Buller, A. R. *et al.* Directed evolution of the tryptophan synthase β -subunit for stand-alone function recapitulates allosteric activation. *Proc. Natl. Acad. Sci. U.S.A.* **112**, 14599-14604 (2015).
- 137 Lee, S. J. *et al.* Conformational changes in the tryptophan synthase from a hyperthermophile upon $\alpha 2\beta 2$ complex formation: Crystal structure of the complex. *Biochemistry* **43**, 11417-11427 (2005).
- 138 Harris, R. M., Ngo, H. & Dunn, M. F. Synergistic Effects on Escape of a Ligand from the Closed Tryptophan Synthase Bienenzyme Complex. *Biochemistry* **44**, 16886-16895 (2005).
- 139 Walkup, G. K. *et al.* Translating slow-binding inhibition kinetics into cellular and in vivo effects. *Nat. Chem. Biol.* **11**, 416-423 (2015).
- 140 Zarzycka, B. *et al.* Stabilization of protein–protein interaction complexes through small molecules. *Drug Discov. Today* **21**, 48-57 (2016).
- 141 Peracchi, A. & Mozzarelli, A. Exploring and exploiting allostery: Models, evolution, and drug targeting. *Biochim. Biophys. Acta* **1814**, 922-933 (2011).
- 142 Chen, Y.-N. P. *et al.* Allosteric inhibition of SHP2 phosphatase inhibits cancers driven by receptor tyrosine kinases. *Nature* **535**, 148-152 (2016).
- 143 Kasbekar, M. *et al.* Selective small molecule inhibitor of the Mycobacterium tuberculosis fumarate hydratase reveals an allosteric regulatory site. *Proc. Natl Acad. Sci.* **113**, 7503-7508 (2016).
- 144 Nussinov, R. & Tsai, C.-J. Allostery in Disease and in Drug Discovery. *Cell* **153**, 293-305 (2013).
- 145 Cornish-Bowden, A. Why is uncompetitive inhibition so rare? *FEBS Letters* **203**, 3-6 (1986).

- 146 Spyarakis, F., Raboni, S., Cozzini, P., Bettati, S. & Mozzarelli, A. Allosteric communication between alpha and beta subunits of tryptophan synthase: Modelling the open-closed transition of the alpha subunit. *BBA-Proteins Proteom.* **1764**, 1102-1109 (2006).
- 147 Lowe, J. T. *et al.* Synthesis and Profiling of a Diverse Collection of Azetidine-Based Scaffolds for the Development of CNS-Focused Lead-like Libraries. *J. Org. Chem.* **77**, 7187-7211 (2012).
- 148 Snavelly, M. D., Gravina, S. A., Cheung, T. T., Miller, C. G. & Maguire, M. E. Magnesium transport in *Salmonella typhimurium*. Regulation of *mgtA* and *mgtB* expression. *J. Biol. Chem.* **266**, 824-829 (1991).
- 149 Li, W. *et al.* The EMBL-EBI bioinformatics web and programmatic tools framework. *Nucleic Acids Res.* **43**, W580-584 (2015).
- 150 Dieckman, L., Gu, M., Stols, L., Donnelly, M. I. & Collart, F. R. High Throughput Methods for Gene Cloning and Expression. *Protein Expr. Purif.* **25**, 1-7 (2002).
- 151 Kim, Y. *et al.* High-throughput Protein Purification and Quality Assessment for Crystallization. *Methods* **55**, 12-28 (2011).
- 152 Aslanidis, C. & de Jong, P. J. Ligation-independent cloning of PCR products (LIC-PCR). *Nucleic Acids Res.* **18**, 6069-6074 (1990).
- 153 Eschenfeldt, W. H., Stols, L., Millard, C. S., Joachimiak, A. & Donnelly, M. I. A Family of LIC Vectors for High-Throughput Cloning and Purification of Proteins. *Methods Mol. Biol.* **498**, 105-115 (2009).
- 154 Klock, H. E. & Lesley, S. A. The Polymerase Incomplete Primer Extension (PIPE) Method Applied to High-Throughput Cloning and Site-Directed Mutagenesis. *Methods Mol. Biol.* **498**, 91-103 (2009).
- 155 Nocek, B. *et al.* Structural Studies of ROK Fructokinase YdhR from *Bacillus subtilis*: Insights into substrates binding and fructose specificity. *J. Mol. Biol.* **406**, 325-342 (2011).
- 156 Smith, O. H. & Yanofsky, C. Enzymes involved in the biosynthesis of tryptophan. *Methods Enzymol.* **5**, 794-806 (1960).
- 157 Minor, W., Cymborowski, M., Otwinowski, Z. & Chruszcz, M. HKL-3000: the integration of data reduction and structure solution - from diffraction images to an initial model in minutes. *Acta Cryst.* **D62**, 859-866 (2006).
- 158 French, S. & Wilson, K. On the treatment of negative intensity observations. *Acta Cryst.* **A34**, 517-525 (1978).

- 159 Padilla, J. E. & Yeates, T. O. A statistic for local intensity differences: robustness to anisotropy and pseudo-centering and utility for detecting twinning. *Acta Cryst.* **D59**, 1124-1130 (2003).
- 160 Winn, M. D. *et al.* Overview of the CCP4 suite and current developments. *Acta Cryst.* **D67**, 235-242 (2011).
- 161 McCoy, A. J. Solving structures of protein complexes by molecular replacement with *Phaser*. *Acta Cryst.* **D63**, 32-41 (2007).
- 162 Adams, P. D. *et al.* *PHENIX*: a comprehensive Python-based system for macromolecular structure solution. *Acta Cryst.* **D66**, 213-221 (2010).
- 163 Emsley, P. & Cowtan, K. Coot: model-building tools for molecular graphics. *Acta Cryst.* **D60**, 2126-2132 (2004).
- 164 Murshudov, G. N., Vagin, A. A. & Dodson, E. J. Refinement of Macromolecular Structures by the Maximum-Likelihood Method. *Acta Cryst.* **D53**, 240-255 (1997).
- 165 Krissinel, E. & Henrick, K. Secondary-structure matching (SSM), a new tool for fast protein structure alignment in three dimensions. *Acta Cryst.* **D60**, 2256-2268 (2004).
- 166 Chwastyk, M., Jaskolski, M. & Cieplak, M. Structure-based analysis of thermodynamic and mechanical properties of cavity-containing proteins – case study of plant pathogenesis-related proteins of class 10. *FEBS J* **281**, 416-429 (2013).
- 167 Pettersen, E. F. *et al.* UCSF Chimera—A visualization system for exploratory research and analysis. *J. Comput. Chem.* **25**, 1605-1612 (2004).
- 168 D'Elia, M. A., Pereira, M. P. & Brown, E. D. Are essential genes really essential? *Trends Microbiol.* **17**, 433-438 (2009).
- 169 Turner, K. H., Wessel, A. K., Palmer, G. C., Murray, J. L. & Whiteley, M. Essential genome of *Pseudomonas aeruginosa* in cystic fibrosis sputum. *Proc. Natl Acad. Sci.* **112**, 4110-4115 (2015).
- 170 Lee, S. A. *et al.* General and condition-specific essential functions of *Pseudomonas aeruginosa*. *Proc. Natl Acad. Sci.* **112**, 5189-5194 (2015).
- 171 Eymann, C., Homuth, G., Scharf, C. & Hecker, M. *Bacillus subtilis* functional genomics: global characterization of the stringent response by proteome and transcriptome analysis. *J. Bacteriol.* **184**, 2500-2520 (2002).
- 172 Dahl, J. L. *et al.* The *relA* Homolog of *Mycobacterium smegmatis* Affects Cell Appearance, Viability, and Gene Expression. *J. Bacteriol.* **187**, 2439-2447 (2005).

- 173 Swaim, L. E. *et al.* Mycobacterium marinum Infection of Adult Zebrafish Causes Caseating Granulomatous Tuberculosis and Is Moderated by Adaptive Immunity. *Infect. Immun.* **74**, 6108-6117 (2006).
- 174 Hess, I. & Boehm, T. Intravital Imaging of Thymopoiesis Reveals Dynamic Lympho-Epithelial Interactions. *Immunity* **36**, 298-309 (2012).
- 175 Wolf, A. J. *et al.* Initiation of the adaptive immune response to Mycobacterium tuberculosis depends on antigen production in the local lymph node, not the lungs. *J. Exp. Med.* **205**, 105-115 (2008).
- 176 Nguyen, D. *et al.* Active starvation responses mediate antibiotic tolerance in biofilms and nutrient-limited bacteria. *Science* **334**, 982-986 (2011).
- 177 Dahl, J. L. *et al.* The role of RelMtb-mediated adaptation to stationary phase in long-term persistence of Mycobacterium tuberculosis in mice. *Proc. Natl Acad. Sci.* **100**, 10026-10031 (2003).
- 178 Duan, X. *et al.* Mycobacterium Lysine ϵ -aminotransferase is a novel alarmone metabolism related persister gene via dysregulating the intracellular amino acid level. *Sci. Rep.* **6**, 19695 (2016).
- 179 Stanley, S. A. & Hung, D. T. Chemical Tools for Dissecting Bacterial Physiology and Virulence. *Biochemistry* **48**, 8776-9786 (2009).
- 180 Hung, D. T. & Rubin, E. J. Chemical biology and bacteria: not simply a matter of life or death. *Curr. Opin. Chem. Biol.* **10**, 321-326 (2006).
- 181 Sieger, D., Stein, C., Neifer, D., Sar, A. M. v. d. & Leptin, M. The role of gamma interferon in innate immunity in the zebrafish embryo. *Dis. Model. Mech.* **2**, 571-581 (2009).
- 182 Kirksey, M. A. *et al.* Spontaneous Phthiocerol Dimycocerosate-Deficient Variants of Mycobacterium tuberculosis Are Susceptible to Gamma Interferon-Mediated Immunity. *Infect. Immun.* **79**, 2829-2838 (2011).
- 183 Stanley, S. A. *et al.* Identification of Host-Targeted Small Molecules That Restrict Intracellular Mycobacterium tuberculosis Growth. *PLoS Pathog.* **10**, e1003946 (2014).
- 184 Dean, A. G., Sullivan, K. M. & Soe, M. M. *OpenEpi: Open Source Epidemiologic Statistics for Public Health, Version 3*, < www.OpenEpi.com > (2013).
- 185 Nüsslein-Volhard, C. & Dahm, R. *Zebrafish: a practical approach*. (Oxford University Press, 2002).
- 186 Shishkin, A. A. *et al.* Simultaneous generation of many RNA-seq libraries in a single reaction. *Nat. Meth.* **12**, 323-325 (2015).

- 187 WHO. Global tuberculosis report 2014. (World Health Organization, Geneva, Switzerland, 2014).
- 188 Zumla, A., Raviglione, M., Hafner, R. & von Reyn, C. F. Tuberculosis. *N. Engl. J. Med.* **368**, 745-755 (2013).
- 189 McCune, R. M., Feldmann, F. M. & McDermott, W. Microbial persistence. II. Characteristics of the sterile state of tubercle bacilli. *J. Exp. Med.* **123**, 469-486 (1966).
- 190 Gomez, J. E. & McKinney, J. D. M. tuberculosis persistence, latency, and drug tolerance. *Tuberculosis (Edinb)* **84**, 29-44 (2004).
- 191 Connolly, L., Paul Edelstein, Lalita Ramakrishnan. Why is Long-Term Therapy Required to Cure Tuberculosis? *PLoS Med.* **4**, 0435-0442 (2007).
- 192 Zhang, Y. & Yew, W. W. Mechanisms of drug resistance in *Mycobacterium tuberculosis*. *Int. J. Tuberc. Lung Dis.* **13**, 1320-1330 (2009).
- 193 Yano, T. *et al.* Reduction of clofazimine by mycobacterial type 2 NADH:quinone oxidoreductase: a pathway for the generation of bactericidal levels of reactive oxygen species. *J. Biol. Chem.* **286**, 10276-10287 (2011).
- 194 Williams, K. *et al.* Sterilizing activities of novel combinations lacking first- and second-line drugs in a murine model of tuberculosis. *Antimicrob. Agents and Chemother.* **56**, 3114-3120 (2012).
- 195 Fraaije, M. W., Kamerbeek, N. M., Heidekamp, A. J., Fortin, R. & Janssen, D. B. The Prodrug Activator EtaA from *Mycobacterium tuberculosis* Is a Baeyer-Villiger Monooxygenase. *J. Biol. Chem.* **279**, 3354-3360 (2004).
- 196 DeBarber, A. E., Mdluli, K., Bosman, M., Bekker, L.-G. & Barry, C. E. Ethionamide activation and sensitivity in multidrug-resistant *Mycobacterium tuberculosis*. *Proc. Natl Acad. Sci.* **97**, 9677-9682 (2000).
- 197 Dover, L. G. *et al.* EthA, a Common Activator of Thiocarbamide-Containing Drugs Acting on Different Mycobacterial Targets. *Antimicrob. Agents and Chemother.* **51**, 1055-1063 (2007).
- 198 Bonsor, D. *et al.* Ligation independent cloning (LIC) as a rapid route to families of recombinant biocatalysts from sequenced prokaryotic genomes. *Org. Biomol. Chem.* **4**, 1252-1260 (2006).
- 199 Prakash, P., *et al.* Computational prediction and experimental verification of novel IdeR binding sites in the upstream sequences of *Mycobacterium tuberculosis* open reading frames. *Bioinformatics* **21**, 2161-2166 (2005).

- 200 Pandey, R. & Rodriguez, G. M. IdeR is required for iron homeostasis and virulence in *Mycobacterium tuberculosis*. *Mol. Microbiol.* **91**, 98-109 (2014).
- 201 Gold, B. e. a. The *Mycobacterium tuberculosis* IdeR is a dual functional regulator that controls transcription of genes involved in iron acquisition, iron storage and survival in macrophages. *Mol. Microbiol.* **42**, 851-865 (2001).
- 202 Voskuil, M. I., Bartek, I. L., Visconti, K. & Schoolnik, G. K. The Response of *Mycobacterium Tuberculosis* to Reactive Oxygen and Nitrogen Species. *Front. Microbiol.* **2**, 105 (2011).
- 203 Festa, R. A. *et al.* A novel copper-responsive regulon in *Mycobacterium tuberculosis*. *Mol. Microbiol.* **79**, 133-148 (2011).
- 204 Nishida, C. R. & Ortiz de Montellano, P. R. Bioactivation of antituberculosis thioamide and thiourea prodrugs by bacterial and mammalian flavin monooxygenases. *Chem. Biol. Interact* **192**, 21-25 (2011).
- 205 Singh, A., Jain, S., Gupta, S., Das, T. & Tyagi, A. K. *mymA* operon of *Mycobacterium tuberculosis*: its regulation and importance in the cell envelope. *FEMS Microbiol Lett* **227**, 53-63 (2003).
- 206 Singh, A. *et al.* Requirement of the *mymA* operon for appropriate cell wall ultrastructure and persistence of *Mycobacterium tuberculosis* in the spleens of guinea pigs. *J. Bacteriol.* **187**, 4173-4186 (2005).
- 207 Zampieri, D. *et al.* Antimycobacterial activity of new 3,5-disubstituted 1,3,4-oxadiazol-2(3H)-one derivatives. Molecular modeling investigations. *Bioorg. Med. Chem.* **17**, 4693-4707 (2009).
- 208 Macaev, F. *et al.* Synthesis of novel 5-aryl-2-thio-1,3,4-oxadiazoles and the study of their structure-anti-mycobacterial activities. *Bioorg. Med. Chem.* **13**, 4842-4850 (2005).
- 209 Casali, N. *et al.* Evolution and transmission of drug-resistant tuberculosis in a Russian population. *Nat. Genet.* **46**, 279-286 (2014).
- 210 Eldholm, V. *et al.* Four decades of transmission of a multidrug-resistant *Mycobacterium tuberculosis* outbreak strain. *Nat. Commun.* **6**, 67119 (2015).
- 211 Merker, M. *et al.* Whole Genome Sequencing Reveals Complex Evolution Patterns of Multidrug-Resistant *Mycobacterium tuberculosis* Beijing Strains in Patients. *PLoS One* **8**, e82551 (2013).
- 212 Bird, L. J., Coleman, M. L. & Newman, D. K. Iron and Copper Act Synergistically To Delay Anaerobic Growth of Bacteria. *Appl. Environ. Microbiol.* **79**, 3619-3627 (2013).

- 213 Barry, C. E., 3rd, Slayden, R. A., Sampson, A. E. & Lee, R. E. Use of genomics and combinatorial chemistry in the development of new antimycobacterial drugs. *Biochem. Pharmacol* **59**, 221-231 (2000).
- 214 Torres Pazmino, D. E., Fraaije, M.W. in *Future Directions in Biocatalysis* (ed T. Matsuda) 364 (Elsevier, 2007).
- 215 Torres Pazmino, D. E., Dudek, H. M. & Fraaije, M. W. Baeyer-Villiger monooxygenases: recent advances and future challenges. *Curr. Opin. Chem. Biol.* **14**, 138-144 (2010).
- 216 Baulard, A. R. *et al.* Activation of the pro-drug ethionamide is regulated in mycobacteria. *J. Biol. Chem.* **275**, 28326-28331 (2000).
- 217 Vannelli, T. A., Dykman, A. & Montellano, P. R. O. d. The Antituberculosis Drug Ethionamide Is Activated by a Flavoprotein Monooxygenase. *J. Biol. Chem.* **277**, 12824-12829 (2002).
- 218 Morlock, G. P., Metchock, B., Sikes, D., Crawford, J. T. & Cooksey, R. C. *ethA*, *inhA*, and *katG* Loci of Ethionamide-Resistant Clinical Mycobacterium tuberculosis Isolates. *Antimicrob. Agents and Chemother.* **47**, 3799-3805 (2003).
- 219 Ehrt, S. *et al.* Controlling gene expression in mycobacteria with anhydrotetracycline and Tet repressor. *Nucleic Acids Res.* **33**, e21-e21 (2005).
- 220 Loughheed, K. E. A., Bennett, M. H. & Williams, H. D. An in vivo crosslinking system for identifying mycobacterial protein–protein interactions. *J. Microbiol. Methods* **105**, 67-71 (2014).
- 221 Sassetti, C. M., Boyd, D. H. & Rubin, E. J. Comprehensive identification of conditionally essential genes in mycobacteria. *Proc. Natl Acad. Sci.* **98**, 12712-12717 (2001).
- 222 Nonejuie, P., Burkart, M., Pogliano, K. & Pogliano, J. Bacterial cytological profiling rapidly identifies the cellular pathways targeted by antibacterial molecules. *Proc. Natl Acad. Sci.* **110**, 16169-16174 (2013).
- 223 Hutter, B. *et al.* Prediction of Mechanisms of Action of Antibacterial Compounds by Gene Expression Profiling. *Antimicrob. Agents and Chemother.* **48**, 2838-2844 (2004).